Master's thesis

NTNU
Norwegian University of Science and Technology
Faculty of Natural Sciences
Department of Materials Science and Engineering

Charlotte Amalie Leinebø

Improving the Dynamic Sensing Range of Electrochemical Enzymatic Lactate Biosensors for Sweat Monitoring Applications

Master's thesis in Nanotechnology
Supervisor: Frode Seland
Co-supervisor: Erik Andrew Johannessen
June 2023

NTNU
Norwegian University of
Science and Technology

Charlotte Amalie Leinebø

Improving the Dynamic Sensing Range of Electrochemical Enzymatic Lactate Biosensors for Sweat Monitoring Applications

Master's thesis in Nanotechnology
Supervisor: Frode Seland
Co-supervisor: Erik Andrew Johannessen
June 2023

Norwegian University of Science and Technology
Faculty of Natural Sciences
Department of Materials Science and Engineering

NTNU
Norwegian University of
Science and Technology

Abstract

Sweat is a readily available body fluid for non-invasive, continuous and real-time monitoring of lactate during athletic activity. Electrochemical enzymatic biosensors present a promising and viable option for rapid, accurate and sensitive sweat lactate wearable monitoring. A major hurdle to overcome for realising a sweat lactate biosensor is the limited detection range compared to physiologically relevant sweat lactate concentrations. The overall aim of this work was to identify the mechanisms limiting the maximum signal of the lactate biosensors employed in previous work and examine formulation adjustments increasing the upper lactate detection limit.

Amperometric lactate biosensors were assembled by modifying the working electrodes of screen-printed electrode substrates with a thin film of Prussian Blue, an enzymatic layer of lactate oxidase and single-walled carbon nanotubes immobilised in a chitosan matrix and an outer Nafion membrane. The Prussian Blue film was electrodeposited whereas the enzyme and membrane layers were manually drop cast onto the electrode. The biosensors were chronoamperometrically tested in a phosphate buffer with stepwise lactate concentration increments until reaching current signal saturation. Cyclic voltammetry was employed to evaluate the stability of Prussian Blue.

Experimental findings indicated that the maximum current signal was ultimately limited by availability of dissolved oxygen in the test solution. Testing sensors in oxygen-enriched solution enhanced the maximum current response by 104% compared to standard testing conditions. Efforts to enhance the activity of the enzyme layer did not increase the maximum current signal, further reinforcing that sensors were ultimately limited by oxygen availability and not by catalytic activity of the enzymatic layer. To increase the dynamic range, the sensor membranes were modified to reduce the lactate flux over the outer membrane. Employing membranes made from sulfophenylated-polyphenylene with biphenyl linker did not improve sensor performance compared to Nafion. Incorporating cerium into the Nafion membranes induced polymer cross-linking, and an extended detection limit from 8 mM to 10 mM lactate was demonstrated with a cerium-Nafion composite membrane sensor. The achieved sensor performance supports the feasibility of cerium to reduce membrane lactate permeability and increase the dynamic range, but test data was limited to only 3 sensors due to the lack of a convenient and biosensor-compatible method of cerium incorporation. Given the low sensor reproducibility, larger sample sizes are needed to conclude a significant effect of the cerium composite membranes. Identifying a suitable incorporation method and cerium loading could further increase the dynamic range. An additional 10-fold increase would be necessary for lactate monitoring in undiluted sweat, approaching concentrations of 100 mM.

Sammendrag

Svette er en lett tilgjengelig kroppsvæske for ikke-invasiv og kontinuerlig sanntidsmåling av laktat under fysisk aktivitet. Elektrokjemiske enzym-baserte biosensorer er lovende for integrering i en bærbar sensorenhet, da de gir rask, nøyaktig og sensitiv laktatmåling. Et stort hinder for realiseringen av en svettelaktatsensor er det begrensede deteksjonsområdet til biosensoren sammenliknet med fysiologisk relevante laktatkonsentrasjoner. Det overordnede målet med denne oppgaven er å identifisere hvilke faktorer som begrenser deteksjonsområdet til laktatbiosensorene og å undersøke mulige endringer i sensorformuleringen som kan øke den øvre deteksjonsgrensen.

Amperometriske laktatbiosensorer ble laget ved å funksjonalisere arbeidselektroden på trykte elektrodesubstrater med en Prussian Blue tynnfilm, et enzymlag bestående av laktat oksidase og enkeltvegget karbonnanorør immobilisert i en matriks av chitosan og en ytre Nafionmembran. Elektrodeponering ble brukt til å legge på Prussian Blue-filmen, mens både enzym- og membranlagene ble påført manuelt ved å legge dem dråpevis på arbeidselektroden. Biosensorene ble testet kronoamperometrisk i fosfatbuffer, med en gradvis økning av laktatkonsentrasjon i løsningen frem til signalet ble mettet. Syklisk voltammetri ble brukt til å vurdere stabiliteten til Prussian Blue.

De eksperimentelle funnene indikerte at det maksimale strømsignalet fra sensorene var begrenset av mengden oppløst oksygen i testløsningen. Ved å teste en sensor i en oksygen-beriket løsning ble strømsignalet 104% høyere enn når den samme sensoren ble testet under standard forhold. Det maksimale strømsignalet ble ikke forbedret ved å øke kapasiteten til enzymlaget, hvilket underbygget hypotesen om at signalet var begrenset av oksygentilgang og ikke av lav enzymaktivitet. For å likevel kunne øke den øvre deteksjonsgrensen så ble egenskapene til sensormembranen modifisert med formålet om å redusere fluksen av laktat gjennom membranen. Å bruke sulfofenylert-polyfenylen med bifenyl-linker som membran istedenfor Nafion viste ingen forbedring. Derimot, inkorporering av cerium i Nafion-membranene hadde en kryss-linkende effekt, og en økning i deteksjonsområdet fra 8 mM til 10 mM ble demonstrert av en sensor med cerium-Nafion-membran. Denne sensorresponsen styrket hypotesen om at cerium kan brukes til å redusere permeabiliteten av laktat i membranen og dermed utvide deteksjonsområdet. Dataene var imidlertid begrenset til bare 3 sensorer grunnet mangelen på en praktisk og biosensor-kompatibel metode å inkorporere cerium i membranen på. Ettersom sensorene var lite reproduserbare så er det nødvendig med mer testdata for å kunne konkludere med en signifikant effekt. Ved å finne en egnet inkorporeringsmetode og optimal cerium-dose kan deteksjonsområdet muligens utvides ytterligere. For å kunne monitorere laktat i ufortynnet svette må deteksjonsområdet ytterligere økes med en faktor 10, da laktatkonsentrasjonen kan bli opp mot 100 mM.

Preface

This thesis is the final result of a 5-years integrated Master of Science in Nanotechnology with specialisation in Bionanotechnology at the Norwegian University of Science and Technology. The experimental work presented in this thesis was carried out during the fall of 2022 and spring of 2023, and the thesis is a continuation of the *TMT4510 Nanotechnology, specialisation course* project work finished in December 2022. Both projects were supervised by Frode Seland (NTNU) and Erik Andrew Johannessen (USN), and the experimental work was performed at the Department of Materials Science and Engineering. The project task was provided by Zimmer & Peacock AS, who also supplied necessary materials, equipment and guidance. Most chemicals and standard laboratory equipment were provided by the NTNU university department.

All the experimental work in this thesis was performed by me, whereas some of the employed solutions were pre-prepared by Zimmer & Peacock. The sensor assembly procedures, formulations and testing formats are adapted from Zimmer & Peacock's protocols, while adjustments and changes have been introduced by the author based on experimental findings, experiences, literature reviews and discussions with my academic supervisors. The proposal of incorporating cerium into the polymer membranes was put forward by Professor Steven Holdcroft at Simon Fraser University. Professor Holdcroft additionally gifted me with a sample of polymer proton exchange membranes to test on the sensors. I wish to acknowledge and thank for the help, inputs and guidance from all involved parties.

C. Amalie Leinebø
23rd June 2023

Acknowledgements

This thesis marks the end of 5 fantastic years as a Nanotechnology student at NTNU. I somehow ended up in the world of electrochemistry for my Master's Thesis, a field I have barely touched upon before. So, I can only say as Pippi Langstrømpe would: "Det har jeg aldri prøvd før, så det klarer jeg sikkert!"

Despite a positive attitude, I would not have managed this task without an amazing team of good helpers around me. I would like to thank my supervisors Frode Seland and Erik Andrew Johannessen. You have not only been skilful academic supervisors and available to answer all my stupid and (some) less stupid questions, but also encouraging and entertaining to be around. It has been a pleasure to wake up to the early-morning Tuesday meetings, discussing everything and nothing, and occasionally touching upon my experimental lab work and thesis. The entire electrochemistry group at IMA has been a great support, both in the academic and not-so-academic fields. There was never a boring day in the lab or in the reading hall with such great company. Thank you!

I would also like to thank Zimmer & Peacock for the interesting task and the guidance on the way. I would especially like to thank Youssef Lattach, who has been readily available for discussion sessions whenever necessary. Solrun Lid has also been of great help whenever I needed new materials and took great care of me during my summer internship at ZP.

A huge thank you also goes to Henrik Erring Hansen, Erik and Ruben for thorough and helpful feedback on the first draft of my thesis, both on the academic content and on the writing. Thanks to Vilde for always helping me out, whether it is academic or not. My parents have also been of great help. Not so much on the academic part, but they have supported and encouraged me whenever I have felt tired or annoyed and shared my happiness whenever I have been excited and cheerful.

Last, but definitely not least, I would like to express my gratefulness to Timini Kull 18 for being the most including, supportive, entertaining and engaged group of people I have met, and for making the last 5 years an adventure. Thank you for the ever-lasting lunch breaks, creative activities and the many hours spent together in lectures, reading halls and especially outside of campus. I have made friends for life. Despite that I still don't know what 'Nanotechnology' actually means or exactly what I have been studying for the last five years, I definitely know I would choose it again if we would do it together.

List of Acronyms

Abbreviations

CA	Chronoamperometry
CE	Counter Electrode
Ce	Cerium
CV	Cyclic Voltammetry
EDS	Energy-Dispersive X-ray Spectroscopy
Et	Ethanol
Glu	Glucose
Gly	Glycerol
L	Lactate Oxidase
LOx	Lactate Oxidase
N	Nafion
Ox	Oxidised specie
PB	Prussian Blue
PBS	Phosphate Buffered Saline
PBB	Sodium Phosphate Buffer
RE	Reference Electrode
Red	Reduced specie
RT	Room temperature
S	Sulfophenylated-polyphenylene wih biphenyl linker
SEM	Scanning Electron Microscopy
std dev	Standard deviation
SPE	Screen Printed Electrode
SPPB	Sulfophenylated-polyphenylene with biphenyl linker
SWCNT	Single Walled Carbon Nanotubes
WE	Working Electrode
ZP	Zimmer & Peacock
wt%	Weight percentage

Latin Letters

$\boldsymbol{A}$	Electrode area	m^2
$\boldsymbol{a_{red}}$	Activity of reduced specie	1
$\boldsymbol{a_{ox}}$	Activity of oxidised specie	1
$\boldsymbol{c}$	Concentration	$\mathrm{mol\,L^{-1}}$
$\boldsymbol{c_{max}}$	Highest significantly detected lactate concentration	mM
$\boldsymbol{D}$	Diffusion Coefficient	$\mathrm{m^2\,s^{-1}}$
$\boldsymbol{\Delta} E$	The peak-to-peak separation	V
$\boldsymbol{E}$	Electrode potential	V
$\boldsymbol{E^0}$	Standard electrode potential	V
$\boldsymbol{E^{0\prime}}$	Formal electrode potential	V
$\boldsymbol{E_{1/2}}$	Half-wave potential	V
$\boldsymbol{E_p}$	Peak potential	V
$\boldsymbol{E_{p,a}}$	Anodic peak potential	V
$\boldsymbol{E_{p,c}}$	Cathodic peak potential	V
$\boldsymbol{F}$	Faraday's constant	$96\,485\,\mathrm{C\,mol^{-1}}$
$\boldsymbol{I}$	Current	A
$\boldsymbol{I_{init}}$	Current signal at the first lactate addition	A
$\boldsymbol{I_{max}}$	Current signal at the highest significantly detected lactate concentration	A
$\boldsymbol{I_p}$	Peak current	A
$\boldsymbol{I_{p,a}}$	Anodic peak current	A
$\boldsymbol{I_{p,c}}$	Cathodic peak current	A
$\boldsymbol{J}$	Flux	$\mathrm{mol\,m^{-2}\,s^{-1}}$
$\boldsymbol{K_M}$	Michaelis-Menten constant	M
$\boldsymbol{R}$	Universal gas constant	$8.314\,\mathrm{J\,K^{-1}\,mol^{-1}}$
$\boldsymbol{T}$	Absolute temperature	K
$\boldsymbol{t}$	Time	s
$\boldsymbol{z}$	Number of electrons	1

Sensor Notation

PB|-	Sensors where the working electrode was covered with a Prussian Blue film.
PB|N	Sensors where the working electrode was covered with a Prussian Blue film and a Nafion membrane.
PB|L|N	Sensors where the working electrode was covered with a Prussian Blue film, a layer of lactate oxidase enzymes in a matrix of chitosan and single-walled carbon nanotubes and a Nafion membrane.
PB|L^{Glu}**|N**	Sensors where the working electrode was covered with a Prussian Blue film, a layer of lactate oxidase enzymes with added glucose in a matrix of chitosan and single-walled carbon nanotubes and a Nafion membrane.

PB|L^{Gly}|N Sensors where the working electrode was covered with a Prussian Blue film, a layer of lactate oxidase enzymes with added glycerol in a matrix of chitosan and single-walled carbon nanotubes and a Nafion membrane.

PB|1.5L|N Sensors where the working electrode was covered with a Prussian Blue film, a layer of lactate oxidase enzymes with a 1.5 times increase in standard enzyme amount in a matrix of chitosan and single-walled carbon nanotubes and a Nafion membrane.

PB|2L|N Sensors where the working electrode was covered with a Prussian Blue film, a layer of lactate oxidase enzymes with a 2 times increase in standard enzyme amount in a matrix of chitosan and single-walled carbon nanotubes and a Nafion membrane.

PB|L|N* Sensors where the working electrode was covered with a Prussian Blue film, a layer of lactate oxidase enzymes in a matrix of chitosan and single-walled carbon nanotubes and a Nafion-Ce^{3+} composite membrane.

PB|L|N*$^{y}_{(x\%)}$ Sensors where the working electrode was covered with a Prussian Blue film, a layer of lactate oxidase enzymes in a matrix of chitosan and single-walled carbon nanotubes and a Nafion-Ce^{3+} composite membrane. y is a number referring to the method of Ce^{3+} incorporation. x is a number specifying the weight percent of Ce^{3+} in the membrane.

PB|L|N** Sensors where the working electrode was covered with a Prussian Blue film, a layer of lactate oxidase enzymes in a matrix of chitosan and single-walled carbon nanotubes and a Nafion-CeO_2 composite membrane.

PB|L|N$_{(x\%)}$** Sensors where the working electrode was covered with a Prussian Blue film, a layer of lactate oxidase enzymes in a matrix of chitosan and single-walled carbon nanotubes and a Nafion-CeO_2 composite membrane. x is a number specifying the weight percent of CeO_2 in the membrane.

PB|L|S Sensors where the working electrode was covered with a Prussian Blue film, a layer of lactate oxidase enzymes in a matrix of chitosan and single-walled carbon nanotubes and a SPPB membrane.

PB|L|S* Sensors where the working electrode was covered with a Prussian Blue film, a layer of lactate oxidase enzymes in a matrix of chitosan and
single-walled carbon nanotubes and a SPPB-Ce^{3+} composite membrane.

PB|L|S*$_{(x\%)}$ Sensors where the working electrode was covered with a Prussian Blue film, a layer of lactate oxidase enzymes in a matrix of chitosan and single-walled carbon nanotubes and a SPPB-Ce^{3+} composite membrane. x is a number specifying the weight percent of Ce^{3+} in the membrane.

Sensor Terminology

The listed definitions are meant to give the reader an overview of common biosensor terminology actively employed in this work. The definitions are based on a combination of the *Biosensor Glossary* of Zimmer & Peacock [1] as well as the *Recommended Definitions and Classifications* of IUPAC [2]. The terms reproducibility and repeatability are found to be commonly used interchangeably in literature. In this paper, the below definitions of the terms will be used.

Dynamic Range. The concentration interval between the lower and the upper detection limit of the sensor. Within the dynamic range, a change in analyte concentration will generate a change in the signal output.
Linear range. A concentration interval within the dynamic range where the sensor output signal is linear to the concentration of analyte in solution. For enzymatic biosensors, this is dependent on the Michaelis-Menten kinetics of the enzyme.
Limit of Detection (LOD). The lowest analyte concentration required for a reliable sensor signal. This is commonly defined as LOD $\geq$ 3xSD of the blank signal.
Limit of Quantification (LOQ). The lowest analyte concentration required for a reliable analyte quantification signal. This is commonly defined as LOQ $\geq$ 10xSD of the blank signal.
Reproducibility. The ability of a biosensor to generate identical responses when subject to multiple experiments employing identical testing conditions.
Repeatability. The ability of biosensors with identical formulations to generate identical responses when subject to experiments employing identical testing conditions.
Response Time. The required time for the biosensor signal to stabilise after a change in analyte concentration. The signal is considered stable when larger than 90% of the steady-state signal.
Selectivity. The ability of the biosensors to exclusively interact with the analyte of interest, and not to other interfering species present in the sample.
Sensitivity. The change in current signal with a change in analyte concentration. In other words, this will be the slope of the calibration curve of the sensor.
Signal Drift. The ability of the biosensor to produce an even and reliable signal when all other parameters are kept constant.
Signal resolution. The smallest possible change in analyte concentration that can be distinguished, thus generating a significant change in sensor signal. The signal change should be $\Delta S \geq$ 3xSD. The resolution is often dependent on experimental noise, such as magnetic stirrers or electric noise.

Stability. The drift in sensor signal, either during operational use or storage. The signal drift will be dependent on ambient conditions, such as temperature. High stability implies low signal drift.

Contents

List of Figures

Chapter 1

Introduction

1.1 Background

Wearable healthcare technology represents a huge step within the field of personalised medicine, with the potential to improve the quality of life for millions of people and transform the healthcare system [3, 4]. By taking patient-specific factors into consideration, treatment options can be tailored specifically to meet individual needs. In this manner, one can optimise treatment procedures, circumvent adverse drug reactions and improve diagnostics accuracy [4]. Accurate diagnostics and personalised treatment can be achieved by wearable sensors, offering real-time monitoring of physiological data and health parameters. This will enable point-of-care diagnostics, which relieves the burden on the hospitals and health care systems as well as improving the quality of life for the patients. However, wearable sensors are not only useful in hospital and disease monitoring settings, but also for daily routines and activities [3].

A famous example of wearable sensors is the Apple Watch, tracking fitness parameters such as motion, number of steps and training intensity, as well as health parameters such as stress levels, sleep patterns and heart rate [5]. Wearable systems can be easily implemented into the daily life and routines of the user. They are small and simple to use, and can be integrated into everyday devices such as watches, clothing or other accessories, with a comfortable fit. Overall, wearable sensors can provide the user with rich information on their personal health and physiological state [3, 6].

Despite the rich insight on health status that can be derived from physical data, a considerable amount of information can only be obtained from analysis at a molecular level [6, 7]. The composition of biochemical markers present in biological fluids such as blood, urine and sweat reflects the molecular state of the body, indicating conditions such as bacterial or viral infections, organ failure, malnutrition and muscle fatigue [8, 9]. For accurate monitoring of biochemical parameters, biosensors are a prominent alternative. By employing recognition elements derived from biological systems, biosensors are extremely accurate and highly specific towards the analyte(s) of interest [10]. Despite the lack of transition to the commercial market, there is a great potential for integrating biosensors into wearable devices to track chemical and biological parameters in real-time. Several biosensor systems are currently under clinical evaluation, while still lacking regulatory approvals and sufficient validation studies [3, 7]. A

success story of commercial wearable biosensors is the Abbott FreeStyle Libre glucose sensor, which is a small wearable skin patch that continuously monitors glucose levels to ease insulin management for people suffering from diabetes mellitus [11]. However, a major drawback is the invasiveness, as the sensor requires skin piercing to access interstitial fluids [6]. This poses discomfort, stress and risk of infections to the users [3, 12]. Current efforts are concerned with the development of non-invasive wearable biosensors, meaning that there is no disruption of skin barriers or blood contact, offering more convenience and comfort to the user. Non-invasive and continuous monitoring of relevant biomarkers can be obtained by analysis of more readily available body fluids, such as saliva, tears and sweat [3, 6].

Sweat is abundant in metabolic biomarkers and is readily available for biosensing applications due to its accessibility and ease of collection. By combining smart microfluidic systems and materials for comfortable wearable systems with efficient transport of sweat to the biological sensing element, a fully wearable biosensor skin platform is achievable [3, 13]. Sweat is secreted to the skin from sweat glands distributed over the entire body, and is mainly used by the body for temperature regulation. The main component of sweat is water, but it also contains small amounts of various solutes partitioned from the sweat glands. Sweat is rich in electrolytes such as sodium and chloride, while also containing metabolites such as glucose, urea and lactate [14, 15].

Lactate is a metabolite product of glucose metabolism, and is produced in excess amounts when there is limited oxygen availability [16]. Especially in muscle tissue and blood, high lactate level is an indication of anaerobic conditions. Lactate levels are especially interesting to assess for endurance athletes, as it is related to performance factors such as working muscle fatigue. Lactate tolerance, threshold, peak and clearance values are all essential parameters to evaluate the physical shape of the athlete [17–20]. For temporary lactate analysis, invasive measurements of blood lactate levels are employed, which is both uncomfortable for the athlete and perturbs the training. In addition, the measurements are discrete and do not provide continuous information on the lactate levels [16, 21]. Lactate is not only partitioned to blood during anaerobic conditions, but also to sweat. Sweat lactate measurements present several advantages, such as continuous, real-time and non-invasive monitoring, as well as the ease of integrating the sensor into a comfortable wearable device [15, 22, 23].

Despite the promising prospect of non-invasive lactate monitoring, there are doubts regarding the clinical value of assessing bioanalytes in sweat [3, 24, 25]. No clear correlation between blood and lactate levels has been reported, which additionally calls for a mapping of sweat lactate value related to the degree of physical exertion, substantiating the clinical value of assessing bioanalytes in sweat [3, 24, 26]. Some researchers have demonstrated a positive correlation between the rate of lactate variation in blood and sweat from the active muscle area [25, 27]. Moreover, sweat lactate concentrations have been found to increase with higher exercise intensity and indicate the level of physical exertion over prolonged exercise [13, 21, 26]. With an increase in exercise intensity, the lactate content in sweat has been found to increase from 4 mM up to values close to and even above 100 mM [25, 28–30]. Consequently, the development of wearable sweat lactate biosensors could potentially enhance performance and training regimes for endurance athletes [22].

A major hurdle to overcome for translation of lactate biosensors to wearable sweat measurement devices is to enable detection of sufficiently high lactate concentration [28, 29]. For the lactate biosensor formulation employed in previous work, the best-performing sensor reached signal saturation at bulk lactate concentrations of 8 mM [31]. It was concluded that the biosensor response was ultimately limited by the availability of dissolved oxygen in the test solution or by capacity of the biorecognition element. Adjusting this biosensor formulation to regulate substrate availability or increase the catalytic activity is thus assumed to increase the upper detection limit, thereby making the biosensor more suitable for quantification of physiologically relevant sweat lactate concentrations.

1.2 Aim of Thesis

The aim of this work was to adjust and improve the lactate biosensor formulation to enable detection and quantification of physiologically relevant sweat lactate concentrations up to 100 mM. The sensing range limitations of the biosensor were identified, assessing whether the current response was constrained by activity of the bioactive component, stability of the mediator layer, substrate availability or combinations thereof. Based on the findings, efforts were made to improve the existing formulation to overcome these limitations and increase the upper limit of the dynamic range. All tested biosensor formulations were based on a similar framework, with a layered structure composed of a screen-printed carbon electrode substrate modified with a Prussian Blue thin film, an enzyme immobilisation matrix and an outer polymer membrane. For each layer, the loading amount, type of materials or post-treatment procedures were varied to identify a formulation and fabrication protocol yielding a stable biosensor response with an extended dynamic range. Considerable work was devoted to the incorporation of additives in the outer polymer membrane, attempting to identify a suitable loading dose and incorporation method. Additionally, ambient conditions such as temperature, lactate availability and oxygen availability were adjusted to investigate their impact on the performance of the bioactive component. The electrochemical activity of Prussian Blue was studied in detail to ensure that its catalytic capacity did not limit the biosensor response.

To quantify the dynamic range of the sensors, ex situ testing in phosphate buffer solutions with a controlled and stepwise increase of lactate concentration was performed. Chronoamperometry was the main method used to study the lactate response. The maximum generated current signal, dynamic range and signal linearity were used to evaluate and compare the performance of the sensors towards a gradual increase in lactate concentrations. Signal linearity was quantified by comparing the size of the initial current step to the maximum generated current signal. Sensor repeatability and reproducibility were also addressed, as they are essential parameters for a reliable sensor response and accurate lactate concentration assessments. Cyclic voltammetry was used to study the electrochemical behaviour of Prussian Blue in different phosphate buffers and the effect of post-treatment procedures. Overall, the experimental work aimed to identify a sensor formulation and fabrication protocol suitable for integration into a wearable system for continuous sweat lactate monitoring.

Chapter 2

Theory

This section will provide the theoretic foundation necessary for understanding the biosensor operation and provides a rationale for the sensor formulation, including findings from previous project work. In addition, the applied electrochemical detection methods and the mechanism behind them will be elaborated on.

2.1 Analytical Electrochemistry

Electrochemistry is a branch within physical chemistry concerned with the transfer of electrons at a polarised electrode surface, thus coupling chemical reactions to electrical processes. Electrochemistry is a versatile field with numerous applications within both industry and research, spanning from energy conversion and corrosion protection to analytical chemistry and biomedical analysis. With electroanalytical techniques, electronic properties such as current, potential and charge can be measured and related to chemical parameters and processes [32, 33]. Electroanalytical methods are especially appealing due to their high sensitivity and selectivity, as well as user-friendliness, affordability and portability of the measuring devices. Only small sample volumes are required for bulk solution analysis, allowing for device miniaturisation. These advantages are among the main motivations behind employing electroanalytical principles to develop sensor devices for point-of-care testing. An example of such an electrochemical device is the blood sugar test, which allows for point-of-care blood glucose assessment for diabetic patients [33, 34].

Reduction-oxidation (redox) reactions are the driving forces of electrochemical processes. Redox reactions can be induced by introducing two or more electronic conductors (electrodes) to an ionic solution (electrolyte) and applying a potential between them. Such a construction, consisting of two or more electrodes immersed in an electrolyte, is termed an electrochemical cell [35–37]. In order to obtain a closed circuit and a current flow in an electrochemical cell, there need to be at least two electrodes. Reduction and oxidation reactions are always coupled, with an oxidation occurring at the anodic electrode (anode) and a reduction at the cathodic electrode (cathode) [37, 38]. The supporting electrolyte should keep a constant ionic strength [32].

The simplest electrochemical cell for electroanalysis consists of a working and a reference electrode [38]. At the working electrode (WE), the electrochemical pro-

cess of interest takes place, being either a reduction or an oxidation reaction. The counter reaction takes place at the reference electrode (RE), thereby completing the electrochemical cell. The RE should additionally provide a stable reference point by delivering a constant potential [36–38]. To separate the counter reaction from the reference point, a third electrode can be introduced, namely a counter electrode (CE). The CE presents a designated electrode for countering the oxidation or reduction reaction occurring at the WE, allowing for more accurate measurements of single reaction events. In a three-electrode set-up, there will be a measurable current flow between CE and WE, while the desired cell potential is applied and controlled between RE and WE. A three-electrode system is more convenient for electrochemical analysis purposes. By avoiding a current flow at the RE, there will be no chemical reactions that may change the electrode environment composition and thus the electrode potential, yielding a more stable point of reference [34, 36–38]. A three-electrode system is commonly operated by a potentiostat. By employing a feedback loop, the potentiostat can accurately control the potential between the WE and RE by adjusting the current flow between WE and CE [34].

2.1.1 Nernst Equation

The potential of an electrode is directly correlated to thermodynamic properties of the surrounding solution and the activity of the electroactive species. This relation can be expressed through the Nernst equation. For the redox reaction $\mathrm{Ox} + \mathrm{ne}^- \rightleftharpoons \mathrm{Red}$, the Nernst expression becomes

$$E = E^0 - \frac{RT}{zF} \ln \frac{a_{Red}}{a_{Ox}} \tag{2.1}$$

where E (V) is the potential between WE and RE, E^0 (V) is the cell potential under standard conditions, R ($8.314\,\mathrm{J\,K^{-1}\,mol}$) is the universal gas constant, T (K) is the absolute temperature, z is the number of electrons transferred in the reaction and F ($96\,485\,\mathrm{C\,mol^{-1}}$) is Faraday's constant. The activity of the electroactive species undergoing reduction and oxidation, Red and Ox respectively, are ideal thermodynamic concentrations. Standard conditions are when the concentration of [Red] and [Ox] are both 1 M, at a temperature of 298.15 K and 1 atm pressure [32, 37].

The above equation can be simplified by introducing the formal electrode potential $E^{0\prime}$, which accounts for the activity coefficients a_{Ox} and a_{Red} when the reactants are solutes [38]. In this case, the Nernst equation can be simplified to

$$E = E^{0\prime} - \frac{RT}{zF} \ln \frac{[Red]}{[Ox]} \tag{2.2}$$

where the activities are replaced by the concentrations [Ox] and [Red]. For most applications, E^0 and $E^{0\prime}$ are approximately equal [34]. By applying the Nernst equation to an electrochemical cell, the electrode potential can be used to directly determine the concentration of analyte(s) [32, 36].

2.1.2 Electrodes

Electrodes are conductive or semi-conductive materials that form an interface towards the electrolyte solution. When the analyte of interest is present in the solution, electron transfer processes occur at this interface. Depending on the role of the electrode, being either the working, counter or reference electrode, the material and composition will vary [34, 37].

At the working electrode, the process of interest takes place. The WE is commonly made of an inert material that is unaffected by the reactions and charge transfers occurring during an analytical measurement. Common electrode materials are platinum, gold and various carbon compounds [38]. The WE can be chemically modified to increase its specificity and selectivity towards a certain species, thereby turning the electrolytic cell into a chemical sensor [32, 38].

The reaction of interest occurring at the WE should not be limited by the processes at the counter electrode. Thus, the CE should provide an accessible and large surface area for the counter reaction. The electrode material should be inert, with common electrode materials being platinum and graphite [32, 39].

The reference electrode should maintain a constant, absolute potential under the given reaction conditions. There should be no or minimal current flow through RE. The most prevalent RE composition is an inert metal surrounded by a salt of low solubility. Common RE materials are silver coated with a film of silver chloride (Ag/AgCl) and mercury coated with a mercury(II)chloride film (Hg/Hg_2Cl_2, the Calomel electrode). The anion of the salt in the film should be present at high concentrations in the surrounding solution to circumvent dissolution from the electrode. Additionally, small changes in anion concentration in the solution will have a low impact on the RE potential, evident from the Nernst equation (Eq. (2.2)) using the Ag/AgCl electrode as an example

$$E_{\mathrm{Ag/AgCl}} = E^{0\prime}_{\mathrm{Ag/AgCl}} - \frac{RT}{zF} \ln[\mathrm{Cl}^-] \tag{2.3}$$

The activity of Ag and AgCl are both 1 as they are both solids, and they are thus terminated from the Nernst expression. With large chloride concentrations, the change in potential E is negligible with small concentration fluctuations [32, 34].

To provide a stable environment for the RE, the electrode is often immersed in a dedicated solution, separated from the CE and WE. However, if currents are sufficiently small, in the pA/nA range, the RE can be included in the same electrolyte as WE and CE. This is termed a pseudo-reference electrode [34].

2.1.3 Mass-transport and Kinetic Limitations

An electrode reaction pathway is influenced and limited by the mass-transport of species to/from the electrode and electron transfer kinetics at the electrode surface. More complex reactions could also take place, such as coupled chemical reactions or surface adsorption. The overall reaction rate and current are ultimately determined by the slowest step, which is either the mass-transport or the reaction kinetics [34, 36].

Electrochemically reversible reactions are purely mass-transport controlled, and obey thermodynamic relationships [32]. For a reaction to occur at the electrode, electrochemically active species must be transported from the bulk to the electrode surface. Modes of mass-transport include diffusion, convection and migration. Diffusion is the random Brownian motion of a specie down a concentration gradient, which results in a net movement from areas of high to low concentrations. Convection is present when an external force, such as a magnetic stirrer or a solution flow, physically moves the solution or the electrode. This can be either forced, such as stirring, or natural, such as density gradients. Migration is the movement of charged species in an electric field. The effect of both migration and convection can often be minimised by tuning the test cell conditions [32, 36].

Diffusion is present in about every electrochemical measurement. As the experiment is initiated, the concentration of electroactive analyte (c_0) will be uniform throughout the solution. As analytes are consumed at the WE, the concentration in close proximity to the solution-electrode interface will be reduced. This will create a concentration gradient, governing diffusion of more analytes from the bulk solution to the electrode surface, where they are consumed. Over time, the diffusion layer will grow further into the bulk. The flux of substrate from the bulk to the electrode surface is dependent on the concentration profile, and is given by Fick's first law of diffusion

$$J(x,t) = -D\frac{\partial c(x,t)}{\partial x} \tag{2.4}$$

where the substrate flux J [$\mathrm{mol\,m^{-2}\,s^{-1}}$] is proportional to the concentration gradient, with D [$\mathrm{m^2\,s^{-1}}$] the diffusion coefficient. The concentration gradient is given as a function of time t [s] and distance x [m] from the electrode surface. Due to natural convection of the supporting solution, the diffusion layer cannot grow indefinitely. Ultimately, a stable diffusion layer will be established. The thickness of the diffusion layer will be reduced in a stirred solution [34, 36].

The current generated in a diffusion-controlled electrode process after applying an overpotential ($E > E^{0\prime}$) is predicted by the Cottrell Equation

$$I = zFAc\sqrt{\frac{D}{\pi t}} \tag{2.5}$$

where I [A] represents the cell current, z the number of electrons transferred, F [$96\,485\,\mathrm{C\,mol^{-1}}$] Faraday's constant, A [$\mathrm{m^2}$] the electrode area, D the diffusion coefficient, c [$\mathrm{mol\,L^{-1}}$] the bulk substrate concentration and t [s] the time since the potential step was applied. The Cottrell equation is valid when the operating potential is larger than the formal potential of the electrochemical reaction [34].

When the mass-transport between the bulk and electrode is sufficiently fast, but the reaction kinetics between analyte and electrode is slow, the reaction is electrochemically irreversible. The charge transfer is left as the rate-limiting step, and the system is under kinetic control. Since the current is not limited by diffusion, the Cottrell equation cannot be employed to predict the current [32, 34, 39]. In the case of an irreversible system, considerable kinetic and mechanistic information can be obtained from electrochemical studies [39].

2.1.4 Electrochemical Methods

Cyclic voltammetry

Cyclic voltammetry (CV) is a widely used electrochemical technique, as it can provide information on thermodynamics of a redox reaction, the kinetics of electron transfer and coupled chemical reactions such as adsorption [32, 34]. During a measurement, the current is recorded while the cell potential is swept linearly over a predefined interval [E_1, E_2]. When the upper interval limit E_2 is reached, the sweep direction is reversed, returning the potential to E_1. This gives a triangular potential waveform as a function of time, as illustrated in Figure 2.1a). At the starting potential, E_1, there should be no electrochemical activity of the analytes. The vertex potential, E_2, should be in the mass-transport controlled region. $E^{0\prime}$ of the redox system under study should be in between E_1 and E_2. Another crucial parameter is the scan rate v, which controls the speed of the potential sweep. The scan rate is the change in potential per time, and is typically set to a few $\mathrm{mV\,s^{-1}}$ or $\mathrm{V\,s^{-1}}$. The potential sweep can be performed a single or multiple times, depending on the information one wishes to obtain. Multiple scans are commonly used to study the stability of a system [34, 39].

Data from a CV scan is represented in a cyclic voltammogram, where the recorded current is plotted as a function of potential. From this plot, both mechanistic and kinetic information about the system at hand can be derived [39]. A generic, simple cyclic voltammogram is presented in Figure 2.1b). When the potential is increasing, an anodic peak appears. When the potential is reversed, a cathodic peak is formed. The shape and position of the peaks are dictated by a combination of electrochemical activity, described by the Nernst equation for the redox couple, and the mass-transport of analytes between the electrode surface and bulk solution, described by Fick's law of diffusion [34]. At the initial potential E_1, the redox couple is not electrochemically active, and mainly the reduced form Red of the compound is present in the solution. As the potential is gradually swept towards E_2 and approaches the formal potential $E^{0\prime}$ of the redox couple, the current gradually increases as Red is oxidised to Ox at the electrode surface, dictated by the Nernst equation (2.2). Due to the depletion of Red at the electrode surface, a diffusion gradient from the bulk solution is established. The gradient will continue to grow until complete depletion of Red at the electrode surface, at which the peak anodic current $I_{p,a}$ is reached. The subsequent current decay is purely diffusion controlled, and exhibits at $t^{-1/2}$ dependence according to the Cottrell equation (2.5). Approaching E_2, the diffusion layer will reach a finite thickness, and the current stabilises. At E_2, the potential sweep is reversed, and the process is repeated with Ox as the dominating species in the solution. A cathodic peak will appear due to the reduction of Ox to Red. Thus, the current peaks represent the continuous change of the concentration gradient and redox activity around the electrode with a change in cell potential [34, 39].

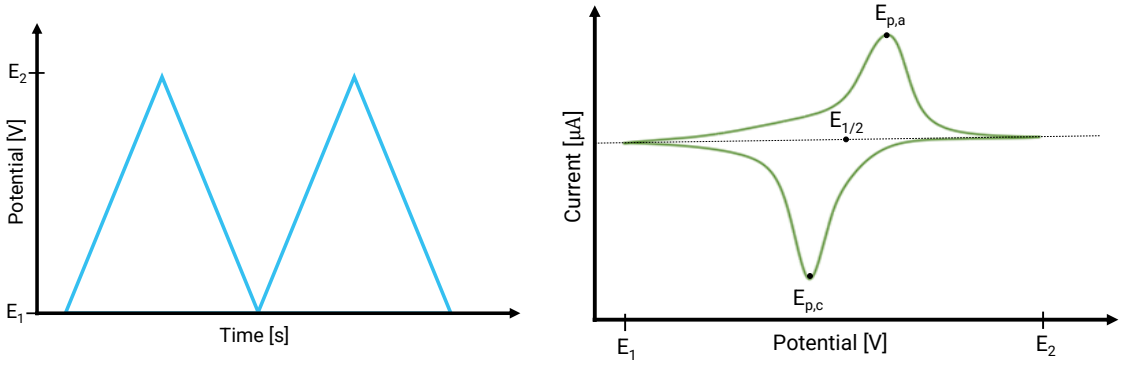

(a) **(b)**

Figure 2.1. a) The potential as a function of time in a CV measurement over two cycles. b) A CV cycle for a reversible electrochemical reaction. $E_{p,a}$ and $E_{p,c}$ are anodic and cathodic peak potentials, respectively. $E_{1/2}$ is the half-wave potential.

The peak potentials (E_p) in a voltammogram can be used to approximate the formal potential of a reversible redox reaction. If the reaction is purely controlled by the electrode potential and diffusion, the formal potential will be somewhere in between the anodic ($E_{p,a}$) and cathodic ($E_{p,c}$) peak. The exact position will depend on the diffusive properties of Red and Ox. If the diffusion constant is identical for oxidised and reduced species, $E^{0\prime} = E_{1/2}$. Moreover, the E_p of a reversible redox system is independent of the scan rate v. The time scale of the experiment is slower than the reaction kinetics, and a Nernstian equilibrium is rapidly established with a change in potential. The peak separation ΔE_p for a reversible system is given by

$$\Delta E_p = \frac{59mV}{z} \tag{2.6}$$

where z is the number of electrons transferred in the redox reaction. Contrastingly, when there are kinetic limitations and thus slow reaction rates, increasing the scan rate will shift the peak potentials and increase the peak separation ΔE_p. The reaction kinetics are slower than the mass transport, and thus more negative/positive potentials are required to observe a reduction/oxidation. This is referred to as electrochemical irreversibility [34, 35, 39].

The shape and position of the voltammetric peaks are not only influenced by electron transfer rates and diffusion, but also by processes such as surface adsorption and coupled chemical reactions [32]. Performing CV at different scan rates can be used to determine whether surface adsorption of the redox species occurs. Increasing the scan rate will reduce the relaxation time of the diffusion layer and make it thinner, which will generate larger peak currents. When the reactants are adsorbed to the electrode after reaction, there is a direct proportionality between peak current and scan rate. When the species are freely diffusing, the peak current is proportional to the square root of the scan rate. Thus, adjusting the scan rate can give information on surface adsorption of the redox species [32, 34, 39].

Cyclic voltammetry can be used to deposit material on an electrode, a process

known as electrodeposition. If one or both of the redox species are involved in an adsorption-desorption process, multiple cycling around the electrochemically active area can give rise to a growing adsorbed layer on the electrode surface. This is reflected in the gradual increase in cathodic and anodic peak current as a function of cycle number. The amount of deposited material can be derived from the peak area [32].

Chronoamperometry

Chronoamperometric (CA) measurements record the current-time behaviour of the electrochemical system at a constant direct current potential. The applied potential is typically set to ensure a mass-transport-limited reaction. When diffusion is the main mode of mass-transport, the Cottrell equation (2.5) will be valid, and can be used to determine either the diffusion constant, the electrode area or the concentration of the electroactive analyte [32]. According to the Cottrell equation, the current will decay exponentially with time due to the gradual extension of the diffusion layer, ultimately reaching a steady state. By introducing convection in the form of constant stirring, the thickness of the diffusion layer is reduced, which facilitates a more rapid current stabilisation. If the stirring rate is kept constant during the experiment, there is a direct proportionality between the recorded current and analyte concentration. Consequently, the concentration of analyte in the test solution can be determined by dividing the current signal by an experimental calibration factor [34].

CA is a useful method for continuous monitoring of analyte concentration in a solution. Changes in analyte concentration could be induced by direct addition or depletion, or by natural changes in the system [10]. A typical chronoamperometric measurement is shown in Figure 2.2. The annotated plateaus c1, c2 and c3 represent three distinct analyte concentrations, which results in generation of three distinct current signals.

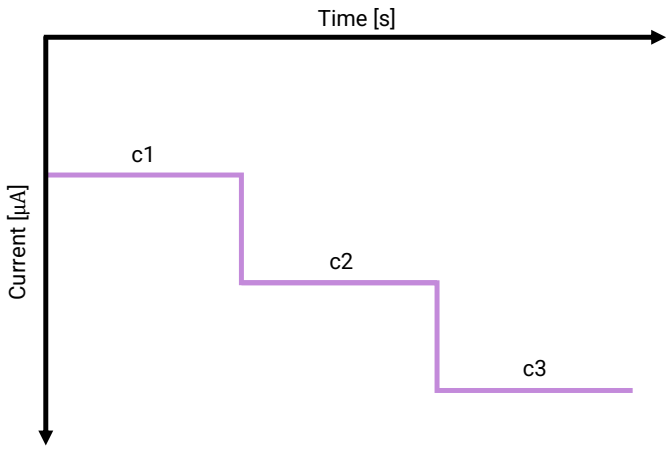

Figure 2.2. An example of a chronoamperometric measurement. c1, c2 and c3 represent different analyte concentrations under a constant WE potential.

2.2 Electrochemical Enzymatic Biosensors

Sensors are devices consisting of a recognition element that registers a physical, chemical or biological change, and a transducer that converts this interaction into a measurable signal [10, 19, 32]. A signal processor will collect, amplify and present the detected signal. In a chemical sensor, the recognition element interacts with the analyte(s) and generates a chemical change, which is used to produce a signal [40]. Electrochemical biosensors are a subclass of chemical sensors, in which the recognition element is a biological component and the transducer element is an electrode [32]. A schematic of an electrochemical biosensor is found in Figure 2.3. The electrochemical biosensors are valuable analytical tools, with high specificity offered by the biorecognition element and accuracy, sensitivity and analytical power provided by electrochemical techniques [32]. The devices have a simple design and cheap instrumentation, making them inexpensive. In addition, they are compact and easy to use, allowing for device miniaturisation [10].

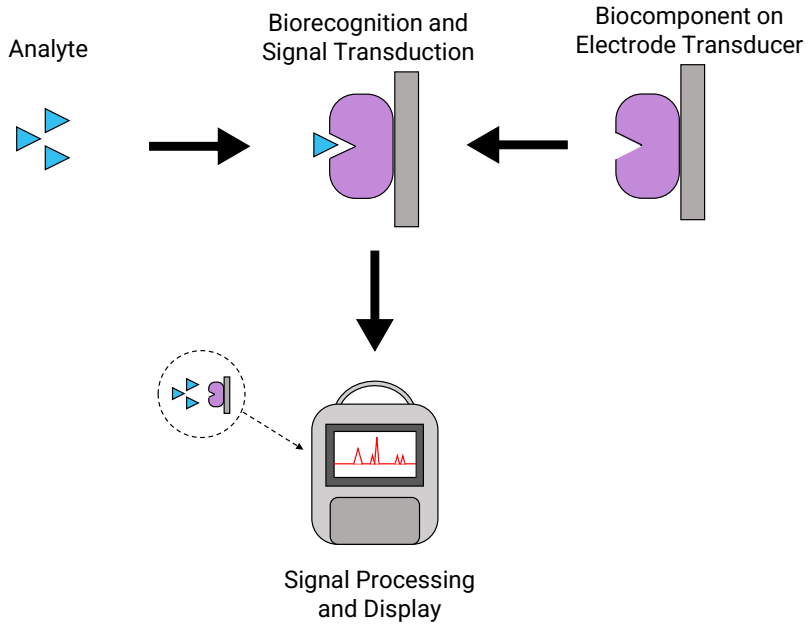

Figure 2.3. Schematic of an electrochemical biosensor. In the presence of the analyte of interest, there will be a binding event between biorecognition element and analyte which generates a change in output signal. The figure is adapted from Biorender [41].

The recognition element determines the selectivity of the sensor. By utilising highly specific elements derived from biological systems prone to years of evolution, biosensors interact highly specifically with their target analytes. There are primarily two groups of biological recognition elements employed for biosensing, yielding either a biocatalytic or an affinity sensor. Affinity electrochemical biosensors utilise the strong binding of molecular recognition elements to their substrates based on complementary size, shape

or charge, among others. Examples are antibodies, membrane receptors and nucleic acids (DNA). For biocatalytic electrochemical biosensors, the biorecognition element is a species that converts the analyte(s) into an electroactive product. This could be enzymes, cell organelles or microorganisms, among others [10, 32].

Using an electrochemical transducer, the biosensor produces an electrical signal that is related to the concentration of analyte in the sample [32]. Amperometric biosensors are the most common type of electrochemical biosensors and exploit the current that is generated when an oxidation or a reduction takes place at an electrode, which will be directly proportional to the concentration of the electroactive species. By applying an appropriate potential between the WE and RE, the electrochemical reaction of interest can take place at the electrode surface [19, 32]. For electrochemical biosensors using enzymes as the biorecognition element, either the substrate or the product of the enzymatic reaction is detected at the electrode. Amperometric biosensors are commonly based on enzymes that consume oxygen and produce hydrogen peroxide as a by-product, namely oxidase enzymes [19]. There exist multiple methods for sensitive detection of hydrogen peroxide, including both direct oxidation or the use of an electrocatalyst [42, 43].

2.2.1 Enzyme-Based Sensing

Enzymes are proteins that function as biological catalysts within living systems. Approximately every metabolic process that takes place within a cell requires enzymes to obtain sufficient reaction rates and to control the catalytic processes [44]. Enzymes are highly specific towards the substrate of the reaction they are catalysing, even in complex sample mixtures, which makes them the most commonly employed biorecognition element for biosensing purposes [40]. A typical enzyme-catalysed reaction can be described as follows

$$\mathrm{S + E \underset{k_{-1}}{\overset{k_1}{\rightleftharpoons}} ES \xrightarrow{k_2} E + P} \tag{2.7}$$

where S is the enzymatic substrate, E is the enzyme, ES is the intermediate enzyme-substrate complex and P is the product [32, 40]. The k_1, k_{-1} and k_2 denote the reaction rates of the individual reactions. When the concentration of enzymes is constant, the overall reaction rate of the enzyme-catalysed reaction can be expressed by the Michaelis-Menten equation

$$v = \frac{\mathrm{V_M\,[S]}}{\mathrm{K_M + [S]}} \tag{2.8}$$

where v is the overall reaction rate, V_M is the maximum reaction rate and $[S]$ is substrate concentration. K_M is the Michaelis-Menten constant, which corresponds to the substrate concentration $[S]$ when the reaction rate equals $\frac{1}{2}V_M$ [32]. Enzymes employed in biosensing should have a high V_M for a wide linear range, and a low K_M to obtain high sensitivity and maximum catalytic activity at low substrate concentrations [10]. This is illustrated in Figure 2.4, displaying a generic Michaelis-Menten plot. At low substrate concentration, there is a large availability of enzymes, resulting in a linear relationship between substrate concentration and reaction rate. At larger

substrate concentrations, the enzymes are saturated, and a further increase in substrate concentration will have little or no effect on the reaction rate. The enzymes are already at their full catalytic capacity [32]. To increase the linear range of a biosensor, a diffusion-limiting membrane can be applied on top of the enzymatic layer. This will result in a lower substrate concentration in the local, enzymatic layer compared to the bulk solution [2, 32].

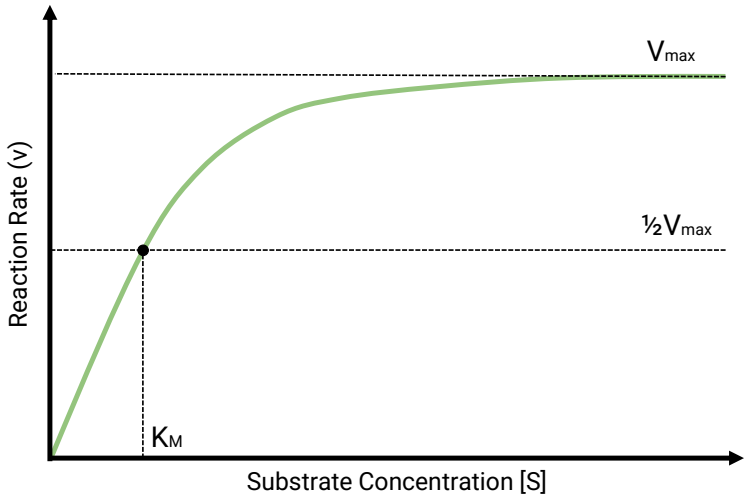

Figure 2.4. Schematic of a generic Michaelis Menten plot. K_M is the Michaelis Menten constant. The figure is adapted from [32].

2.2.2 Enzyme Immobilisation and Stability

Enzyme immobilisation is an important step in the construction of an electrochemical biosensor. The enzymes should be properly attached and in close proximity to the electrode surface for efficient signal transduction [40]. This process is termed immobilisation. It is paramount that the enzymes are retained at the surface and do not leak out to the bulk medium, but must concurrently be available for diffusion of substrate and product in and out of the sensing area. In addition, the microenvironment should retain or enhance enzymatic activity, providing a favourable environment with regards to temperature, pH, ionic strength and chemical composition [16, 19, 40].

The immobilisation is essential for sensor performance in terms of sensitivity, response time and operational and storage stability. Methods for enzyme immobilisation are either physical or chemical. With chemical methods, covalent bonds are induced either between the enzymes or between enzymes and electrode material [10, 45]. Covalent bonding gives the most stable immobilisation and is better at retaining the enzymes at the electrode, but may result in considerable loss in enzymatic activity due to conformational changes in the enzyme structure. Physical methods do not involve a structural change in the native enzyme and are thus better for retaining inherent activity. Physical methods include adsorption, micro-encapsulation or entrapment within a gel or film. For physical adsorption, the enzymes are only held in place by weak van der Waals interactions and hydrogen bonds, which gives low stability and lifetime of the sensor. With micro-encapsulation, the enzymes are kept

in place at the electrode by applying a membrane on top. For physical entrapment, the enzymes are embedded into the interstitial spaces of a gel or film, providing the most durable physical immobilisation method. However, with physical entrapment, the immobilisation gel will present a diffusion barrier for the enzymatic substrate and product, which reduces the response time of the sensor [10, 40]. Chitosan is an example of a polysaccharide suitable for enzyme immobilisation by physical entrapment, forming complexes with and stabilising the enzymes [45].

Maintaining long-term stability is a common challenge for enzymatic biosensors. Most enzymes have low intrinsic stability when removed from their natural environment inside the cell. Several mechanisms give rise to loss of enzyme activity or inactivation, such as aggregation, protein unfolding, chemical alteration or inhibition [46]. The method of immobilisation should retain or enhance enzymatic activity by preventing damage and alterations to the native enzyme conformation. Ambient conditions such as pH and temperature also affect enzyme conformation and activity, and should thus be kept relatively constant if possible [10]. Moreover, several enzymes are regulated by a negative feedback mechanism in which their activity is down-regulated when excessive amounts of product are present. This phenomenon is known as product inhibition, and will contribute to fluctuation of enzymatic activity in a biosensor over time [44, 47].

In addition to an appropriate immobilisation method, other techniques can be used to enhance enzyme stability and compromise inhibition effects. Protein engineering can be used to directly enhance protein stability and to improve properties such as specificity, selectivity, pH and temperature stability and activity [48]. However, there is an intricate interplay between protein structure and function [22, 48]. Even minor adjustments improving the stability of the enzyme could influence protein folding and alter other important functions, such as substrate binding and conversion. Compared to protein engineering, optimising immobilisation is more straight-forward technique [48]. The process of protein engineering is iterative and requires thorough screening, rendering it time-consuming and possibly with only minor improvements regarding stability and activity [49, 50]. Another option is to introduce enzyme-stabilising agents. The addition of cosolvents has been shown to greatly enhance protein stability and activity for applications within biotechnology. The exact mechanism is not thoroughly understood, but it is assumed that the cosolvents shift the protein conformation towards more stable states and counteract protein unfolding. Glycerol has been routinely used for this purpose, inducing effects such as lower protein flexibility, protein compaction, stabilisation of unfolded intermediate state and aggregation prevention [51].

2.3 Electrochemical Biosensor for Lactate Detection

In this section, the layers comprising an electrochemical enzymatic lactate biosensor will be described, namely the WE, inner mediator layer, enzymatic layer, and outer permselective membrane. In combination, the biosensor layers ensure accurate and sensitive lactate detection, while interference from other species is limited.

2.3.1 Screen Printed Electrodes

Screen-printed electrodes (SPEs) have been widely employed for biosensing purposes and offer several advantages for electrochemical measurements. The low production costs allow for disposable sensors, which eliminates the need for electrode cleaning and polishing after use, improving the user-friendliness. To produce SPE sensors, a mask containing the electrode pattern can be placed on top of a support material, often polyester, and an electrode paste can be accurately pressed through the mesh and onto the support material. The electrodes can be made up of different pastes due to the ease of applying a mask. CE is often made of a carbon paste, and RE of silver paste with silver chloride. The material of the CE can vary, and for simplicity it is often made from the same material as either the WE or RE. [34].

2.3.2 Lactate Oxidase

L-Lactate, hereby referred to as lactate, is a key metabolite in the anaerobic respiratory pathway. Lactate is an important biomarker for hypoxia, which occurs when the energy demand of the cell exceeds the oxygen availability [19]. Lactate oxidase (LOx) enzymes are commonly employed in enzymatic lactate biosensors. LOx is highly specific towards lactate, has a simple enzymatic reaction and is simple to integrate into biosensor devices [16, 52–54]. Lactate Oxidases are expressed in several bacteria, *Aerococcus viridans* among them. In the presence of dissolved oxygen, LOx catalyses the oxidation of lactate to pyruvate, and hydrogen peroxide (H_2O_2) is formed as a by-product [16, 19]. The LOx-catalysed reaction can be summarised as follows

$$\text{Lactate} + O_2 \longrightarrow \text{Pyruvate} + H_2O_2 \tag{2.9}$$

H_2O_2 is electrochemically active and can be directly oxidised by the following reaction scheme [19]

$$H_2O_2 \longrightarrow O_2 + 2\,H^+ + 2\,e^- \tag{2.10}$$

The above reaction occurs at a potential of approximately 0.6 V vs Ag/AgCl [55]. H_2O_2 generated by the LOx enzyme can thus be directly oxidised at the WE, generating a current signal directly proportional to the amount of lactate present. Hence, coupling of the two above equations can be used for accurate determination of the lactate concentration in a sample [10].

A major challenge in using LOx for biosensing applications is the limited stability when the enzyme is removed from its natural matrix [53, 56]. This restricts both the performance and the lifetime of the biosensor. Efforts to improve the stability and performance of lactate oxidase involve both enzyme engineering and identifying immobilisation techniques that can contribute to increased stability. LOx has been thoroughly studied, and its amino acid sequence and three-dimensional shape have been analysed and modelled [16]. Taurino et al. managed to improve the detection limit and long-term stability of LOx by site-directed mutagenesis [52]. However, protein engineering increases the complexity and cost of biosensor development [56]. Optimising immobilisation procedures have provided techniques and materials that significantly

improve LOx stability, with especially sol-gel immobilisation demonstrating retention of enzymatic activity [16, 53, 57].

A second hurdle for lactate oxidase-based biosensors is the oxygen dependency, as seen in Equation (2.9). Fluctuations in oxygen content will affect the detection limit of the sensor, reduce the reliability of the measurements and limit sensor miniaturisation. Alternatively, the enzyme lactate dehydrogenase has an oxygen-independent reaction mechanism and could be employed to circumvent oxygen limitation issues. However, lactate dehydrogenase enzymes face challenges in sensor integration, making LOx the preferred choice for biosensing purposes [16, 19].

The activity of LOx is dependent on pH and temperature [54, 58]. Lactate oxidase from *Aerococcus viridans* has a pH optimum between 6.5-7.5 and temperature 37°C. The catalytic activity of an enzyme in a catalyst solution mix is given in units (U). One unit (1 U) of LOx is defined as the amount of enzyme necessary to convert 1 µmol of lactate to pyruvat and H_2O_2 at pH 6.5 and a temperature of 37°C [58].

2.3.3 Nanomaterials and Carbon Nanotubes

Nanotechnology refers to the creation and utilisation of materials, systems and devices where either one, two or three dimensions are on the scale of 1 - 100 nm. Nowadays there exists a wide range of available nanomaterials of different compositions, shapes and sizes, with the possibility of tailoring the properties for specific applications [59]. Due to the versatility of nanomaterials, there are numerous application areas, biosensing among them. 1D nanomaterials are especially appealing owing to properties such as high surface-to-volume ratio and excellent electron transfer properties. The effective surface area of the active electrode can be increased by implementing nanomaterials, increasing the overall current response. Moreover, nanomaterials may contribute to enzyme immobilisation and cross-linking, as they show strong adsorption properties [19].

The most commonly employed nanomaterials for lactate biosensing purposes are carbon nanotubes (CNTs), gold nanoparticles (AuNPs) and zinc oxide nanostructures (ZNO) [19]. CNTs are a 1D nanomaterial with unique electronic and mechanical properties owing to their structure. CNTs are formed by rolling up single or multiple sheets of graphite, resulting in either single-walled or multi-walled tube [59]. These tubes can have a length of several micrometres, whereas the diameter is on the nanometer scale. Within the hollow tube structure, CNTs can accommodate guest molecules, rendering them appropriate for immobilisation and retention of enzymes at the WE of an electrochemical biosensor. Additionally, their large surface area enhances the effective area of the working electrode, increasing the sensor sensitivity [8, 59, 60]. Lastly, CNTs possess exceptional electron transfer characteristics and can reduce the necessary overpotential for H_2O_2 reduction [45, 61, 62].

CNT-based sensors can be prepared by dispersing the CNTs in an aqueous solution and casting them onto the sensor surface. However, CNTs have low solubility in most conventional solvents and have a tendency to aggregate. The natural and biocompatible polysaccharide chitosan can be used to homogeneously disperse CNTs and the CNT-chitosan solution can simply be drop cast onto the biosensor electrode [45, 61, 62]. The solution preserves the CNT structure, has a uniform CNT distribu-

tion and shows good stability. Furthermore, chitosan has proven useful for enzyme immobilisation. Chitosan-CNT dispersions have a higher tensile modulus and mechanical strength than pure chitosan films, which is more suitable for efficient enzyme immobilisation [45].

2.3.4 Permselective Membranes

A permselective outer membrane is a critical component of an enzymatic biosensor, adjusting the linear range, dynamic range and sensitivity of the sensor. An outer membrane decreases substrate diffusion into the enzymatic layer, and thus the substrate in the local area is lower than in the bulk solution [2, 63, 64]. As a result, the apparent K_M value increases [65]. Moreover, the membrane blocks interfering agents from interacting with the enzyme or the electrode, thus enhancing sensor specificity [16, 63]. The outer diffusion membrane should limit the flux of lactate into the enzymatic layer, but not significantly affect availability of oxygen (O_2). If the local O_2 concentration is low, the sensor response will be limited by O_2 availability rather than lactate. An appropriate outer membrane will eliminate the complications of O_2 dependence by allowing for O_2 transport while limiting the lactate flux [66].

Nafion is one of the most commonly employed polymer membranes for lactate biosensors [16]. Nafion is a sulfonated fluoropolymer, consisting of a hydrophobic backbone of polytetrafluoroethylene with hydrophilic sulfonated side groups [16, 67, 68]. The molecular structure of Nafion is shown in Figure 2.5a). The morphology and microstructure of Nafion membranes are complex. It is challenging to obtain structural info on Nafion due to the random chemical structure and distribution of the co-polymer, complexity in the organisation of crystalline and ionic domains, low degree of crystallinity and dependence on membrane swelling state. Despite a heterogeneous structure, it is generally accepted that there is an aggregation of the ionic groups in the perfluorinated polymer matrix. There exists a connected network in which the anionic sulfate groups form clusters and channels through which both polar solvents and cations can migrate. Upon water swelling, the number of ionic clusters decreases while the size of the remaining clusters increases. Thus, the membrane becomes more permeable to larger species. The morphology of the Nafion membrane will change depending on water and ion content, and is thus dependent on the properties of the supporting electrolyte. Pre-treatment procedures, such as processing, temperature treatment and swelling history can have a large impact on the membrane morphology. Thus, specific casting and post-treatment procedures can be selected to control and tailor the properties of Nafion films and membranes [67].

Nafion membranes are commercially available as ionomer solutions, which can be used to cast uniform thin film membranes. The properties of the membrane are highly dependent on the deposition method, as this will influence the crystallinity and supramolecular organisation in the film. Recast membranes have different properties and performance than melt-produced membranes regarding morphology, physical properties and chemical characteristics. As-received membranes are flexible, though and insoluble in about any solvent up to 200 degrees. Recast membranes are often more brittle and are soluble at room temperature in several organic solvents. Nafion membranes cast and treated at room temperature are essentially amorphous, and thus have

low resistance to swelling. Heating of recast membranes can increase the crystallinity, making them more similar to the melt extruded membranes [67].

Recast Nafion membranes are one of the most commonly employed polymers for membrane construction in lactate biosensors, and are known to exclude interfering species and anions [16]. However, the membrane is still susceptible to lactate passage [64, 69]. Recast Nafion membranes have an amorphous structure, thus constituting a diffusion barrier while still being partly lactate permeable [67]. Diffusion rates through amorphous materials are known to be much greater than in crystalline materials due to the more open structure [70].

A current field of research is the development of various sulfonated polymers as an alternative to Nafion membranes. These sulfonated membranes are likewise based on the presence of both hydrophobic and hydrophilic moieties, giving rise to the formation of ionic clusters and channels that allows for passage of polar solvents and cations. By developing polymers with a more controlled synthesis procedure, properties such as ion exchange capacity, water adsorption, ion conductivity and durability of the membrane can be tailored more accurately. Especially sulfophenylated-polyphenylene with biphenyl linker (SBBP) membranes constitute a promising alternative to the existing perfluorinated membranes, as it has a high backbone stability, simple synthesis and favourable ion conductive properties [71]. The structure of SBBP membrane monomers is found in Figure 2.5b).

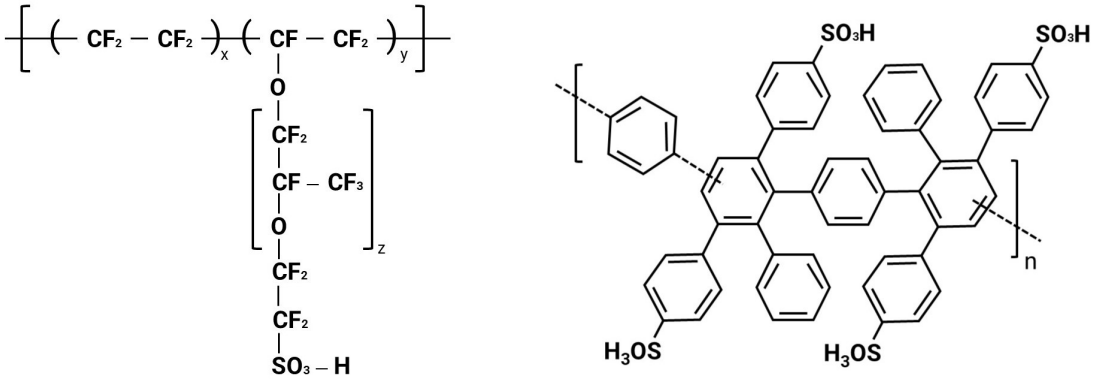

(a) **(b)**

Figure 2.5. The chemical structures of Nafion (a) and SBBP (b) polymers. The figures are adapted from Yu [72] and Tian [73].

Cerium can be introduced to Nafion or SBBP membranes to enhance the chemical stability, and simultaneously reduce their proton conductivity, water uptake and permeability. There are several reports in literature on incorporation of either Ce^{3+} or CeO_2 in proton exchange membranes to function as radical scavengers, thereby improving the lifetime of the membranes in fuel cells [73–75]. Both CeO_2 nanoparticles and Ce^{3+} ions have been found to associate with the anionic sulfate groups of the membranes by replacing up to three or four membrane protons. This proposed mechanism is shown in Figure 2.6. Consequently, the cerium functions as ionic cross-linkers and perturbs the proton transport pathway within the membrane [73, 76]. Research

on incorporation of cerium in anion exchange membrane is mainly concerned with the radical scavenging effect of cerium, whereas reduced membrane conductivity is an undesirable side effect [73, 74, 77, 78]. There exists little literature on the fabrication of cerium composite membranes with the main objective of controlling and reducing membrane properties for biosensing applications. Nevertheless, findings on cerium as radical scavengers can be used to establish a minimum of cerium content to obtain a significant reduction in membrane conductivity and permeability. For Ce^{3+} incorporation, Tian concluded that concentration up to 2 wt% of pristine membrane polymer content had little impact on membrane conductivity [73, 74]. In the same manner, Zhao et al. found that 10 wt% CeO_2 resulted in a significant reduction in membrane conductivity [76]. These findings imply that cerium loading should exceed 2 wt% and 10 wt% for Ce^{3+} and CeO_2, respectively, to observe a significant effect.

Several methods for preparation of composite membrane-cerium have been described, mainly concerned with direct mixing of cerium and membrane solution or solution immersion. For direct mixing, CeO_2 particles or Ce^{3+} salts are added to the membrane solution and subsequently cast and cured at elevated temperatures [74, 78, 79]. A second option is to immerse previously cast polymer membranes in Ce^{3+} solutions for a prolonged time and allow for ion exchange with the membrane protons [73, 75, 77]. The immersion technique is challenging to employ with CeO_2, being practically insoluble in aqueous solutions. Nevertheless, the cross-linking effect of CeO_2 is achieved despite the presence of the oxide lattice [78]. Overall, CeO_2 or Ce^{3+} Nafion and SBBP composite membranes could present a more efficient and stable diffusion barrier for solution cast membranes by lowering the substrate flux across the membranes [74, 75].

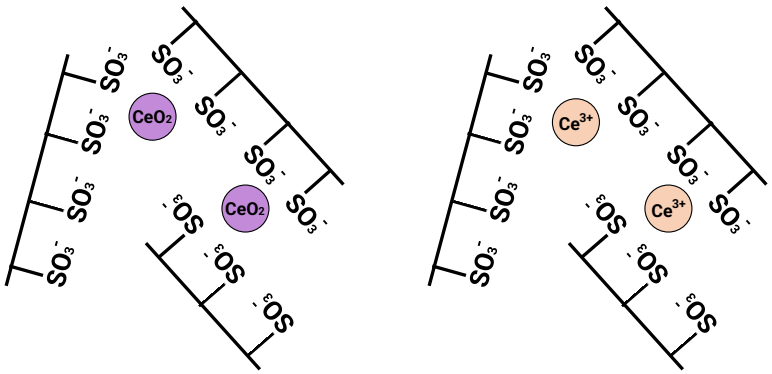

Figure 2.6. The cross-linking effect of incorporating either CeO_2 or Ce^{3+} in sulfonated polymer membranes. The Figure is adapted from Zhao [76].

2.3.5 Prussian Blue

Prussian Blue (PB), or ferric hexacyanoferrate, is a polymeric inorganic semiconductor with electrocatalytic properties [42, 80]. PB is a complex between divalent (Fe^{2+}) and trivalent (Fe^{3+}) iron and cyanide ions (CN^-), produced from iron salts and hexacyanoferrate ($[Fe^{II}(CN)_6]^{4-}$) [34]. The exact stoichiometry and composition of PB are not completely understood, and are dependent the method of deposition and subsequent

conditioning [80]. Both structural complexity, risk of impurity inclusion and tendency to form colloids facilitates several possible stochiometries. From spectroscopic investigations and diffraction measurements, it has been established that PB forms a three-dimensional polymeric network, similar to that of a face-centred cubic lattice cell [81–83]. Divalent and trivalent iron ions are placed alternately on the lattice nodes, with cyanide ligands in between. The Fe^{2+} ions are coordinated by the carbon atom of the cyanide complex and Fe^{3+} by the nitrogen [81, 83, 84]. As seen from the chemical formula $Fe^{III}{}_4[Fe^{II}(CN)_6]_3$, there is an excess of ferric ions compared to hexacyanoferrate complexes. Thus, each unit cell will on average contain a vacant $Fe^{II}(CN)_6{}^-$ lattice site. A schematic of a PB unit cell with a vacant $Fe^{II}(CN)_6{}^-$ lattice site is displayed in Figure 2.7). The vacant site can be occupied by water molecules (insoluble PB) or potassium ions (soluble PB) for necessary charge compensation [83, 84].

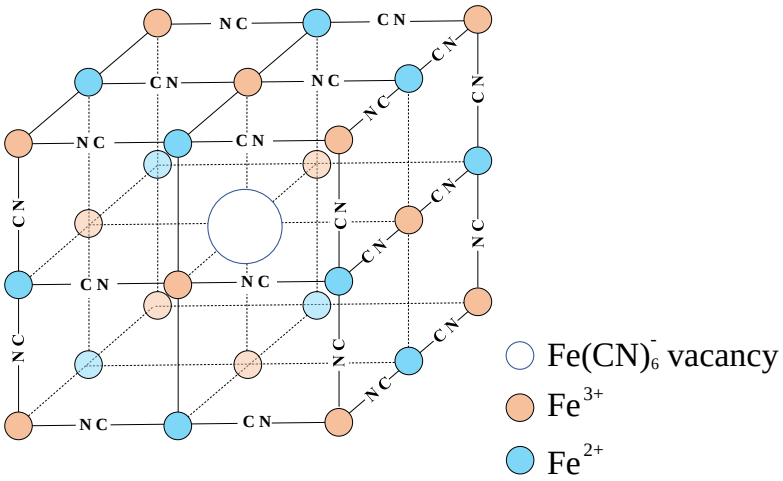

Figure 2.7. Crystal structure of Prussian Blue.

PB can be found in two main stochiometric forms, referred to as either soluble or insoluble PB. The terms do not refer to aqueous solubility, as neither forms are water soluble, but have a historic origin [83, 84]. In soluble PB, the lattice vacancies are occupied by potassium ions, resulting in the chemical formula $KFe^{III}Fe^{II}(CN)_6$. For the insoluble form, water molecules are incorporated to coordinate of excess Fe^{3+}, yielding the chemical formula $Fe^{III}{}_4[Fe^{II}(CN)_6]_3 \cdot nH_2O$. The interstitial water molecules are normally omitted from the insoluble formula, writing only $Fe^{III}{}_4[Fe^{II}(CN)_6]_3$ [84, 85].

Both forms of PB are electrochemically active, and their reduction requires participation from cations in the supporting electrolyte to counterbalance the electron transfer and maintain electroneutrality [42, 83]. The crystal framework of PB has large channels, which allows for efficient insertion and desertion of cations upon reduction and oxidation. Potassium ions are found to be the most efficient cation for charge compensation during electrochemical processes, though electroactivity of PB is stable in solutions of other cations as well [42, 84]. The reduction and oxidation of insoluble and soluble PB in a potassium-rich solution are given by

$$Fe^{III}{}_4[Fe^{II}(CN)_6]_3 + 4\,e^- + 4\,K^+ \rightleftharpoons K_4Fe^{II}{}_4[Fe^{II}(CN)_6]_3 \tag{2.11}$$

for insoluble PB, and

$$KFe^{III}Fe^{II}(CN)_6 + e^- + K^+ \rightleftharpoons K_2Fe^{II}{}_2(CN)_6 \tag{2.12}$$

for soluble PB [34, 86]. Due to the potassium dependency, the redox potential at which the reaction takes place is dependent on the K^+ activity in the electrolyte, according to the Nernst equation (2.2)

$$E = E^0 + \frac{RT}{4F} \ln \frac{a(PB_{Ox})}{a(PB_{Red})} + \frac{RT}{4F} \ln a(K^+) \tag{2.13}$$

with PB_{Ox} and PB_{Red} being the oxidised and reduced form of PB, respectively. The activity of PB_{Ox} and PB_{Red} are 1, as both are solids. Thus, the voltammetric potential is purely a function of potassium activity and temperature [42, 83]. Most electrochemical studies of PB are performed in electrolytes where the ionic strength of potassium is larger than 0.1 M [15, 85–87]. A typical voltammogram obtained for PB in a potassium-rich electrolyte solution is shown in Figure 2.8, including the reduction and oxidation reactions associated with the respective peaks.

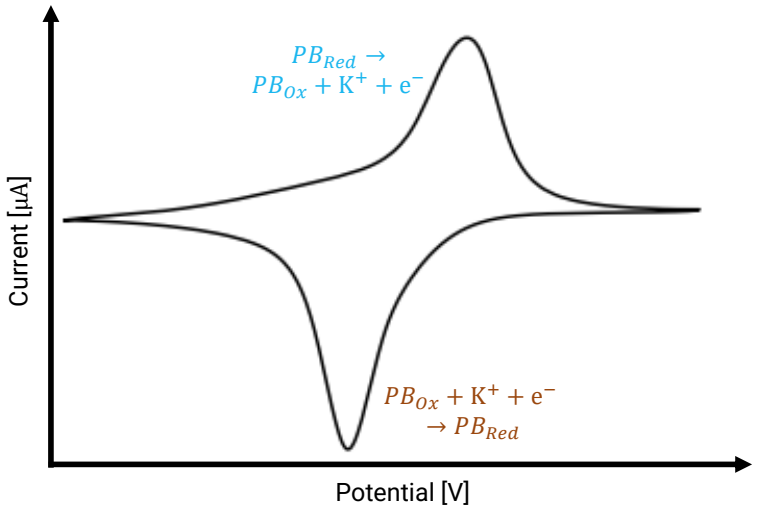

Figure 2.8. Typical voltammetric behaviour of PB in a potassium electrolyte solution, showing both the reduction and oxidation reactions.

PB has a selective catalytic activity towards hydrogen peroxide at low electrode potentials. PB has been attributed as an "artificial peroxidase" due to its excellent catalytic rate of H_2O_2 reduction, which is similar to that for the peroxidase enzyme [34, 42]. Deposition of a PB film on the working electrode is a suitable alternative for selective H_2O_2 detection in the construction of biosensors based on oxidase enzymes. By employing PB, the operating potential of the biosensor can be reduced from 0.6 V, where H_2O_2 is oxidised, to around 0.0 V vs Ag/AgCl. By lowering the operating

potential, interference from other electrochemically active species such as urate and ascorbate, which are present in complex solutions like sweat, is circumvented [34].

The selective catalytic effect of PB towards H_2O_2 is owed to its open lattice structure. The size of the PB channels allows for efficient transport of H_2O_2, which has a low molecular weight, whereas larger molecules are excluded. When inside the lattice structure of PB, the H_2O_2 molecules are surrounded by iron ions enabling reduction of H_2O_2 and subsequent rapid electron transport to the active electrode. The reaction between H_2O_2 and PB can be summarised in the following reaction schemes

$$K_4Fe^{II}{}_4[Fe^{II}(CN)_6]_3 + 2\,H_2O_2 \rightleftharpoons Fe^{III}{}_4[Fe^{II}(CN)_6]_3 + 4\,K^+ + 4\,OH^- \tag{2.14}$$

$$2\,K_2Fe^{II}{}_2(CN)_6 + H_2O_2 \rightleftharpoons 2\,KFe^{III}Fe^{II}(CN)_6 + 2\,K^+ + 2\,OH^- \tag{2.15}$$

for insoluble and soluble PB, respectively. Both reactions take place at approximately 0.0 V vs. Ag/AgCl [34].

A PB electrode can be prepared by electrodeposition from an aqueous HCl solution containing $Fe[CN]_6$, $FeCl_3$ and KCl. By running multiple CV scans within the electrochemically active region of PB, a thin film is deposited on the electrode [88]. Another option for PB deposition is chemical synthesis, where the electrode is simply placed in a ferric ferricyanide solution for several minutes [34, 89]. Post-deposition treatments can contribute to increasing PB film stability, and include electrochemical activation in a 0.1 M KCl/HCl solution using CV to increase the potassium content and/or drying procedures [43, 83, 90, 91]. The hydration state of PB film presumably affects its conductivity and thus stability, with the presence of excess water lowering its electrochemical activity. Both heat treatment 100-120 °C and desiccator drying of PB films are found to have a positive effect on PB performance [34, 83, 85, 91].

A major disadvantage of utilising PB for H_2O_2 detection is poor operational stability in neutral and alkaline solutions. In the presence of hydroxyl ions, $Fe(OH)_3$ complexes will form and dissolve the PB film [34]. The three-dimensional structure of PB dictates the accessibility of iron for the hydroxyl ions. Consequently, the method of deposition and post-deposition treatments affecting the structure of PB will impact the stability in neutral and alkaline solutions [34]. In addition, deposition of PB on carbon substrates has been shown to improve operational stability. It is suggested that the amorphous carbon structure limits the transport of hydroxyl ions into the PB crystal structure, enhancing its stability in neutral and alkaline media [83, 89].

It is known from literature the cycling performance of PB is highly dependent on the alkali ion composition of the electrolyte with respect to voltammetric shape and formal potential, while the mechanism behind this dependency is unknown [55, 80, 85, 92–95]. PB electroactivity requires the entry of counterions to support the charge transfer upon PB reduction, as seen from Equations (2.11) and (2.12), using potassium as an example. The PB crystal framework has an open structure, containing channels with a radius of approximately 0.16 nm, which is highly suitable for insertion and expulsion of appropriately sized cations. Cations of similar size as K^+ have been found to also promote PB activity, such as $NH_4{}^+$, Cs^+ and Rb^+, as they are efficiently inserted and expelled from the PB structure. For cycling in electrolyte solutions dominated

by Na^+, findings are scattered. Some authors report on cycling stability [85], whereas other concludes that sodium disrupts electrochemical activity of PB [43, 83, 86, 94]. It has been suggested that the ease of cation insertion is related to alkali ion hydration energy [92]. K^+ has a large ionic radius and low hydration energy, and can thus be dehydrated upon insertion. Smaller ions such as Na^+ and Li^+ are intensively hydrated, and presumably enters the PB lattice with their hydration shell [84, 91, 92]. These ions have a too large hydrated radius to be efficiently transported through the PB lattice, possibly blocking the electrochemical activity of PB and/or deforming and ultimately delaminating the film [43, 83, 86, 92]. Cycling stability of PB in sodium-rich solutions is presumably dependent on the stochiometry, hydration state and crystallinity of the PB film, giving rise to the scattered findings on stability of PB cycling in sodium solutions in literature [80, 85].

2.4 Lactate and Electrolytes in Sweat

The prospect of assessing biomarker composition in sweat to accurately determine physiological data has been gaining momentum over the last years, as it present a non-invasive alternative to blood sampling [3, 13, 28, 29, 96]. Sweat is rich in metabolites and is a readily available fluid for continuous monitoring, avoiding complications such as risk of infections and human trauma associated with blood level measurements. The contemporary use of sweat analysis is partially limited by the scattered research on correlation between blood and sweat biomarker levels, as well as uncertainty in the correlation between regional and whole-body sweat [15, 23, 25, 97]. There is a gap in literature with respect to biomarker partition to sweat and the physiological significance of sweat content [23, 97, 98]. Moreover, there is a clear dependence on sweat collection and sweat stimulation methodologies [15, 23]. Traditional sweat sampling techniques suffer from uncertainties such as contamination and sweat evaporation, as the sweat needs to be collected from the test objects and subsequently analysed [15, 23, 97]. With modern microfluidic systems, sweat can be immediately transported into the active sensing area, thereby avoiding contamination and evaporation issues. Further research on the topic and smart microfluidic sampling systems is likely to give a better understanding of the correlation between sweat biomarker content and the physiological state of the individual [99].

Sweat is an aqueous mix consisting mainly of water and NaCl, but also contains several other solutes in various concentrations, such as ionic species, lactate, glucose and vitamins, among others [15]. In Table 2.1, the range in sweat biomarker concentrations for Na^+, Cl^-, K^+ and lactate are listed. The reported values have a large range, which is partly a consequence of the dependence on sweat collection and stimulation methodologies. Nevertheless, the table provides an overview of the order of magnitude in which the electrolytes and lactate are present in sweat. The values are adapted from a review by Sonner et al., and correspond well with intervals reported by Baker et al. and median values reported by Harvey et al. [15, 23, 100]. An upper limit of 116 mM sweat lactate concentrations was detected by Mitsubayashi et al. and is included in the Table [30].

Table 2.1. An overview of normal physiological concentration ranges of Na^+, Cl^-, K^+ and lactate in sweat. Values are adapted from [23]. The 116 mM lactate limit was reported by Mitsubayashi et al [30].

Sweat Biomarker	Sweat Concentration Range
Na^+	10 - 100 mM
Cl^-	10 - 100 mM
K^+	4 - 24 mM
Lactate	5 - 60 mM (116 mM)

Finding a correlation between blood and sweat lactate level has proven difficult. Several authors have reported on a non-existing relation between blood and sweat lactate levels [14, 24, 101, 102], while others have found a clear correlation between the lactate concentration variation rates in sweat and blood [25, 27]. However, due to the varying sampling methodologies across literature and issues such as evaporation and contamination from sweat sampling to analysis, previous findings could be limited. Moreover, sweat lactate content is regional, and there is little correlation between whole body and specific body site levels [15, 23, 25, 103]. Thus, a whole-body sweat analysis is not representative of the metabolic state of the body. Karpova et al. reported on the variation in sweat lactate content from working and latent muscles during exercise, proving a positive correlation between lactate concentration variation rates in working muscle and blood [25]. Consequently, a wearable lactate biosensor should be positioned on the skin area above the working muscle to evaluate level of physical exhaustion [25, 27]. In addition, sweat lactate proved to be the faster indicator of muscle metabolism, as sweat lactate level from the working muscle changed more rapidly than blood levels [25]. Another aspect to consider is the variance in sweat rates during exercise, with a possible need to normalise detected lactate concentration values over sweat volumes to obtain a better correlation to blood lactate values [26]. Overall, recent studies have reported a positive correlation between blood and lactate levels by employing wearable sensor systems, providing a proof-of-concept for non-invasive sweat lactate assessment to improve athlete performance [26, 104].

The lactate level is 20-30 times higher in sweat compared to blood, and increases dramatically upon exhaustive exercise [14, 25, 28, 105]. Estimated values for sweat lactate content during exercise is again difficult to establish due to the large variation in sampling protocols between research groups [14, 15]. Reported lactate concentration at high exercise intensity in literature are as low as 25 mM and as high as 116 mM [24, 30]. Other reported values are 80 mM and 102 mM [25, 106]. Thus, a biosensor for real-time sweat monitoring of lactate requires a wide dynamic range, and should ideally be able to sense lactate concentrations well above 80 mM [105].

Applying a Ag/AgCl electrode for sweat sensing purposes requires the presence of a relatively constant amount of Cl^- to provide a stable reference point. The reference potential of such an electrode will be dependent on the concentration of Cl^-, as given by the Nernst equation for the Ag/AgCl electrode shown in Equation (2.3). For a concentration range of Cl^- between 10 and 100 mM, as reported in Table 2.1, a potential shift of approximately 47 mV is expected with maximum $[Cl^-]$ variation.

2.5 Summary of Previous Work

During the fall of 2022, a preliminary project work on amperometric lactate biosensors was performed. All data and conclusions presented below are gathered from this work [31]. The sensor formulation consisted of a screen-printed electrode substrate where the WE was covered with a Prussian Blue mediator film, LOx immobilised in a matrix of Chitosan/SWCNT and an outer Nafion membrane. A total of 7 sensors were tested with chronoamperometric titrations against lactate and H_2O_2. The thickness of the Nafion membrane was varied, having 1 sensor with no membrane (0N), 4 sensors with 3 layers (3N) and 2 sensors with 5 layers of solution-cast Nafion membrane (5N).

Figure 2.9 summarises the chronoamperometric current response of all 7 sensors towards lactate increments of +1 mM. The maximum current response (I_{max}) was achieved by S0, having no Nafion membrane. S0 also had a large initial current (I_{init}), as it had no outer membrane to limit the flux of lactate and O_2 to the enzymatic layer. To achieve a linear-like response and large dynamic range, it was desirable to have a small I_{init} while having a high I_{max}. As can be seen from the figure, the highest dynamic range was obtained with S5, with a maximum detected lactate concentration (c_{max}) of 8 mM. This sensor also exhibited the most linear-like behaviour, as it had a small I_{init} compared to I_{max} signal. Both S5 and S6 had the thickest Nafion membranes (5N) and the most linear-like responses, reflected by the ratio between I_{init} and I_{max}. The I_{init}/I_{max} ratio for each sensor is explicitly given in Table 2.2. It is evident that the 5N sensors had lower I_{init}/I_{max} ratios, while S0 had the lowest, indicating that increasing the Nafion membrane thickness reduced the lactate flux through the membrane at the initial current step and extending the dynamic range.

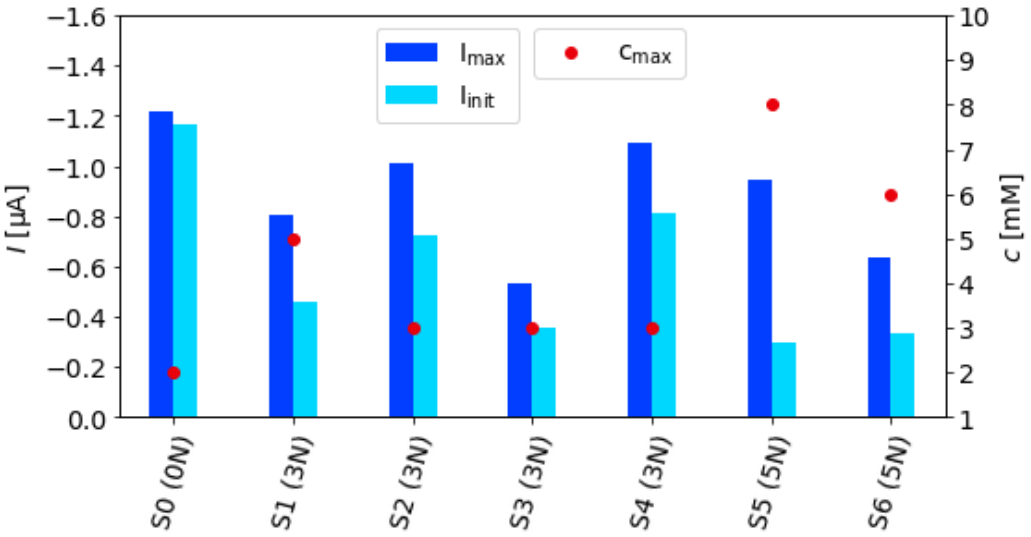

Figure 2.9. Responses of sensors S0-S7 tested in previous work to increasing lactate concentrations, displaying the current signal at the first (I_{init}) and last (I_{max}) lactate increment (left axis). The c_{max} markers denote the maximum detected lactate concentration (right axis). The x-axis specifies the number of Nafion membrane layers (0,3,5) on the sensors.

Table 2.2. Ratio between initial current step (I_{init}) and maximum current signal (I_{max}) and maximum detected lactate concentration (c_{max}) for sensors with 0 (S0), 3 (S1-S4) or 5 (S5-S6) layers of Nafion membrane.

Sensor	$\boldsymbol{I_{init}/I_{max}}$	$\boldsymbol{c_{max}}$ **[mM]**	$\boldsymbol{I_{max}}$ [µA]
S5 (5N)	0.294	8	-0.935
S6 (5N)	0.491	6	-0.633
S1 (3N)	0.557	5	-0.803
S3 (3N)	0.660	3	-0.509
S2 (3N)	0.710	3	-0.996
S4 (3N)	0.743	3	-1.079
S0 (0N)	0.957	2	-1.220

All 7 sensors were subject to both lactate and H_2O_2 chronoamperometric titration measurements. The resulting current responses of sensors with either 0, 3 or 5 layers of Nafion membrane (S0, S1, S5) are shown in Figure 2.10, with 2.10a) lactate and 2.10b) H_2O_2 titrations. Based on the experimental findings and literature reviews, it was suggested that biosensor response was limited by availability of O_2 in the test solution, efflux of enzymatically produced H_2O_2 to the bulk solution, enzyme saturation, enzyme activity fluctuations, low enzyme stability or combinations thereof. The H_2O_2 reduction capacity of the Prussian Blue film was disregarded as the response-limiting factor, as H_2O_2 titration of the S0 sensor generated a 5-fold increase in I_{max}

compared to lactate titration measurements. The lower response of 3N and 5N sensors to lactate titration measurements was mainly attributed to the efflux of H_2O_2 to the bulk solution.

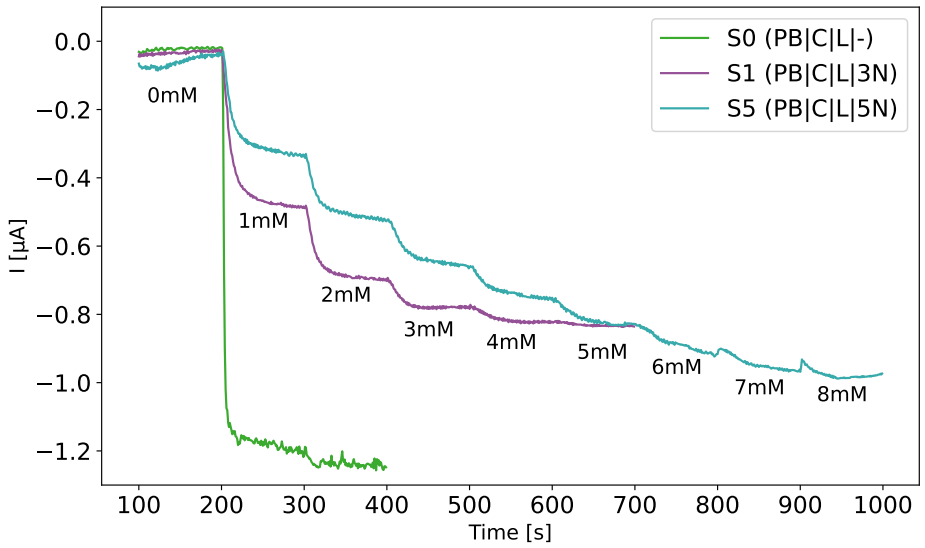

(a)

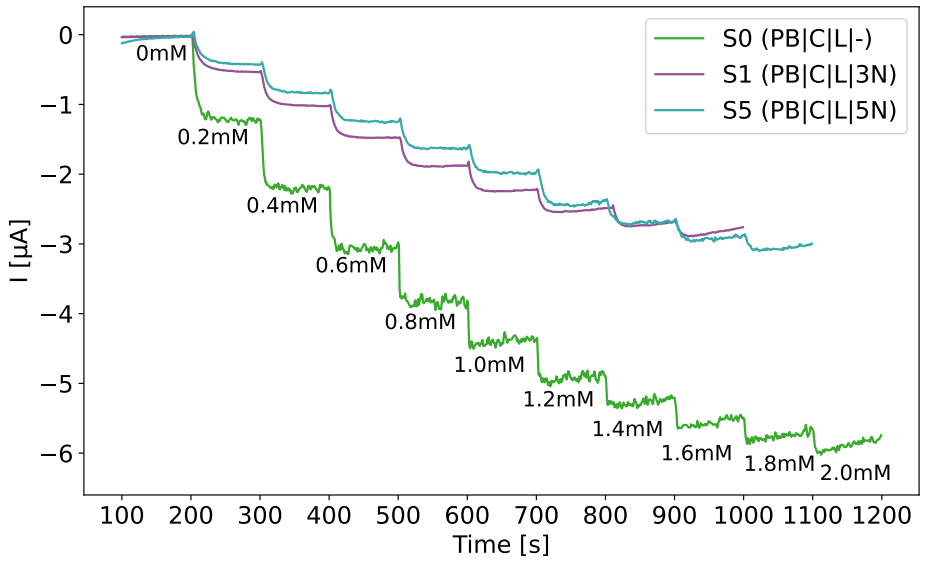

(b)

Figure 2.10. The chronoamperometric responses of lactate biosensors towards increasing a) lactate and b) H_2O_2 concentrations in PBS (pH 7.11). The sensor had either 0, 3 or 5 layers of Nafion membrane (S0, S1, S5, respectively). Operational potential was 0.0 V vs Ag/AgCl.

Both repeatability and reproducibility of the sensors with respect to lactate concentration assessment were low. There were large variations in inter- and intra-sensor responses with respect to dynamic range and maximum generated current signal. Low repeatability was expected from the challenges associated with the manual sensor fab-

rication process, with microliter volumes applied to small sensor area surfaces by hand. The low reproducibility was presumably owed to a change in properties of the Nafion membrane during operational use and from repeated hydration and dehydration over multiple testing rounds. Fluctuations in enzymatic activity were also proposed to contribute to low sensor reproducibility.

Chapter 3

Experimental

3.1 Materials

3.1.1 Reagents

A list of all reagents used is given in Table 3.1.

Table 3.1. List of reagents used. VWR = VWR Chemicals (US), SA = Sigma Aldrich (US) and ZP = Zimmer & Peacock AS (NO)

Reagent	**Distributor**
Disodium phosphate, Na_2HPO_4	SA
Monosodium phosphate, NaH_2PO_4	SA
Dipotassium phosphate, K_2HPO_4	SA
Monopotassium phosphate, KH_2PO_4	SA
Potassium ferricyanide, K_3FeCN_6	SA
Nafion ionomer solution (5 wt% in mixture of aliphatic alcohols and 45% water)	SA
Nafion 117 containing solution (5 wt% in mixture of aliphatic alcohols and water)	SA
Hydrochloric acid (37%), HCl	SA
L-(+)-lactic acid solution (50%), $C_3H_6O_3$	SA
L-(+)-lactic acid (lyophilized powder), $C_3H_6O_3$	SA
Cerium(IV)Oxide, CeO_2 (powder, <5 µm, 99.9% trace metals basis)	SA
Cerium(III) chloride heptahydrate, $CeCl_3{\cdot}7H_2O$	SA
Sodium chloride, NaCl	VWR
Potassium chloride, KCl	VWR
Iron(III) chloride anhydrous, $FeCl_3$	VWR
Ethanol analytical reagent (96%), C_2H_5OH	VWR
Lactate (LOx) Catalyst Solution	ZP
Lactate (LOx) Catalyst Solution w/1 wt% glycerol (gly)	ZP
Lactate Catalyst Solution w/1 wt% glucose (glu)	ZP
Single walled carbon nanotubes (SWCNT) in chitosan solution	ZP

All aqueous solutions were prepared with ultra pure water (18.2 MΩ cm) from Merck Millipore Milli-Q (GE), and will hereby only be referred to as water. Solid sulfophenylated-polyphenylene wih biphenyl linker (SPPB-H^+, hereby only referred to as SPPB) membranes were received as a gift from Professor Steven Holdcroft at Simon Fraser University (CA).

3.1.2 Equipment

A list of all equipment used is given in Table 3.2.

Table 3.2. List of reagents used. ZP = Zimmer & Peacock AS (NO),

Equipment	**Distributor**
Hyper Value Screen Printed Electrodes (SPE)	ZP
Potentiostat (EmStat 3)	ZP
SPE connector	ZP
SPE connector (2 mm banana)	Palm Instruments (NE)
PHM210 Standard pH Meter	Radiometer Analytical (FR)
S-3400N SEM/EDS	Hitachi (J)
Ultrasonic cleaner	VWR (US)
Drying oven (TS8136)	Termaks (NO)
Ar (5.0) gas tank	Aga (NO)
O_2 (5.0) gas tank	Linde Gas (SE)

The PSTrace 5.9 software from PalmSense was used to control and visualise all potentiostat measurements (Palm Instruments, NE).

3.2 Solution Formulations

The following section describes the preparation, conditioning and storage of all solutions used in the sensor formulation or for sensor testing.

3.2.1 Phosphate Buffers

A stock solution of 10x phosphate buffered saline (PBS) was prepared by dissolving 17.8 g Na_2HPO_4, 2.4 g KH_2PO_4, 80.0 g NaCl and 2.0 g KCl in water to a total volume of 500 mL. The solution was vortexed until all the salt had dissolved. 10x PBS stock solution was diluted to 1x PBS by adding water in a 1:10 ratio. The 1x PBS solution (12 mM) was the explicit test solution used in all experiments unless otherwise stated. The molarity of the 1x PBS solution with respect to K^+, Na^+ and Cl^- can be found in Table 3.3.

A base phosphate buffer solution of pH 7 was prepared by dissolving 1.87 g K_2HPO_4 and 1.26 g KH_2PO_4 in water to a total volume of 200 mL. The solution was vortexed until all the salt had dissolved. From the base phosphate buffer, potassium and sodium-potassium phosphate buffers were prepared. To make a potassium phosphate buffer (PPB), 1.118 g KCl was added to 100 mL phosphate buffer base to obtain a final $[Cl^-]$ of 0.15 M. To make a potassium-sodium phosphate buffer (PPB+NaCl), 0.878 g NaCl was added to 100 mL phosphate buffer base to obtain a final $[Cl^-]$ of 0.15 M. Table 3.3 gives an overview of the ionic strength and measured pH of all buffer solutions used.

Table 3.3. Calculated ionic strength and measured pH of all employed buffer solutions.

Buffer	**[K^+]**	**[Na^+]**	**[Cl^-]**	**pH**[1]
PBS	0.02	0.16	0.14	7.48
PPB	0.304	0	0.15	6.83
PPB+NaCl	0.15	0.15	0.15	6.78

[1]pH was measured using a pH meter after solution preparation.

3.2.2 Prussian Blue Solution

A 50 mL centrifuge tube was filled with 40 mL of HCl [0.1 M]. 0.3725 g KCl was weighed out and added to the tube, and the solution was vortexed for a few seconds until the salt was completely dissolved. This procedure was repeated for 0.0411 g $K_3Fe(CN)_6$ and 0.0203 g $FeCl_3$, respectively. Lastly, HCl [0.1 M] was added until a total volume of 50 mL was reached. The centrifuge tube was covered with aluminium foil to avoid light exposure. The PB solution was stored in the fridge at 4°C if not immediately employed. Unused solution was stored for a maximum of 2 days before being discarded due to precipitation of PB.

3.2.3 Lactate Catalyst Solutions [2000 U/mL]

Lactate catalyst solutions with lactate oxidase (LOx) enzymes were prepared by ZP and used as-received. The enzyme solutions were stored in the freezer at -20°C. Upon application, the lactate catalyst solution was thawed for 30 minutes at room temperature by placing the tube on an icing element. Thawing was performed slowly to avoid enzyme denaturation.

3.2.4 Chitosan-SWCNT Mixture

Chitosan-single walled carbon nanotubes (SWCNT) mixture was prepared by ZP and used as-received. Upon application, the chitosan-SWCNT solution was placed in an ultrasonic bath for 20 minutes and thereafter vortexed for a few seconds to ensure a homogeneous SWCNT dispersion.

3.2.5 SPPB Membrane Solutions

The solid, as-received sulfophenylated-polyphenylene wih biphenyl linker (SPPB) membranes were dissolved to enable membrane casting onto the sensors. A total of three different SPPB membrane solutions were made, with varying weight percentages and solvent compositions. The following solutions were prepared:

- 7.5 wt% SPPB in Ethanol
  0.100 g solid SPPB membrane was dissolved in 1.563 mL ethanol. The solution was stirred using a magnetic stirrer until completely dissolved.

- 2.5 wt% SPPB in Ethanol
  A 2.5 wt% SPPB solution was made by diluting 0.317 mL of the 7.5 wt% SPPB solution with 0.636 mL ethanol.

- 2.5 wt% SPPB in Ethanol and water
  0.0890 g solid SPPB membrane was dissolved in 2.482 mL ethanol and 1.513 mL H_2O. The solution was stirred using a magnetic stirrer until completely dissolved.

3.2.6 Cerium-Nafion Membrane Solutions

Two different cerium salts were employed to directly mix cerium into the Nafion membrane solutions, namely CeO_2 and $CeCl_3{\cdot}7H_2O$. The weight percentage of cerium is given relative to the pristine Nafion content. The following cerium-containing Nafion solutions were prepared:

- 24.8 wt% CeO_2 in Nafion 117 containing solution
  A stock solution of 650 wt% CeO_2 was made by dissolving 0.0615 g CeO_2 in 0.205 mL Nafion 117 containing solution. The solution was vortexed for a few hours to disperse the CeO_2. To make a 24.8 wt% CeO_2 solution, 6.1 µL stock solution was diluted with 0.308 mL Nafion 117 containing solution.

- N/Awt% CeO_2 in Nafion ionomer solution
  A solution with an unknown content of CeO_2 was made by mixing 0.216 mL Nafion solution with CeO_2. The CeO_2 content was unknown due to difficulties in obtaining an accurate weight for low CeO_2 amounts.

- 3.1 wt% Ce^{3+} in Nafion ionomer solution
  A stock solution of 66.2 wt% $CeCl_3$ was made by dissolving 0.0176 g $CeCl_3$ in 0.216 mL Nafion ionomer solution. To make a 3.1 wt% $CeCl_3$ solution, 0.005 g stock solution was diluted with 0.103 mL Nafion ionomer solution. The cross-linking effect of Ce^{3+} on Nafion was immediate. Consequently, the solution was not suited for storage and had to be employed instantly.

3.2.7 Aqueous $CeCl_3$ Solutions

$CeCl_3$ was dissolved in water at various concentrations, namely: 1 M $CeCl_3$ (aq), 0.413 M $CeCl_3$(aq), 0.076 M $CeCl_3$, 0.038 M $CeCl_3$(aq). 0.01 M and 0.016 mM $CeCl_3$(aq).

3.2.8 Lactic Acid Test Solution

Solutions of 0.5 M lactic acid was prepared both from stock solution and from powder. Using a 50 wt% lactic acid stock solution, 0.901 g of stock solution was diluted with water to a final volume of 10 mL. To prepare 5 mL lactic acid solution [0.5 M] from powder, 0.230 g was added to a glass vial and water was added to the 5 mL mark. The solution was vortexed until all salt had been dissolved.

3.3 Experimental Setup

Similar experimental setups were used for electrochemical sensor characterisation and PB electrodeposition. The sensors were coupled to the potentiostat via a connector and positioned in a sample holder to keep the sensor in place. The sensor was immersed in a beaker containing the test solution. 10 mL beakers with PBS were used for sensor testing, whereas 5 mL beakers were used for PB electrodeposition and post-treatment. All three electrodes were submerged, whereas the connector was kept dry and above the solution interface. The setup was arranged with a magnetic stirrer for mechanical mixing for lactate sensors, while no stirrer was applied for PB electrodeposition, post-treatment and testing. For electrodeposition of PB, two sensors were immersed in the same solution, using two separate connectors. One sensor functioned as the deposition substrate, whereas the second sensor provided a sacrificial counter and reference electrode. The sensors were placed facing each other in the solution to ensure an even deposition. A schematic view of the experimental setups can be found in Figure 3.1, with 3.1a) showing the setup for sensor performance testing and 3.1b) for PB deposition.

For testing at 37°C, the hot plate was turned on, and a thermometer was used to monitor the temperature in the test solution every 100 s.

When Ar or O_2 gas was purged into the test solutions, a glass pipette was inserted in the outlet of the gas supply tube and placed in the test solution. A flow rate of 1-3 gas bubbles per second was employed.

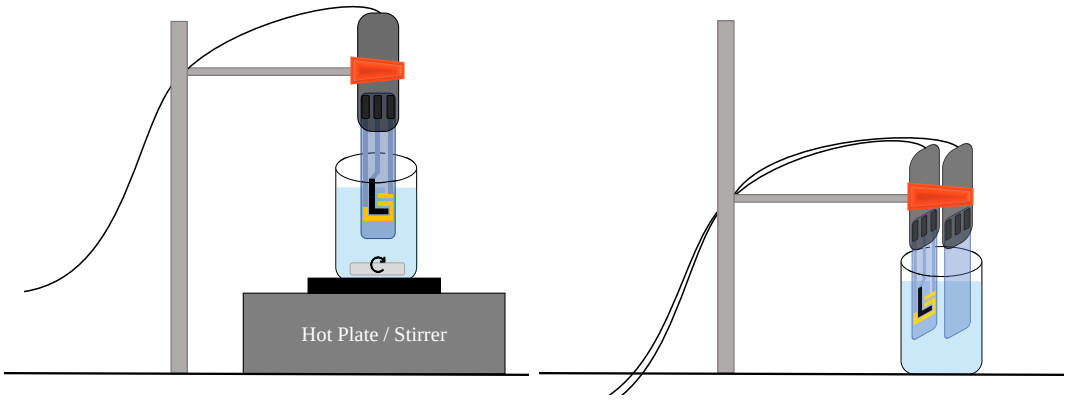

Figure 3.1. Schematic view of the general experimental setups for a) sensor testing and characterisation and b) PB deposition.

3.4 Biosensor Assembly

A general schematic of a fully assembled lactate biosensor is found in Figure 3.2, showing the screen-printed electrode substrate and an enlargement of the modified carbon working electrode. The WE was coated with 3 consecutive layers, namely a thin film of Prussian Blue, Lactate Oxidase enzymes and single-walled carbon nanotubes entrapped in a chitosan-matrix and an outer polymer membrane, being either Nafion or SPPB. Biosensor were prepared with different formulation variations, with modifications including post-treatment procedures for the PB film, increasing the enzyme loading volume, incorporating additives in the enzyme or membrane layer, and changing the membrane material. An overview of all biosensor compositions that were fabricated is found in Table 3.4. The table additionally includes the notation that will be used to refer to the distinct sensor compositions throughout the paper.

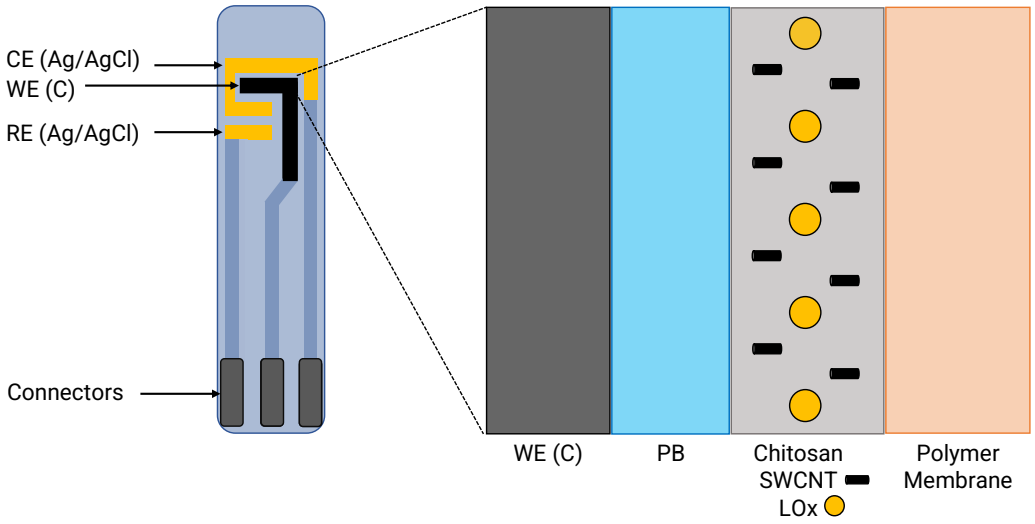

Figure 3.2. The general composition of a fully assembled lactate biosensor. The SPE substrate is shown to the left, with an enlarged view of the successive layers applied to the WE to the right.

Table 3.4. Overview of biosensor formulation variations. The presence of a layer is marked with ("x"). Layer-specific modifications are given in the footnotes.

PB	LOx	Nafion	SPPB	Notation
x	-	-	-	PB|-
x	-	x	-	PB|N
x	x	x	-	PB|L|N
x	1.5x[1]	x	-	PB|1.5L|N
x	2x[1]	x	-	PB|2L|N
x	x (Glu)[2]	x	-	PB|L^{Glu}|N
x	x (Gly)[2]	x	-	PB|L^{Gly}|N
x	x	x (Ce^{3+})[3]	-	PB|L|N*
x	x	x (CeO_2)[4]	-	PB|L|N**
x	x	-	x	PB|L|S
x	x	-	x (Ce^{3+})[3]	PB|L|S*

[1] LOx loading was increased by a factor 1.5 or 2. This is represented by 1.5L or 2L.
[2] Glycerol or Glucose was incorporated in the LOx catalyst solution. This is represented by L^{Glu} or L^{Gly}.
[3] Ce^{3+} was incorporated in the polymer membrane. This is represented by N* or S*.
[4] CeO_2 was incorporated in the Nafio membrane. This is represented N**.

3.4.1 Prussian Blue Film Deposition

Cyclic voltammetry (CV) was used to deposit a PB film onto the WE of the sensor substrates. The scan interval was set to [-0.2, 0.5] V, with step size 1 mV and scan rate 50 mV s^{-1} for a total of 10 cycles. The sensors were submerged in a 5 mL beaker filled with fresh PB solution. The beaker was carefully shaken by hand at each cycle to prevent depletion of analyte at the electrode surface. The shaking was performed in the potential interval [0.40, 0.50] V to not perturb the oxidation and reduction processes.

When the deposition was completed, the sensor was transferred to a 0.1 M KCl in 0.1 M HCl solution and cycled for a total of 10 cycles. The scan interval was set to [-0.05, 0.35] V, with step size 1 mV and scan rate 50 mV s^{-1}. The newly deposited sensor was shaken dry and kept in a petri dish covered with aluminium foil to prevent light exposure, as light can induce photochemical reactions and result in a structural change. PB-deposited sensors were stored in a desiccator until further use, and for at least 5 days. When necessary to accelerate the drying process, the PB sensors were annealed at 100°C for 1 hour. The process of cycling the PB sensors in KCl and annealing are hereby referred to as post-treatment of PB sensors.

3.4.2 Enzyme Layer

LOx was immobilised in a matrix of SWCNT-chitosan by drop casting solutions onto the WE of the sensor and letting the droplets dry at room temperature. First, 2 x 0.5 µL CNT-Chitosan solution was cast on the PB-WE using a pipette, and allowed to dry for 10-15 minutes. Next, a layer of lactate catalyst solution was added on top. The amounts were either 0.5 µL, 0.75 µL or 1.0 µL. If not otherwise specified, 0.5 µL enzyme catalyst solution was the explicit volume used. The layer was allowed to dry for 10-15 minutes. Lastly, a second layer of 2 x 0.5 µL CNT-Chitosan solution was applied. The sensors were kept in a petri dish covered in aluminium foil and left to dry at 4°C for 12-16 hours.

3.4.3 Polymer Membrane

For Nafion-coated sensors, 5 consecutive layers of 2 x 0.5 µL Nafion solution were cast on top of the enzymatic layer. For SPPB-coated sensors, 5 consecutive layers of 2 x 0.5 µL SPPB solution were cast on top of the enzymatic layer. The drying period of each layer was 20-30 minutes to allow for the solvent to evaporate. After applying all 5 layers, the sensors were stored at 4°C for minimum 48 hours to allow for the membranes to cure. Sensors with membranes containing cerium were stored at room temperature in the fume hood. Only one type of membrane solution was employed per individual sensor.

Polymer membranes with incorporated cerium ions were prepared by employing one of the three following approaches:

1. Direct addition of cerium to the Nafion membrane solution. The Ce-polymer membrane solution was cast onto the sensor using the approach described above. Both 24.8 wt% CeO_2, N/A wt% CeO_2 and 3.1 wt% Ce^{3+} Nafion solutions were used for this purpose.

2. $CeCl_3$ (aq) immersion. A Nafion membrane was applied as described above. After membrane curing (48 hours), the sensor was immersed in a 0.016 mM $CeCl_3$(aq) solution for 24 hours.

3. Co-casting of polymer solution and $CeCl_3$ (aq). The polymer membrane was applied as described above. In between one of the membrane layers, 2x or 4x 0.5 µL of 1 M, 0.42 M, 0.076 M or 0.076 M $CeCl_3$(aq) was drop cast onto the sensor and left to dry for 30 minutes before a new membrane layer was applied.

Due to the multiple methods and loading amounts employed to incorporate cerium ions into the polymer membranes, it is convenient to introduce a notation to distinguish between variations of PB|L|N*, PB|L|S* and PB|L|N** sensors with respect to the cerium incorporation method and contebt. The cerium content was calculated in percent with respect to the mass of pristine Nafion or SPPB in the membrane, assuming that all added cerium was incorporated. The notation that will be used for this purpose is given in Table 3.5.

Table 3.5. Notation for sensors with cerium (%) incorporated in the membranes. 1,2,3 refers to the incorporation method. * = Ce^{3+} and ** = CeO_2.

Method of Cerium Incorporation	**Notation**
Direct mixing of CeO_2(s) and Nafion solution	PB|L|N$^{**}_{24.8\%}$
Direct mixing of CeO_2(s) and Nafion solution	PB|L|N$^{**}_{N/A\%}$
Direct mixing of $CeCl_3$(s) and Nafion solution	PB|L|N$^{*1}_{3.1\%}$
Immersing PB|L|N in 0.0016 mM $CeCl_3$ (aq)	PB|L|N$^{*2}_{50\%}$
Co-casting of Nafion and 1 M $CeCl_3$ (aq)	PB|L|N$^{*3}_{60.7\%}$
Co-casting of Nafion and 2 x 0.413 M $CeCl_3$ (aq)	PB|L|N$^{*3}_{50\%}$
Co-casting of Nafion and 0.413 M $CeCl_3$ (aq)	PB|L|N$^{*3}_{25\%}$
Co-casting of Nafion and 2 x 0.076 M $CeCl_3$ (aq)	PB|L|N$^{*3}_{9.3\%}$
Co-casting of Nafion and 0.076 M $CeCl_3$ (aq)	PB|L|N$^{*3}_{4.6\%}$
Co-casting of Nafion and 0.038 M $CeCl_3$ (aq)	PB|L|N$^{*3}_{2.3\%}$
Co-casting of SPPB and 0.076 M $CeCl_3$ (aq)	PB|L|S$^{*3}_{9.3\%}$

Figure 3.3 gives a brief schematic summary of the entire biosensor assembly process.

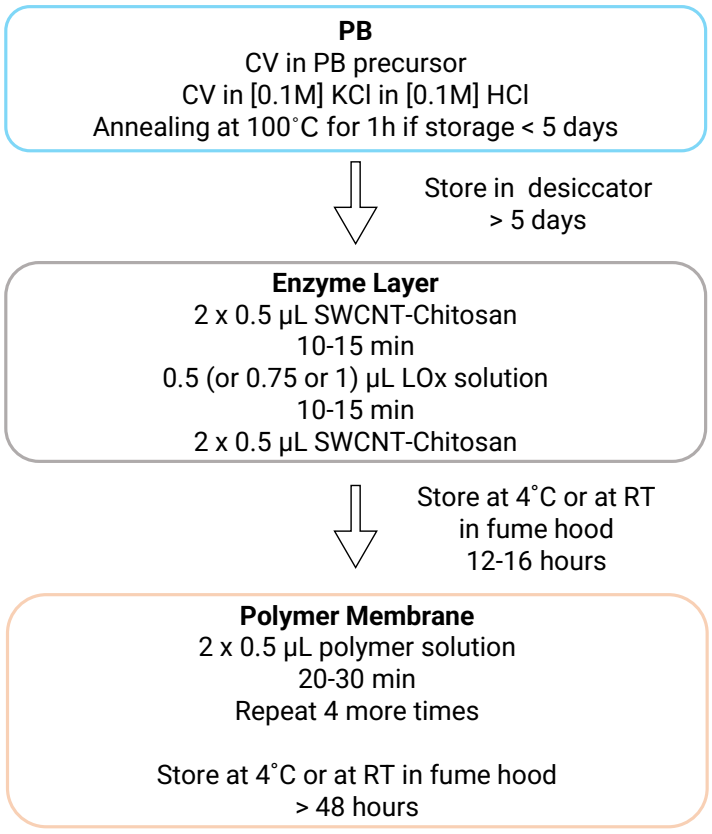

Figure 3.3. Flow chart summarising the general sensor assembly procedure. The polymer solution was either Nafion or cerium-Nafion solution, SPPB or cerium-SPPB. Only one type of polymer solution was employed per sensor.

3.5 Characterisation and Testing

3.5.1 Prussian Blue Characterisation

CV studies of PB-deposited sensors (PB|- and PB|N) were carried out using the experimental setup described in Experimental Setup (3.3). Voltammograms were recorded using a potential interval of [-0.3, 0.5] V and scan rate $50\,\mathrm{mV\,s^{-1}}$. The following test solutions were used: PBS, PPB and PPB+NaCl. A total of 30 cycles were performed per CV measurement.

EDS analysis of two PB|- sensors subject to different conditioning was performed in a Hitachi S-3400N SEM. One sensor had only been subject to post-deposition treatment (KCl-cycling and annealing), whereas the second sensor had been post-treated, tested in PBS solution for a total of 30 cycles and thereafter dried at 100°C for 1 hour. The images were captured using a 15 kV acceleration voltage and a magnification of x500.

3.5.2 Lactate Sensor Testing

Lactate responses were evaluated by chronoamperometric measurements, using the experimental setup described in Experimental Setup (3.3). A potential of 0.0 V vs Ag/AgCl was found to be optimal for PB activity in previous work, and was the explicit WE potential applied in all experiments [31]. After the formation of a stable baseline, approximately 500 s, lactate concentration was incremented stepwise every 100-300 s, after the signal had properly stabilised (when the gradient was less than approximately $-0.02\,\mu\mathrm{A}$ per 50 seconds). Standard lactate increments were +1 mM and used throughout unless otherwise specified, while +0.1 mM increments were used for step size testing.

Lactate sensor response was additionally evaluated by adjusting ambient conditions such as solution temperature or dissolved oxygen content, with the setup described in Experimental Setup (3.3). Standard testing conditions refer to testing at ambient temperature without gas purging, using lactate addition increments of +1 mM. An overview of all sensor formulation variations and testing conditions are summarised in Figure 3.4.

All sensors were chronoamperometrically tested 2-3 times. In between testing rounds, the sensor was rinsed carefully with DI water to remove remnant test solution from the sensor surface. The sensors were allowed to dry for at least 1 hour before initiating the next testing round. Drying of the sensors ruptured the outer membranes, altering the sensor architecture between testing rounds. Thus, reproducibility could not be evaluated. Repeated rounds of sensor testing should be performed immediately after one another, only rinsing the sensor with DI water in between subsequent testing rounds and changing the test solution. Mainly chronoamperometric data from the first testing rounds will thus be presented in this work, while chronoamperometric data from all 3 testing rounds can be found in Appendix B.

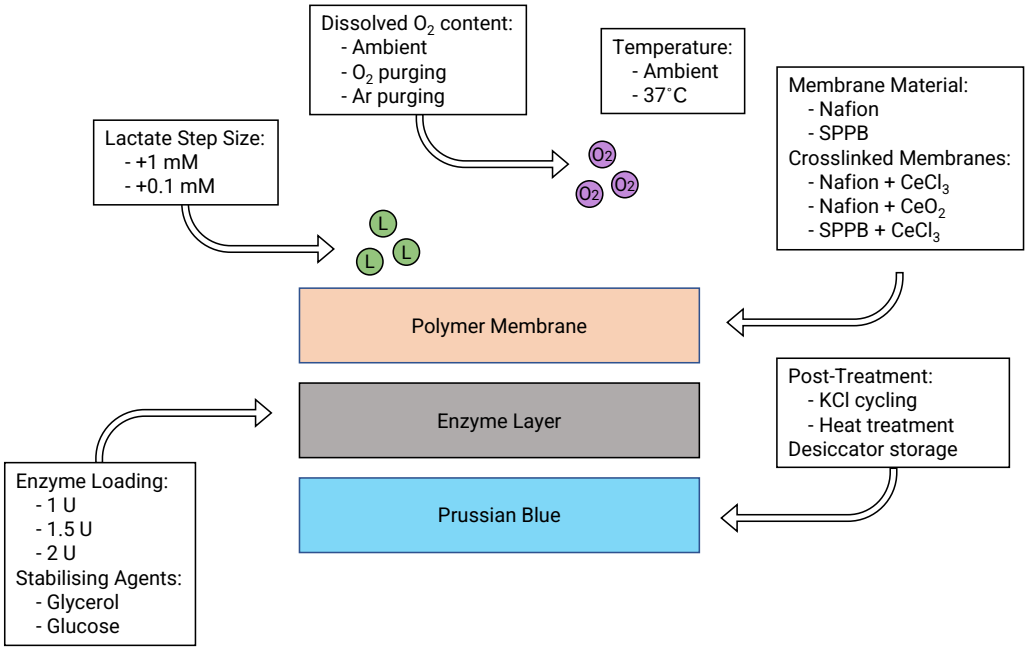

Figure 3.4. Overview of all sensor formulation adjustments and testing conditions employed, achieved by tuning properties of either the distinct biosensor layers or the test solution. L (green) is lactate and O_2 (purple) is dissolved oxygen.

3.6 Data Analysis and Visualisation

Experimental data was recorded using PSTrace 5.9 and exported to Python Spyder (Anaconda 3) for visualisation and analysis. Before export, all chronoamperometric curves were post-processed in the PSTrace software using the "low" smoothing filter to minimise interference effects from the magnetic stirrer and/or electrical noise. PSTrace uses the Savitzky–Golay method for smoothing, which is similar to a low-pass filter. 5 points were used for the smoothing (corresponding to the "low" filter).

The average value and standard deviation (std dev) were calculated at each amperometric concentration step, using the last 55 seconds of the measurement at each step. The current values for the first seconds at each step were not included in the average to allow for signal stabilisation. The last 5 seconds at each step were additionally omitted to avoid interference from the subsequent lactate addition. The average current at each concentration step was plotted against concentration for all tested sensors. All measurements were baselined to 0.0 V at 0 mM lactate concentration. An amperometric current step was accepted if the average current signal of the subsequent step was larger than three times the std dev of the previous step, by biosensor signal resolution definition [1]. The upper concentration cut-off for the chronoamperometry plots was when an addition gave a current step smaller than 3 x std dev. All standard deviations were calculated using the following formula,

$$stddev = \sqrt{\frac{\sum(x - \overline{x})^2}{N}} \tag{3.1}$$

with x the individual values, $\overline{x}$ the average over all the measured values and N the total number of measurement values.

For voltammetry measurements, the second and the last cycle was extracted from the measurement and plotted. The first cycle was not included, since the signal had to stabilise. The cathodic and anodic current values were extracted at 0.0 V.

Chapter 4

Results

In the following section, the results from sensor testing and characterisation are presented. The first section shows the results from chronoamperometric measurements of fully assembled lactate sensors in PBS solutions with a stepwise increase in bulk lactate concentration. In the last section, the results from the Prussian Blue characterisation are shown. All presented potential values are measured against a Ag/AgCl reference electrode in phosphate buffer solutions. An overview of the sensor notations used can be found in Tables 3.4 and 3.5.

4.1 Lactate Sensor Testing

A total of 36 lactate biosensors of various sensor formulations were chronoamperometrically tested. The primary chronoamperometric measurements for all tested sensors can be found in Appendix B. To investigate the sensing range limitations of sensors made with the standard PB|L|N formulation, PB|L|N sensors were tested with various lactate concentration increment sizes and in solutions where the content of dissolved oxygen was increased or decreased. Thereafter, various sensor formulation adjustments were introduced to increase the maximum current signal (I_{max}) and upper limit of the dynamic range (c_{max}) of the sensors. The following section will present the results from initial PB|L|N sensor testing and efforts to improve the sensor response by introducing adjustments in the enzyme or outer membrane sensor layers.

4.1.1 Lactate Increment Size

The chronoamperometric response of a PB|L|N sensor towards lactate increments of either +0.1 mM or +1 mM are compared in Figure 4.1, displaying the average current signal at each lactate concentration step. The sensor was subject to a total of 3 testing rounds, with two rounds of +0.1 mM increments and a round in between using the standard +1 mM increments. The +0.1 mM increment testing is shown in the figure as the average over the two testing rounds, with standard deviation included. The two testing rounds reached signal saturation at different currents, giving rise to the gradually increasing error bars.

It can be seen that lowering the lactate increment size to +0.1 mM reduced the upper limit of the dynamic range from 4 mM to 2 mM, but also increased the total number of distinct current steps before signal saturation was reached. In the +0.1 mM testing rounds, the sensor was sensitive to minimum 20 lactate additions. A linear relationship between the current signal and lactate concentration was observed up to approximately 1 mM lactate concentrations when the increment size was reduced.

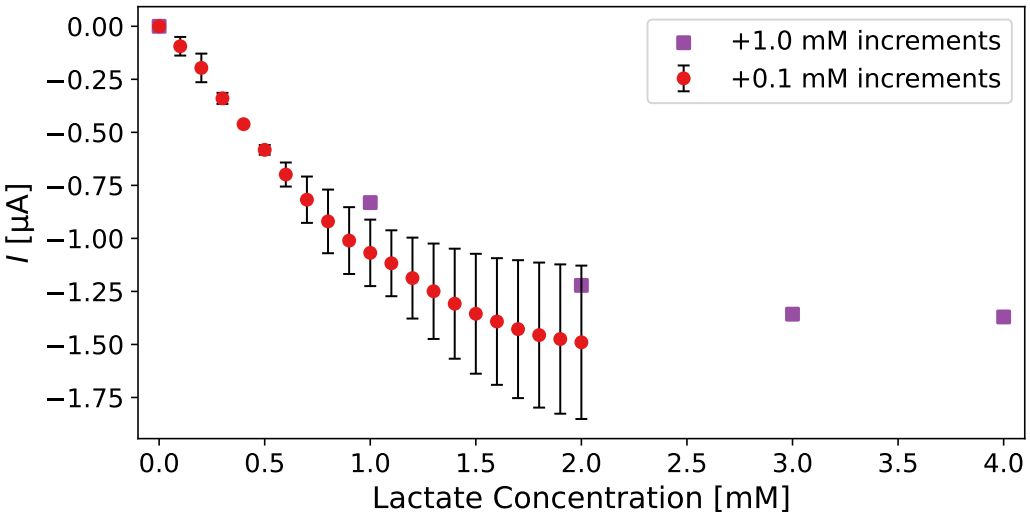

Figure 4.1. Responses of 1 PB|L|N sensor to +0.1 mM or +1 mM lactate increments (number of measurements $n_{0.1\,mM} = 2$ and $n_{1\,mM} = 1$). Error bars correspond to ±1 std dev. The average current signal at each lactate concentration is displayed, with ±1 std dev for a single measurement in the nA-range (not visible in fig.).

4.1.2 Dissolved Oxygen Availability

To assess the dependence of I_{max}, c_{max} and signal linearity on the availability of dissolved oxygen in the test solution, PB|L|N sensors were tested in O_2-enriched and -deprived solutions. O_2 purging was used to increase the availability of O_2, whereas Ar purging was used to deprive the solution of oxygen.

The chronoamperometric response of a PB|L|N sensor under standard testing conditions and under O_2 purging conditions are compared in Figure 4.2a), displaying the average current signal at each lactate concentration step. The sensor was tested twice under standard conditions, with one round in between using O_2 purging. The standard conditions testing is shown in the figure as the average over the two testing rounds, with standard deviation included. Similarly, Figure 4.2b) shows the response of a PB|L|N with the average of two testing rounds with Ar purging and one round with standard condition testing.

For both sensors, there was a significant difference between the current signal at standard conditions testing and gas purging testing at all lactate concentration steps. O_2 purging increased the relative current signal, whereas Ar purging reduced the relative current signal. It can also be observed that testing with O_2 purging generated

a quite linear response over the entire responsive range of the sensor. Upon increasing the lactate concentration from 11 mM to 12 mM during testing, the signal started to drift, resulting in a gradually increasing current despite continued lactate additions (Appendix B Fig. B.2). In contrast, standard and Ar purging testing conditions showed a hyperbolic saturation behaviour with increasing bulk lactate concentrations.

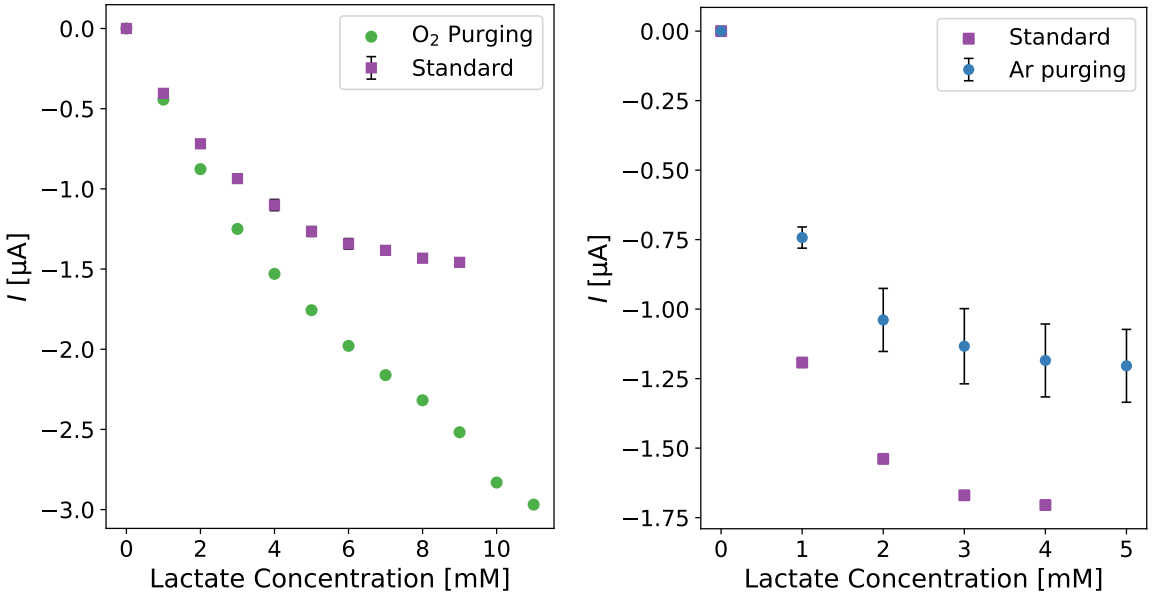

(a) O2 Purging **(b)** Ar Purging

Figure 4.2. Responses of 2 PB|L|N sensor subject to (a) oxygen purging compared to at standard conditions (number of measurements $n_{std} = 2$ and $n_{O_2} = 1$). (b) shows a similar test, but with a reduced oxygen content due to argon purging (number of measurements $n_{std} = 1$ and $n_{Ar} = 2$). Error bars correspond to ±1 std dev. The average current signal at each lactate concentration is displayed, with ±1 std dev for a single measurement in the nA-range (not visible in fig.).

The maximum detected lactate concentrations (c_{max}) and the associated current signal (I_{max}) for both the O_2 and Ar purging tests are given in Table 4.1. Compared to the standard testing rounds, purging O_2 into the solution resulted in a 104% increase in I_{max} and extended the upper limit of the dynamic range. Testing in an O_2-enriched solution resulted in the highest I_{max} and c_{max} obtained for all sensors tested in this and previous work. Conversely, purging Ar gas into the solution during testing generated a relatively lower I_{max} value compared to the standard conditions testing round.

Table 4.1. Maximum generate current signal (I_{max}) and detected lactate concentration (c_{max}) for sensors subject to oxygen or argon purging compared to standard conditions. Averages and ±1 std dev are over n=2 testing rounds. c_{max} are given for all n=3 test rounds.

Sensor	**Testing Conditions**	$\boldsymbol{I_{max}}$ **[μA]**	$\boldsymbol{c_{max}}$ **[mM]**
PB|L|N	Standard	-1.458 ± 0.002	9, 9
	O_2 Purging	-2.97	11
PB|L|N	Standard	-1.705	4
	Ar Purging	-1.204 ± 0.131	5, 5

4.1.3 Adjusting Enzyme Activity

To increase the maximum current response of the sensors, properties of the enzymatic layer were adjusted to increase enzyme stability and catalytic activity. This included testing in 37°C solutions, increasing the enzyme loading or adding enzyme stabilising agents, either glucose or glycerol, to the enzyme catalyst solution. Table 4.2 summarises the I_{max} and c_{max} obtained from the chronoamperometric testing towards increasing lactate concentrations for a total of 10 enzyme layer-modified sensors. The sensors are listed from the highest to the lowest I_{max}. Sensors made with an identical formulation are listed after one another, with the sensor having the highest I_{max} dictating the listing position.

Table 4.2. Maximum generated current signal (I_{max}) and detected lactate concentration (c_{max}) for sensors with enzyme layer modifications. 37°C refers to testing in solutions of T = 37°C. 1.5L and 2L indicate increased enzyme loadings. Gly and Glu denote incorporation of glycerol or glucose.

Sensor	$\boldsymbol{I_{max}}$ **[μA]**	$\boldsymbol{c_{max}}$ **[mM]**
PB|L^{Glu}|N	-1.199	4
PB|L^{Glu}|N	-0.155	4
PB|L|N (37°C)	-0.953	6
PB|L|N (37°C)	-0.713	2
PB|L|N (37°C)	-0.691	5
PB|1.5L|N	-0.943	8
PB|1.5L|N	-0.552	6
PB|L^{Gly}|N	-0.809	3
PB|L^{Gly}|N	-0.545	7
PB|2L|N	-0.762	7

None of the enzyme-modified sensors achieved a maximum current response larger than $-1.199\,\mu A$. The maximum obtained current response for all enzyme-modified sensors was obtained with a sensor where glucose had been added to the enzyme catalyst solution. Contrastingly, the lowest current response was obtained by the second PB|L^{Glu}|N sensor. Despite the large spread in I_{max} values, the two sensors had an identical c_{max}. With the exception of the PB|L^{Glu}|N sensors, there was no repeatability in c_{max} and I_{max} for sensors with identical formulations.

The highest detected lactate concentration was 8 mM, obtained with a sensor where the enzyme loading had been increased to 1.5 U. Further increasing the enzyme loading to 2 U did not result in a further increase in c_{max}.

4.1.4 Adjusting Membrane Permeability

Properties of the sensor polymer membrane were adjusted to reduce the lactate diffusion into the enzyme layer. 23 sensors were tested in total, employing various methods to reduce the permeability of lactate across the outer polymer membrane. Membrane modifications included either replacing the Nafion membrane with a SBBP membrane or incorporating cerium into the Nafion membrane to induce polymer cross-linking.

To enable comparison and evaluation of the performance of the membrane-modified sensors, the chronoamperometric response of each sensor will be represented by 3 characteristics: c_{max}, I_{max} and I_{init}. c_{max} is the highest bulk lactate concentration that was significantly detected, thus being the upper limit in the dynamic range of the sensor. I_{max} is the current signal at c_{max}, thus being the maximum current generated at sensor signal saturation. The I_{init} is the detected current signal after the first lactate addition, when the bulk lactate concentration is changed from 0 mM to 1 mM. To achieve a large c_{max} as well as a linear-like response, I_{max} should be large, while I_{init} should be low. To compare the sensor responses, the ratio between I_{init} and I_{max} and the c_{max} values will be used.

SBBP Membranes

Solid SBBP membranes were dissolved to allow for solution casting onto the sensors, employing a total of 3 distinct solvent conditions and/or SBBP concentrations: 7.5 wt% SPPB in ethanol, 2.5 wt% SPPB in ethanol and 2.5 wt% SPPB in ethanol/water. All solvent compositions proved suitable for the dissolution of solid SPPB membranes. The resulting c_{max}, I_{init} and I_{max} from chronoamperometric lactate titration testing of 4 PB|L|S sensors are shown graphically in Figure 4.3, with the x-axis specifying the composition of the SBBP casting solution for the membrane of each sensor.

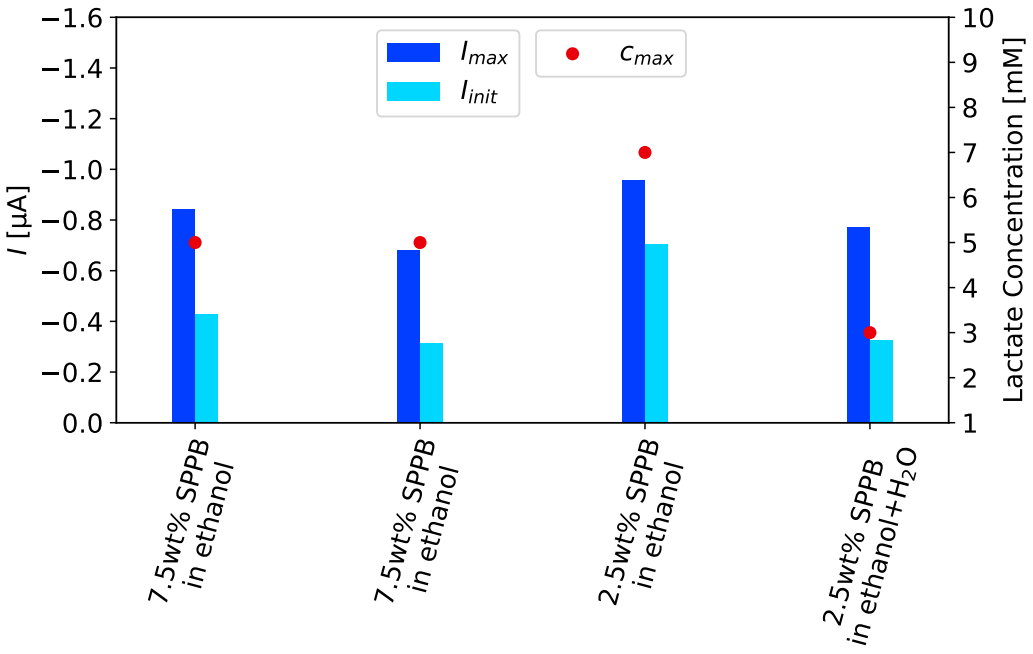

Figure 4.3. Responses of 4 PB|L|S sensor to increasing lactate concentrations, displaying the current signal at the first (I_{init}) and last (I_{max}) lactate increment (left axis). The c_{max} markers denote the maximum detected lactate concentration (right axis). The x-axis specifies the SBBP membrane casting solution composition of each individual sensor.

Table 4.3 gives the I_{init}/I_{max} ratio and c_{max} for all the 4 PB|L|S sensors shown in Figure 4.3. The sensors are listed from the highest to the lowest c_{max}. Sensors made with an identical formulation are listed after one another, with the sensor having the highest c_{max} dictating the listing position.

Table 4.3. Ratio between initial current step (I_{init}) and maximum current signal (I_{max}) and maximum detected lactate concentration (c_{max}) for sensors with SPPB membranes prepared from different casting solutions.

Sensor	**Membrane Solution**	$\boldsymbol{I_{init}/I_{max}}$	$\boldsymbol{c_{max}}$ **[mM]**
PB|L|S	2.5 wt% SBBP in ethanol	0.736	7
PB|L|S	7.5 wt% SBBP in ethanol	0.463	5
PB|L|S	7.5 wt% SBBP in ethanol	0.510	5
PB|L|S	2.5 wt% SBBP in ethanol/H_2O	0.420	3

Casting the membrane from a 7.5 wt% SBBP in ethanol solution generated intermediate sensor responses with respect to both I_{init}/I_{max} ratio and c_{max}. However, the membranes had partly delaminated from the WE after the testing. By reducing the SPPB membrane solutions content 2.5 wt%, no delamination was observed. Lowering

the wt% of SPPB concurrently increased the I_{init}/I_{max} ratio of the sensor. Changing the solvent composition to a mixture of ethanol and water generated the lowest I_{init}/I_{max} ratio sensor response, still showing no membrane delamination after testing.

The highest detected lactate concentration of all PB|L|S sensors was 7 mM, obtained with the sensor where the membrane was cast from a solution of 2.5 wt% SPPB in ethanol.

Cerium-Incorporated Membranes

3 different methods were employed to incorporate various wt% of either CeO_2 or Ce^{3+} into Nafion membranes. An overview of the sensor notation, referring to both the implementation method and cerium loading, can be found in Table 3.5.

Figure 4.4 shows the c_{max}, I_{max} and I_{init} from the chronoamperometric lactate titration testing of PB|L|N* (4.4a) and PB|L|N** (4.4b) sensors. Only 13 out of 19 tested sensors are presented, excluding the data from 3 PB|L|N*^{3}, 1 PB|L|S*^{3} and 2 PB|L|N**$_{24.8\%}$ sensors. Supplementary findings from these sensors did not significantly deviate from or provide any additional information to the presented results. A complete overview of all tested sensors can be found in Appendix A.

For PB|L|N* sensors, the largest c_{max} values were obtained with sensors where the membrane was made from direct mixing of $CeCl_3$ and Nafion solution (PB|L|N*^{1}), as seen in Figure 4.4a). The storage stability of the $CeCl_3$-Nafion solution was low, with the addition of $CeCl_3$ to the Nafion solution resulting in precipitation of cross-linked Nafion within 5 days of storage, rendering the solution useless for fabrication of new PB|L|N*^{1} sensor batches. A picture of the cross-linked Nafion precipitate within the solution can be found in Appendix C in Figure C.1.

The second largest c_{max} values in Figure 4.4a) was obtained by the sensors immersed in $CeCl_3$(aq) solutions (PB|L|N*^{2}), however generating relatively low I_{max}.

The lowest dynamic ranges of the PB|L|N* sensors were observed for the sensor where the composite membrane was made from co-casting of Nafion and $CeCl_3$(aq) solutions (PB|L|N*^{3}). It can also be seen that both c_{max} and I_{max} increased with reduced Ce^{3+} membrane content (%) for the PB|L|N*^{3} sensors.

Incorporation of CeO_2 into the sensor membranes was only performed by direct mixing of Nafion solution and CeO_2. Direct addition of CeO_2 to the Nafion membrane solutions did not yield homogeneous dispersions. Despite prolonged mechanical stirring, non-dispersed CeO_2 particles were readily observed. A picture of the CeO_2-Nafion dispersion can be found in Appendix C in Figure C.2.

The leftmost PB|L|N**$_{N/A\%}$ sensor in Figure 4.4b) stands out, having both the highest I_{max} and lowest I_{init} of all PB|L|N** sensors, as well as the highest c_{max} value of all cerium-modified membrane sensors tested in this work. This PB|L|N**$_{N/A\%}$ was the only PB|L|N** sensor where the CeO_2-Nafion membrane solution was cast onto the sensor immediately after solution preparation. The 24.8 wt% CeO_2-Nafion solution was prepared 12 hours before casting, and the second PB|L|N**$_{N/A\%}$ sensor was made 5 weeks after the N/A wt% CeO_2-Nafion solution had been prepared. The difference in storage time of the CeO_2-Nafion solutions used to fabricate the membranes of the PB|L|N** sensors should be noted.

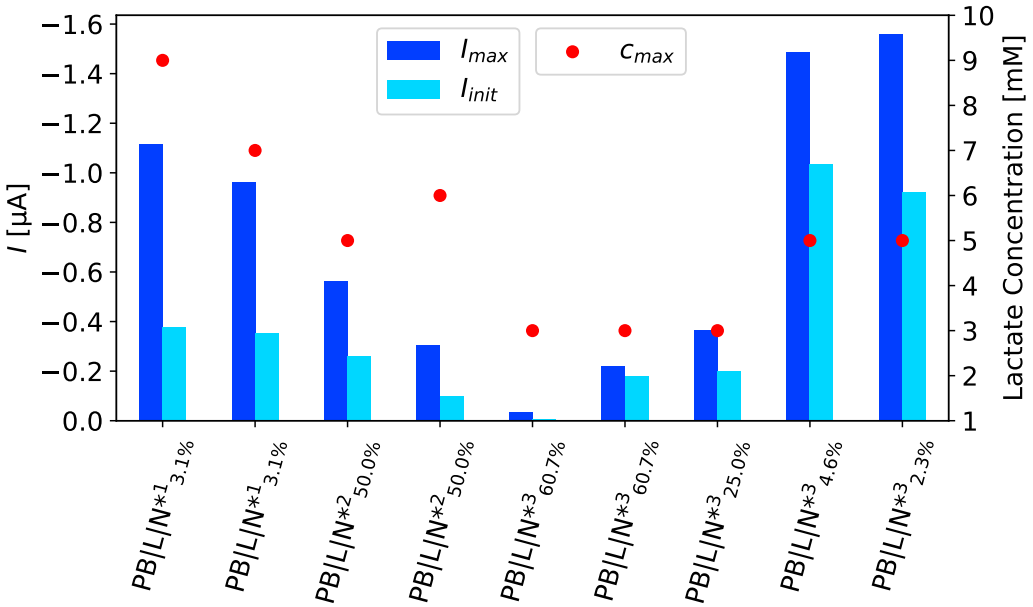

(a) PB|L|N*

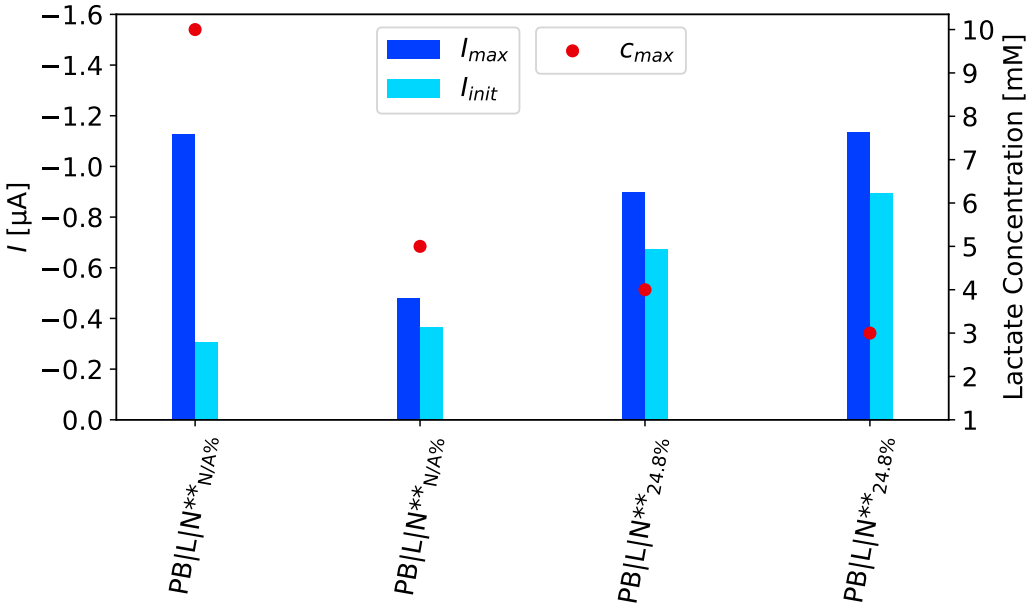

(b) PB|L|N**

Figure 4.4. Responses of (a) 9 PB|L|N* and (b) 4 PB|L|N** sensors to increasing lactate concentrations, displaying the current signal at the first (I_{init}) and last (I_{max}) lactate increment (left axis). The c_{max} markers denote the maximum detected lactate concentration (right axis). The x-axis specifies the sensor formulation, with cerium loading method (1,2,3) and content (%). * = Ce^{3+} and ** = CeO_2.

Table 4.4 gives the I_{init}/I_{max} ratio and c_{max} for all the PB|L|N* and PB|L|N** sensors shown in Figure 4.4. The sensors are listed from the highest to the lowest c_{max}. Sensors made with an identical formulation are listed after one another, with the sensor having the largest c_{max} dictating the listing position. It can be observed that the sensors with the highest lactate detection limit also had the most linear-like responses, reflected by the relatively low I_{init}/I_{max} ratio. The c_{max} values and ratios varied slightly for individual sensors having an identical formulation, with the largest spread seen for the PB|L|N$^{**}_{N/A\%}$ sensors. The largest difference in I_{init}/I_{max} ratio was also observed for the PB|L|N$^{**}_{N/A\%}$ sensors.

Table 4.4. Ratio between initial current step (I_{init}) and maximum current signal (I_{max}) and maximum detected lactate concentration (c_{max}) for sensors with cerium-modified membranes. The sensor formulation is specified, with cerium loading method (1,2,3) and content (%). * = Ce^{3+} and ** = CeO_2.

Sensor	$\boldsymbol{I_{init}/I_{max}}$	$\boldsymbol{c_{max}}$ **[mM]**
PB|L|N$^{**}_{N/A\%}$	0.270	10
PB|L|N$^{**}_{N/A\%}$	0.742	5
PB|L|N$^{*1}_{3.1\%}$	0.336	9
PB|L|N$^{*1}_{3.1\%}$	0.365	7
PB|L|N$^{*2}_{50\%}$	0.347	6
PB|L|N$^{*2}_{50\%}$	0.329	5
PB|L|N$^{*3}_{4.6\%}$	0.551	5
PB|L|N$^{*3}_{2.3\%}$	0.591	5
PB|L|N$^{**}_{24.8\%}$	0.752	4
PB|L|N$^{**}_{24.8\%}$	0.789	3
PB|L|N$^{*3}_{60.7\%}$	0.191	3
PB|L|N$^{*3}_{60.7\%}$	0.811	3
PB|L|N$^{*3}_{25\%}$	0.548	3

Pictures captured of the WE of 5 PB|L|N* sensors and 1 PB|L|N sensor after 3 rounds of chronoamperometric lactate testing are shown in Figure 4.5. Varying the incorporation method and content of Ce^{3+} changed the visual appearance of the membrane. The membranes on PB|L|N$^{*1}_{3.1\%}$ and PB|L|N$^{*2}_{50.0\%}$ sensors were similar to the non-modified PB|L|N Nafion membrane, with a thin and transparent film visible on the WE (Figs. 4.5d to 4.5f). In stark contrast, the membranes of PB|L|N^{*3} sensors had a matt white colour (Figs. 4.5a to 4.5c). Decreasing the cerium content from 60.7 wt% to 4.6 wt% concurrently reduced the intensity of the white colour.

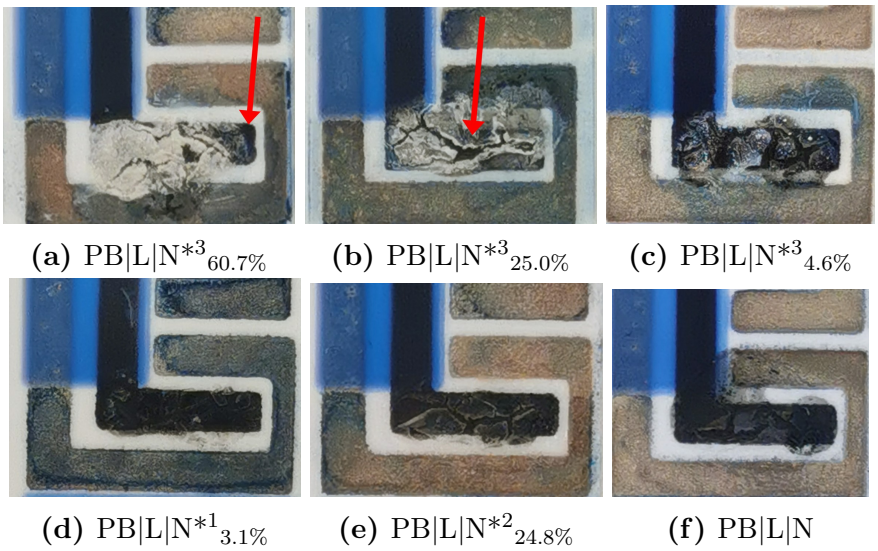

(a) PB|L|N*$^{3}{}_{60.7\%}$ **(b)** PB|L|N*$^{3}{}_{25.0\%}$ **(c)** PB|L|N*$^{3}{}_{4.6\%}$

(d) PB|L|N*$^{1}{}_{3.1\%}$ **(e)** PB|L|N*$^{2}{}_{24.8\%}$ **(f)** PB|L|N

Figure 4.5. Pictures captured of sensors where the membrane was made from (a-c) co-casting of Nafion and $CeCl_3$(aq) of various Ce^{3+}(%) content, (d) direct mixing of Nafion and $CeCl_3$(s), (e) immersion in $CeCl_3$(aq) after casting and (f) a normal Nafion solution after 3 rounds of chronoamperometric lactate titration testing. Arrows indicate openings or cracks in the membranes.

4.2 Prussian Blue Characterisation

This section presents the findings from voltammetric studies of PB without and with a Nafion membrane (PB|- and PB|N). Experiments involved cycling of PB|- sensors in electrolyte solutions of various cationic compositions, and investigating the effect of post-treatment procedures on the voltammetric behaviour of PB|- and PB|N in PBS solution. In addition, EDS elemental analysis of PB|- sensors before and after PBS cycling will be shown.

4.2.1 PB|- Cation Dependency

Figure 4.6 compares the voltammetric behaviour of PB|- sensors in 3 distinct phosphate buffer solutions: PPB, PPB+NaCl and PBS. The ionic strength and pH of the solutions can be found in Table 3.3. Only the second cycle is shown in the figure, while the voltammograms showing both the second and last (30th) cycle can be found in Appendix D in Figure D.1. The voltammograms were relatively stable over 30 scans in all but the PBS solution. Cycling in PPB generated the most narrow and largest current peaks. Increasing the sodium and concurrently increasing the potassium content in the buffer resulted in a peak widening and I_p reduction, both for the anodic and cathodic peaks.

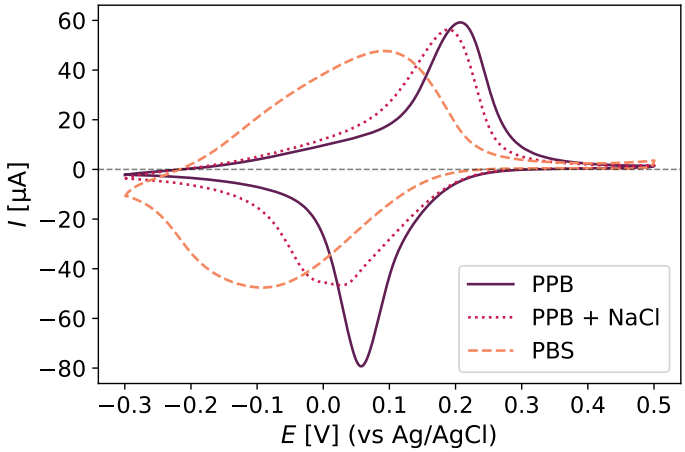

Figure 4.6. CVs of PB|- sensors in PPB (pH 6.83), PPB+NaCl (pH 6.78) and PBS (pH 7.48) at $50\,\mathrm{mV\,s^{-1}}$, showing the 2nd cycle. The scan rate was $50\,\mathrm{mV\,s^{-1}}$.

The cathodic and anodic peak potentials, peak-to-peak separation and half-wave potential for each voltammogram are given in Table 4.5. Decreasing the potassium and increasing the sodium concentrations resulted in a gradual shift of I_p towards lower potential values and a gradual increase in ΔE.

Table 4.5. The peak potentials (E_p), peak-to-peak separation (ΔE) and half wave potential $E_{1/2}$ for PB|- sensors cycled in PPB, PPB+NaCl or PBS solution from voltammograms in Figure 4.6.

Buffer	$E_{p,c}$ [V]	$E_{p,a}$ [V]	ΔE [V]	$E_{1/2}$ [V]
PPB	0.21	0.06	0.15	0.14
PPB+NaCl	0.19	0.03	0.16	0.11
PBS	0.09	-0.09	0.18	0.0

4.2.2 PB Post-Treatment

PBS-cycling of PB|- sensors with and without post-treatment generated distinct voltammograms after multiple scans, as seen in Figure 4.7. Post-treatment refers to cycling in a 0.1 M HCl/KCl solution directly after PB deposition and annealing the sensor at 100°C before use. The PB|- sensor tested in 4.7a) had not been subject to any post-treatment. Approximately all voltammogram features were lost over a total of 30 cycles in PBS. A more stable voltammogram was obtained with a post-treated PB|- sensor, as seen in 4.7b).

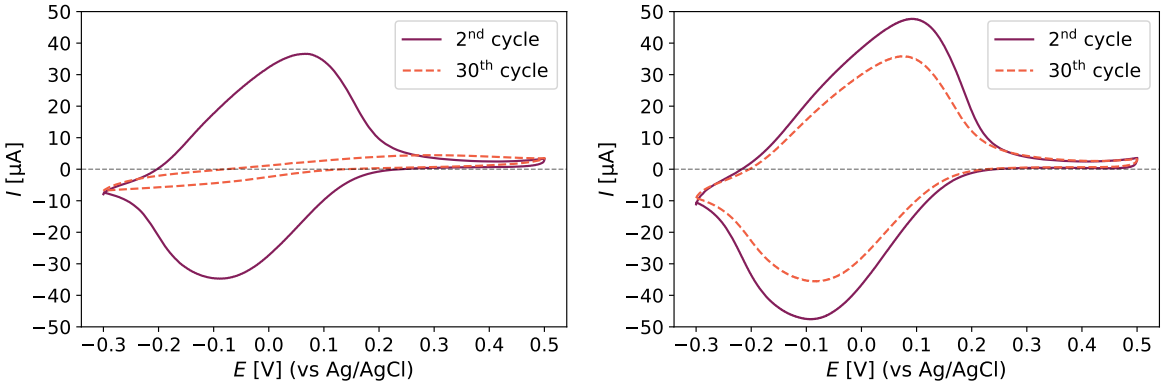

(a) PB|- **(b)** Post-treated PB|-

Figure 4.7. CVs in PBS (pH 7.48) of PB|- sensors with (a) no post-treatment (b) both KCl cycling and annealing. The scan rate was 50 mV s^{-1}.

The relative change in the anodic and cathodic current at 0.0 V from the 2nd to the 30th cycle for the non-treated and post-treated PB|- sensors are given in Table 4.6. The table additionally gives the peak current change from identical testing of non-treated and post-treated PB|N sensors. The corresponding CVs for the PB|N sensors can be found in Appendix D in Figures D.2a) and D.3a). A reduction in cathodic current will give rise to a positive percent change, as the current will become less negative.

Both post-treatment and Nafion membrane coating enhanced the cycling stability, reducing the peak current decay from the 2nd to the 30th cycle at 0.0 V, especially when employed in combination. The post-treated PB|N sensor had the best cycling

stability over a total of 30 cycles, even showing an increase in anodic current from the 2nd to the 30th cycle. Contrastingly, the non-treated PB|- sensor showed a 96% and 91% anodic and cathodic current reduction, respectively, losing approximately all electrochemical activity over 30 cycles.

Table 4.6. Percent change in anodic ($\Delta I_a/I_{a,0}$) and cathodic ($\Delta I_c/I_{c,0}$) current signal at 0.0 V from the 2nd to the 30th CV cycle for PB|- (Fig. 4.7) and PB|N (Figs. D.2a and D.3a) sensors subject to distinct pre-conditioning.

Sensor	KCl-cycling	Annealing	$\Delta I_a/I_{a,0}$ [%]	$\Delta I_c/I_{c,0}$ [%]
PB|-	-	-	-96	91
PB|-	x	x	-22	23
PB|N	-	-	-30	27
PB|N	x	x	25	19

A non-treated PB|- sensor previously cycled in PBS was transferred to and cycled in a 0.1 M KCl/HCl solution. The resulting voltammogram is shown in Figure 4.8. The electrochemical activity of the PB|- sensor was not restored after 30 cycles in 0.1 M KCl/HCl. Conversely, approximately all remaining voltammetric features from the PBS cycling were lost during the subsequent KCl/HCl cycling.

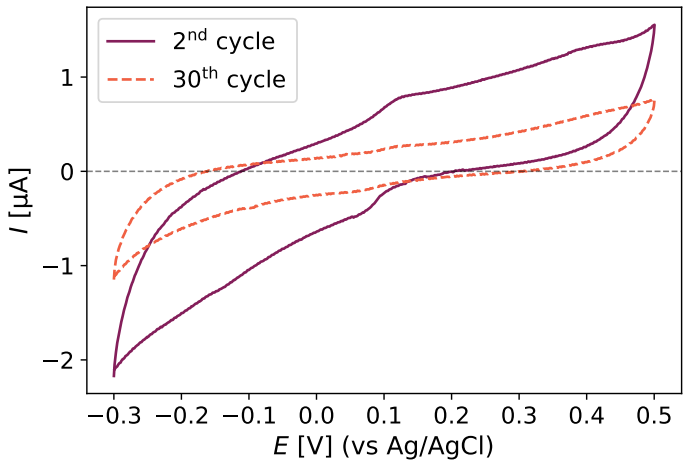

Figure 4.8. CV in 0.1 M KCl/HCl solution (pH 1.16) of a non-treated PB|- sensors previously cycled in PBS. The scan rate was 50 mV s^{-1}.

4.2.3 PB|N Durability Testing

The durability of PB|N sensors in PBS was tested by repeated cycling. A non-treated and post-treated PB|N sensor were subject to a total of 6 repeated CV measurements, with 30 cycles in each testing round. The sensors were stored and dried between each testing round. The resulting CVs are shown in Figure 4.9, with only the last (30th) cycle from each of the 6 testing rounds included in the figure.

The peak currents for both oxidation and reduction peaks were strictly decaying with repeated testing, as indicated by the arrows in the figures. For the non-treated PB|- sensor in 4.9a), the electrochemical activity around −0.05 V was rapidly lost with repeated testing, while the peaks around 1.0 V was better retained. The cathodic peak shifted from −0.05 V to 1.0 V with repeated testing. The post-treated PB|N sensor in 4.9b) displayed a relatively better retention of electrochemical activity at both −0.05 V and 1.0 V.

With the exception of the first testing round, the post-treated PB|N sensor generated a stable signal over all 30 cycles in all testing rounds. The non-treated PB|N sensor showed a slight, gradual current decay from the first to the last cycle in all testing rounds. The voltammograms showing both the 2nd and the 30th cycle for all 6 rounds can be found in Appendix D in Figures D.2 and D.3.

It should be noted that the initial current signal from the post-treated PB|N sensor was twice as large compared to the non-treated PB|N. The electrodeposition process result in PB films of various thicknesses, with a larger area under the deposition curve indicating a thicker PB layer. From the electrodeposition data (Appendix D Fig. D.4) it is evident that the post-treated PB|N sensor had quantitatively more PB and therefore has a higher electrochemical activity. Thus the CV curves of the PB|N sensors must be read relatively.

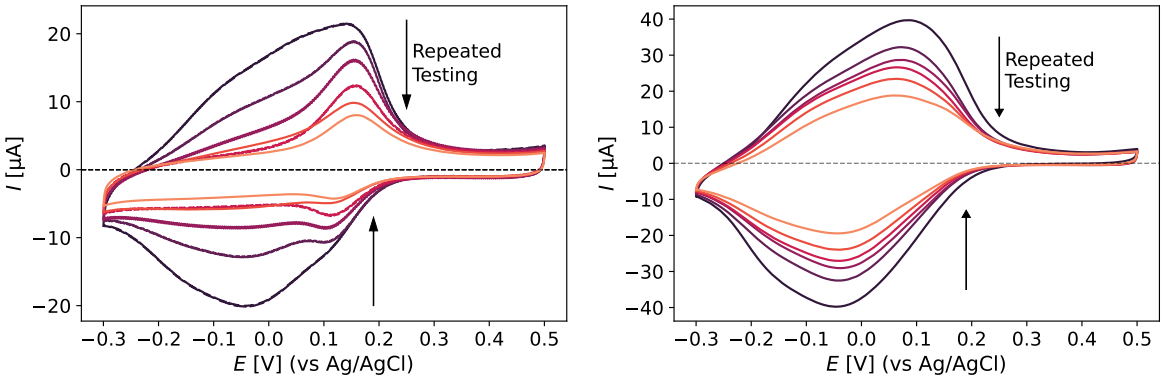

(a) PB|N **(b)** Post-treated PB|N

Figure 4.9. 6 rounds of CV of (a) non-treated and (b) post-treated PB|N sensors, with minimum 5 days storage between testing rounds. Only the last (30th) cycle per testing round is shown. All measurements were performed in PBS (pH 7.48) with scan rate 50 mV s^{-1}.

Table 4.7 summarises the anodic and cathodic current decays at 0.0 V for both the non-treated and post-treated PB|N sensor from the second cycle in the first testing round to the last cycle in the last testing round.

Table 4.7. Change in anodic ($\Delta I_a/I_{a,0}$) and cathodic ($\Delta I_c/I_{c,0}$) current signal at 0.0 V for non-treated and post-treated PB|N sensors from voltammograms in Figure 4.9. Current change is measured from the 2nd cycle in the first testing round to the 30th cycle in the last (6th) testing round.

Sensor	**KCl-cycling**	**Annealing**	$\boldsymbol{\Delta I_a/I_{a,0}}$ [%]	$\boldsymbol{\Delta I_c/I_{c,0}}$ [%]
PB|N	-	-	-89	86
PB|N	x	x	-38	60

4.2.4 EDS Elemental Analysis

EDS data for two post-treated PB|- sensor are given in Table 4.8. One of the sensors had not been prone to PB deposition and post-treatment, whereas the second sensor had been subject to 30 CV cycles in PBS. The elemental analysis showed the presence of both potassium and sodium at the surface of the PBS-cycled PB|- sensor. The full EDS spectra are given in Appendix E.

Table 4.8. Atomic wt% data obtained from EDS of two post-treated PB|- sensors, one of them untested and the second one previously cycled in PBS (pH 7.48) for 30 cycles.

Detected Element	**PB|- [at%]**	**PBS-cycled PB|- [at%]**
C	81.1	85.8
N	8.6	3.5
O	4.7	6.2
Cl	2.5	2.6
Si	1.1	1.1
Fe	1.0	0.5
K	0.9	0.1
S	0.1	0.1
Na	0.0	0.1

Chapter 5

Discussion

5.1 Lactate Sensor Testing

5.1.1 O_2 Availability and Enzyme Layer Capacity

The O_2 purging testing results implies that the sensor current response was ultimately limited by the availability of dissolved O_2 in the test solution. Considering all chronoamperometric lactate titrations tests performed in the present and previous work, the highest current signal obtained under ambient testing conditions was $-1.77\,\mu A$, with the PB|L|N sensor shown in Figure 4.1. Contrastingly, purging O_2 gas into the solution during PB|L|N testing generated a maximum current of $-2.97\,\mu A$ (Tab. 4.1). Testing the same PB|L|N sensor both without and with O_2 supplementation resulted in a signal increase of 104% at the point of signal saturation, confirming that the relatively high I_{max} signal was caused by the increased O_2 availability.

Ar purging testing results further substantiated that availability of dissolved O_2 limited the maximum obtainable current of PB|L|N sensors at standard testing conditions. Depriving the test solution of O_2 resulted in a significant I_{max} reduction. It is evident from Figure 4.2b) that the PB|L|N signal was significantly larger at every concentration step at standard conditions compared to testing with continuous Ar purging. Performing complementary testing with both Ar and O_2 gas purging eliminated the plausibility that the purging process itself affected the sensor responses. Purging of O_2 could possibly have increased the sensor response by inducing a convection effect, thereby reducing the size of the diffusion layer [32]. Considering that Ar and O_2 purging had complete opposite effects, respectively reducing and increasing I_{max}, this can be disregarded.

Adjusting properties of the enzyme layer did not increase the maximum current signal, further reinforcing that the sensor response was limited by O_2 availability. Only 1 out of 10 enzyme-layer modified sensors generated a I_{max} response larger than $-1.0\,\mu A$ (Tab. 4.2), thus showing no pronounced improvement compared to PB|L|N sensors tested in previous work (Tab. 2.2). Moreover, all enzyme layer-modified sensors had profoundly lower I_{max} than the standard conditions testing of the PB|L|N sensors presented in Table 4.1. If the activity or stability of the enzyme layer had been limiting the sensor response, increasing the enzyme loading, adding stabilising agents

or testing the enzyme at temperature optimum should have substantially increased I_{max} [19]. However, when limited by substrate availability, adjusting properties of the enzyme layer has little or no effect, evident from Michaelis-Menten kinetics (Fig. 2.4) [32]. In conclusion, attempts to increase I_{max} by increasing enzymatic activity or loading gave no significant improvement with respect to maximum generated current, implying that the sensor was limited by substrate availability rather than enzyme saturation.

The catalytic capacity of the enzyme layer was possibly not exceeded at the point of current signal saturation in the O_2 purging experiment. Increasing the dissolved O_2 content generated an approximately linear response up to 11 mM lactate (Fig. 4.2a), suggesting that the enzyme layer had not yet reached catalytic saturation levels. From Michaelis-Menten kinetics, enzyme saturation should produce a hyperbolic curve (Fig. 2.4) [32]. Upon increasing the lactate concentration from 11 mM to 12 mM during testing, the current signal started to drift towards more positive current values, and was unresponsive to further lactate additions (Appendix B Fig. B.2). Systems employing pseudo-RE are especially prone to signal drifting, as the RE is immersed directly in the test solution and is subject to a changing electrolyte composition [107]. The observed signal drift could be owed to a change in pH by the addition of lactate or by RE surface adsorption effects, among others [107], but none of the mentioned effects was experimentally measured and thus not confirmed. A shift in the reference potential would affect the catalytic activity of the PB layer and consequently the current signal [34]. PB|L|N sensors could potentially reach even higher c_{max} and I_{max} values by employing O_2 purging if circumventing potential drift effects. Ultimately, I_{max} should be imposed by enzyme saturation, PB saturation or by reaching the limit of dissolved O_2 in the test solution, as the O_2-content in the test solution cannot be infinitely increased by purging. More O_2 purging tests could be performed in future work to identify the linear range and I_{max} for PB|L|N sensors in O_2-enriched solutions.

Lowering the permeability of lactate across the sensor membrane could enable detection of even higher bulk lactate concentrations [2]. For sweat sensing applications of the biosensor, the content of dissolved O_2 cannot be forcedly increased. It would be highly inconvenient to perform endurance training with an O_2 tank. Thus, I_{max} would be limited by O_2 availability. From Figure 4.1 it is evident that reducing the lactate addition increment size simultaneously reduced the current step sizes and increased the total amount of steps, which would be a favourable response to adapt with respect to increasing c_{max} while restricted by an upper I_{max} limit. By reducing the bulk lactate concentration increments from +1 mM to +0.1 mM, the PB|L|N sensor was responsive to minimum 20 additions. Testing the same sensor with the standard +1 mM increments, the sensor response ceased after only 4 lactate additions. The experimental findings demonstrated that lowering lactate flux through the membrane could dramatically reduce the current step size for bulk lactate additions of +1.0 mM, mimicking the sensor responses obtained with the +0.1 mM additions [65, 66]. Both Burmeister et al. and Almeida et al. significantly increased the linear range and apparent K_M of their respective enzymatic biosensors by applying an outer polymer membrane [65, 66]. The membranes limited the lactate flux while simultaneously having a low impact on the O_2 diffusion [66]. Based on the step size testing and literature findings,

it is rational to assume that reducing lactate permeability across the outer membrane could increase the dynamic range of the biosensor when restricted by availability of O_2, thereby approaching physiologically relevant sweat lactate concentration.

Reducing the current step size and membrane permeability could still be insufficient to enable detection of lactate concentrations up to 100 mM, and might need to be combined with other approaches. If the +0.1 mM step sizes in Figure 4.1 was reproduced for +1.0 mM increments, c_{max} would be extended to 20 mM. The step size could be further reduced to increase c_{max}, but excessive step size reduction has a negative impact on the sensitivity of the sensor [66]. The step size must still be large enough to distinguish between two distinct lactate concentration levels. A possible solution could be to supplement with alternative approaches to decrease the local lactate concentration. Firstly, a scavenger could be employed to deplete the bulk solution of a predetermined quantity of lactate. During signal post-processing, the original bulk concentration can be recalculated by combining the measured values and the known depletion. A second approach could be to dilute the bulk solution, similar to the performed step size testing. With respect to the practical application of the sensor with integration into a wearable device, the two above suggestions would complicate the system architecture, involving inclusion of a scavenger and/or a liquid chamber for sweat dilution. Contrastingly, reducing the lactate permeability of the outer diffusion membrane would be more compatible with and simpler to integrate into a wearable device. However, considering that sweat lactate concentrations can reach values up to 100 mM, it might be necessary to ultimately combine multiple approaches to sufficiently increase the dynamic range of the wearable lactate biosensor.

5.1.2 Adjusting Membrane Permeability

New membrane materials were tested in an attempt to reduce the lactate flux over the sensor membrane, with the objective of lowering the current step sizes and increasing the dynamic range. The following section will discuss and evaluate the prospect of the new sensor membranes to lower the current step sizes and increase the dynamic range compared to the PB|L|N sensor formulation employed in previous work. The sensors will be distinguished with respect to both the membrane material, concentrations of membrane materials in the casting solution (wt%) and the method of membrane fabrication.

SBBP Membranes

PB|L|S sensors did not improve sensor response with respect to current step size reduction or dynamic range compared to PB|L|N sensors tested in previous work. c_{max} was lower or equal to 7 mM for all PB|L|S sensors (Tab. 4.3), thus showing no improvement to S5 (c_{max} = 6 mM) and S6 (c_{max} = 8 mM) from previous work. Moreover, membrane permeability of PB|L|S sensors were larger, with I_{init}/I_{max} ratios either between or larger than I_{init}/I_{max} ratios of sensors S5 and S6. In a study by Adamski et al, the properties of SBBP and Nafion 211 membranes were measured and compared, where SBBP membranes were found to have a higher water uptake than Nafion 211 membranes of identical thickness [108]. Assuming that lactate is co-transported

with water through the hydrophilic domains of the polymer membrane during swelling, higher water uptake is expected to increase lactate permeability and result in larger I_{init} [67, 76, 109]. This effect could explain the higher I_{init}/I_{max} ratio for PB|L|S sensors compared to PB|L|N. However, it is difficult to accurately compare Nafion and SBBP membranes with respect to water permeability due to the differences in thickness (wt%) and solvent composition between the Nafion and SBBP solutions employed in this work. Despite no improvement in linear or dynamic range from casting of SBBP membranes from 7.5 wt% or 2.5 wt% in ethanol or ethanol/water solutions was demonstrated, other wt% and solvent compositions could be attempted. Adjusting the weight percentage, solvent composition and curing conditions of the solution cast SBBP membranes could affect the membrane morphology and accordingly water- and lactate transport properties, thereby improving sensor PB|L|S performance [67, 110, 111]. This could be investigated in future work.

The response of PB|L|S sensors was dependent on wt% pristine SBBP and solvent composition of the SBBP casting solution. As seen from Table 4.3, changing the solvent composition from ethanol to a mixture of ethanol and water reduced the I_{init}/I_{max} ratio. Adjusting properties of the solvent might have affected the membrane structure by changing the organisation of polar and non-polar groups, and possibly by prolonging the curing time [51, 112]. However, overall sensor performance was not improved, as both I_{max} and c_{max} were reduced. It should be noted that the sample size of tested PB|L|S sensors was low, with only one or two sensors tested per formulation permutation. Thus, the sensor responses could have been dictated by differences in testing conditions or low sensor repeatability. More tests should be performed to obtain further data on the effect of solvent composition and wt% SPPB on lactate permeability in solution-cast SBBP membranes.

Cerium Incorporation

It was confirmed that Ce^{3+} and possibly CeO_2 had a cross-linking effect on Nafion polymers. Direct addition of $CeCl_3$ to the Nafion ionomer solution resulted in precipitation of cross-linked Nafion upon storage (Appendix C Fig. C.1). In contrast to the $CeCl_3$-Nafion solution, it was not possible to discern precipitation of cross-linked Nafion in the CeO_2-Nafion solutions by eye due to the presence of non-dispersed CeO_2 (Appendix C Fig. C.2). However, considering that the expected mechanism for sulfonate group cross-linking is similar for CeO_2 and Ce^{3+}, it is rational to assume that direct addition of CeO_2 to the polymer solution also resulted in precipitation [73, 76].

Although a precipitate could not be directly observed, the scattered responses of the CeO_2-Nafion composite membrane sensors (Fig. 4.4b) could imply that also CeO_2 induced polymer cross-linking within the casting solution. It is evident from Figure 4.4b) that all but one PB|L|N** sensor responded with a relatively high I_{init}, which was the only sensor where the CeO_2-Nafion membrane was cast from a freshly prepared composite membrane solution. Low storage stability of the casting solution would readily explain the relatively high membrane permeability of the remaining PB|L|N**, reflected by the high I_{init}/I_{max} ratio (Tab. 4.4), as the membranes would be thinner and thus more permeable if cast from a polymer-depleted solution. However, the large variability in the PB|L|N** sensor responses could alternatively be owed

to an inhomogeneous dispersion of CeO_2 in the Nafion membrane solution. The actual weight percentage of CeO_2 in the membrane of each distinct PB|L|N** sensor would be dependent on how well the composite membrane solutions were mixed immediately prior to casting. As the PB|L|N** sensors were made in three different batches, the distinct responses could possibly just reflect a large variation in CeO_2 membrane content. No literature has been found on the explicit shelf life of CeO_2-Nafion solutions, as most research on composite membranes has been directed toward fuel cell applications, where composite membrane preparation is followed by immediate casting and solution storage is irrelevant [74, 78, 113, 114]. A more thorough investigation of the shelf life of CeO_2-Nafion solutions is required to draw a final conclusion on whether precipitation occurs upon solution storage.

The prospect of using cerium-Nafion composite membranes to reduce lactate permeability was not unambiguously demonstrated due to the limited test data. The two sensors made from the $CeCl_3$-Nafion solution before precipitation had a relatively high c_{max} and low I_{init}/I_{max} ratio (Tab. 4.4) compared to sensors tested in both present and previous work (Tab. 2.2). In addition, the lactate diffusion was not excessively hindered, as the PB|L|N*$^1{}_{3.1\%}$ sensors still responded with relatively high maximum currents. Correspondingly, the one PB|L|N**$_{N/A\%}$ sensor with a membrane cast from a non-precipitated CeO_2-Nafion solution achieved the highest c_{max} and lowest I_{init}/I_{max} of all sensors tested under standard conditions both in this and previous work (Tabs. 4.4 and 2.2). These 3 sensors could function as a proof-of-concept for cerium-mediated membrane cross-linking to moderate lactate transport. However, although the reduced step size and increased c_{max} of the sensors could be owed to a cross-linking effect of cerium in the membranes, it could as well have been a result of other variables, such as a complete and homogeneous membrane coverage and high catalytic activity of PB and enzyme layer. The low shelf life of the composite membrane solutions impeded fabrication of new sensor batches to conclude a significant effect of the cerium incorporation. It was not attempted to make new cerium-Nafion mixtures, since relatively large volumes of Nafion ionomer solution were required to enable addition of measurable quantities of $CeCl_3$(s) or CeO_2(s), which was inconvenient for fabrication of a limited amount of sensors. Large amounts of solution would be necessary to screen for and optimise the cerium loading content, and considerable amounts of cerium-Nafion solution going to waste for each fabrication round. In order to obtain more test data on cerium-Nafion composite membranes, these impracticalities must be overcome, or alternative methods for cerium membrane implementation must be identified.

The alternative cerium-incorporation method of immersing PB|L|N sensors in $CeCl_3$ (aq) solutions resulted in low I_{max} signals, presumably owed to low storage stability of the biosensors in aqueous solutions. From Figure 4.4 it can be seen that both the PB|L|N*$^2{}_{50\%}$ sensors had a I_{max} lower than 0.6 µA. The immersion procedure was adapted from Tian, who produced SPPB-Ce^{3+} composite membranes by soaking previously cast SPPB membrane pieces in aqueous solutions of $CeCl_3$ for 24 hours, demonstrating an efficient uptake of Ce^{3+} into the membranes [73]. Employing a similar approach as Tian was expected to increase the dynamic range of the sensors, but soaking the biosensors in solution for 24 hours prior to testing presumably had a negative impact on the maximum sensor response. Enzymatic biosensors with solution-cast

Nafion membranes are found to have low storage stability in aqueous buffer solutions, with a rapid loss of responsiveness as compared to dry storage conditions [69]. Reduced responsiveness could be owed to leaching of enzymes from the immobilisation matrix and out to bulk solution [16, 19, 69]. Moreover, storage of PB films in aqueous solution has been shown to reduce its catalytic capacity towards H_2O_2 reduction, likely due to film dissolution [34, 64, 94]. Lastly, prolonged soaking could result in partial membrane dissolution. Nafion films cast from aqueous solutions and cured at room temperature have proven to be slightly soluble in polar solvents and are readily susceptible to crack formation [51, 67, 115]. Overall, soaking the sensor in aqueous solutions could have had a negative impact on both the PB film, enzyme layer and polymer membrane, thus explaining the low maximum current signals.

The experimental data from the PB|L|N$^{*2}{}_{50\%}$ sensors could further substantiate a positive effect of cerium in reducing membrane lactate permeability, despite the sensors having a low I_{max}. Both sensors had a I_{init}/I_{max} ratio in between that of S5 and S6 from previous work (Tabs. 4.4 and 2.2, respectively). From Figure 4.4 it can be readily observed that the PB|L|N$^{*2}{}_{50\%}$ sensors also had among the lowest I_{init} values, which could indicate a reduced lactate flux across the membrane. However, no improvement in the c_{max} was observed for the PB|L|N$^{*2}{}_{50\%}$ sensors compared to previous work. A reduction in the current step size will have little effect on the dynamic range of the sensors if accompanied by a concurrent reduction in I_{max}. A possible adjustment to be investigated in future work to circumvent a reduction in catalytic activity could be to let the sensors soak in a more concentrated solution of $CeCl_3$(aq) for a shorter period of time. In this manner, the immersion method could be a viable method for cerium ion incorporation and could possibly be employed as an alternative to the direct mixing of $CeCl_3/CeO_2$ and membrane polymer solution.

The method of co-casting $CeCl_3$ and polymer membrane solution presented the simplest method to accurately tune cerium content and circumvent issues related to solution precipitation and low I_{max}, but did not result in efficient incorporation of Ce^{3+} in the membranes. It is clear from comparing the pictures in Figure 4.5 that there was a white substance present within the membranes of the PB|L|N^{*3} sensors (Figs. 4.5a to 4.5c), while the membranes of sensors where cerium was incorporated by direct mixing (Fig. 4.5d) or immersion (Fig. 4.5e) were transparent. The correlation between colour intensity of PB|L|N^{*3} sensor membranes and $CeCl_3$ loading indicates that the white membrane colour originated from solid $CeCl_3$ remnants. The time required for Ce^{3+}-proton exchange when mixing $CeCl_3$ and semi-cured Nafion ionomer solution is not known. Zaton et al. reported on a complete uptake of Ce^{3+} in pre-cured Nafion membranes from a 0.04 mM immersion solution after only 90 minutes, obtaining a final doping of approximately 0.9 wt% Ce^{3+} [75]. During co-casting of alternating Nafion and $CeCl_3$(aq) layers in this experiment, the $CeCl_3$(aq) solvent had completely evaporated after 30 minutes, and loading amounts were at the lowest 2.3 wt%. Thus, both doping time and loading amount differed from the experiments performed by Zaton, in addition to employing semi-cured Nafion membranes. Based on this, it is strongly suggested that evaporation could have occurred faster than the Ce^{3+}-proton exchange process, leaving solid $CeCl_3$ salt remnants within the membrane layers.

The low response of PB|L|N^{*3} sensors with a high wt% Ce^{3+} ($\geq$ 25 wt%) was

presumably owed to solid $CeCl_3$ salt grains forming a physical barrier towards the passage of lactate and O_2 across the membrane. All sensors generated relatively low current responses, with I_{max} consistently lower than $-0.4\,\mu A$ (Appendix A Fig. A.1). From pictures captured of the WE of PB|L|N*3 sensors in Figure 4.5, it is suggested that the low sensor responses were owed to a continuous layer of solid $CeCl_3$ salt rendering the membranes practically impermeable in the first testing round. It is clear from repeated testing of the sensors that the low current response of the sensors was not owed to a low catalytic activity of PB or the enzyme layer (see Appendix B.4 for data on the second and third testing rounds). There was a large increase in I_{max} from the first to the second testing round, presumably owed to crack formation in the membranes upon repeated hydration and re-hydration [67], which would increase the flux of lactate and O_2 in the subsequent testing rounds and enhance the current signal [65]. Solution-cast Nafion membranes are found to be brittle and prone to crack formation [67], which can be readily observed for the PB|L|N*3$_{25\%}$ sensor in Figure 4.5b), indicated by the red arrow. Consequently, it can be excluded that the low I_{max} in the initial testing rounds was owed to low catalytic activity of PB or the enzyme layer, but rather caused by excessively low membrane permeability.

Reducing the cerium loading content in the PB|L|N*3 sensor membranes (wt% $Ce^{3+} \leq 9.3\,wt\%$) did not improve Ce^{3+} incorporation and additionally had a negative impact on the mechanical integrity of the polymer membranes. The relatively high I_{init}/I_{max} and low c_{max} of the sensors (Appendix A Tab. A.1) imply that the membranes were a less efficient barrier towards lactate diffusion than PB|L|N sensors tested in previous work (Tab. 2.2). The increased membrane permeability was presumably owed to the formation of cracks in the membranes, as seen in the picture in Figure 4.5c). Lowering the loading of $CeCl_3$ circumvented formation of a continuous layer of solid $CeCl_3$ completely obstructing lactate transport, but presumably had a negative impact on the mechanical integrity of the Nafion membrane. The presence of sharp notches within a polymer matrix induces points or regions of concentrated stresses [70]. Upon membrane swelling and deswelling, these localised stresses could result in crack formation [70]. Accordingly, the picture of a PB|L|N*3$_{4.6\%}$ sensor in Figure 4.5c) reveals a torn and ruptured membrane. The presence of solid $CeCl_3$ could additionally have interrupted the regular arrangement of the Nafion polymers, obstructing association between Nafion chains layered before and after the $CeCl_3$ layer in the casting process and thus further weakening the membrane. Membrane rupture could be augmented by the hygroscopic properties of dehydrated $CeCl_3$, resulting in excessive swelling of the Nafion [116]. Moreover, hydration of the membranes could result in a gradual dissolution of solid $CeCl_3$ in the membranes, resulting in ion migration. Cerium ions are found to be mobile within the membrane and could migrate with their diffusion gradient out to the bulk solution when dissolved [75, 76, 117]. Hence, several possible mechanisms could have contributed to low mechanical integrity and rupture of the PB|L|N*3 sensor membranes.

In summary, testing results do not discard the prospect of cerium-induced polymer cross-linking to increase the dynamic range without notably affecting the maximum current, but only limited test data was obtained. Sensor membranes produced from either direct addition of cerium to the polymer casting solution or by immersion in

aqueous $CeCl_3$ solutions generated promising responses with respect to both current step size reduction and maximum detected lactate concentration, which could indicate a positive effect of cerium in reducing lactate membrane permeability. Adversely, both methods of cerium incorporation were associated with practical issues, which obstructed the production and testing of more sensors. More sensor data would be advantageous both with respect to confirming a significant effect of cerium incorporation, as well as to optimise the cerium loading content to further reduce the current step sizes and expand the dynamic range. Further increasing the cerium loading content could be necessary to obtain a more pronounced reduction in lactate diffusion across the sensor membrane [73]. Co-casting of polymer membrane solution and aqueous $CeCl_3$ was simple to perform and allowed for a more precisely tuned cerium loading content. However, the $CeCl_3$ solvent evaporated too fast to allow for cerium-proton exchange in the membranes, only leaving solid and dehydrated $CeCl_3$ within the membrane layers, which had a negative impact on sensor performance both at high and low $CeCl_3$ loadings. The method of co-casting should be discarded, whereas further work should be devoted to either solver the practical challenges of direct mixing or immersion, or identifying alternative methods to obtain cerium-induced membrane cross-linking. This will allow for a thorough screening of various cerium loading amounts and result in a final conclusion on the prospect of cerium-composite membranes to increase the sensing range of the lactate biosensors.

5.1.3 Sensor Repeatability

The low sensor repeatability makes it difficult to conclude a significant improvement in sensor performance when based on test data from only 1-3 sensors. Sensors fabricated with identical formulations and similar ambient conditions responded inconsistently with respect to both I_{max} and c_{max} upon chronoamperometric lactate testing. The low sensor repeatability is particularly pronounced for the enzyme-layer modified sensors in Table 4.2. For instance, the two PB|1.5L|N sensors responded with two distinct c_{max} values, ranging from 6 to 8 mM, and a spread in I_{max} from -0.552 to $-0.942\,\mu A$. Also in Figure 4.4, the two PB|L|$N^{*1}{}_{3.1\%}$ show a spread in I_{max} and c_{max} values, despite being made in the same batch and having an identical formulation. Low sensor repeatability was also observed in previous work, as seen by the spread in I_{max}, I_{init} and c_{max} in Figure 2.9. Due to the large variation in individual sensor responses, a final conclusion on whether a sensor formulation resulted in an improved performance should not be based on the data of only a small number of sensors. Especially for the cerium-incorporated membrane sensors, there was limited test data on each distinct sensor formulation. Focus was rather directed towards screening over a wide range of cerium incorporation methods and loading amounts to get an indication of which method and loading was the most suitable. For future work, more tests should be performed on identical sensor formulations to gather sufficient data and conclude whether cerium incorporation significantly improved sensor performance.

The low sensor repeatability was much owed to the manual fabrication process. It was challenging to deposit enzyme and polymer membrane solutions exclusively at the WE, and it could be observed by eye that some solution was commonly delocalised to the junction between WE and CE or on the CE (Fig. 4.5). An instance of insufficient

and non-uniform membrane coverage can be readily observed in the picture in Figure 4.5a), where the red arrow indicates a WE area which received no or little membrane solution upon casting. The PB|L|N*$^3_{60.7\%}$ sensor in the picture was remarkably more responsive than the second PB|L|N*$^3_{60.7\%}$ sensor tested (Fig. 4.4), presumably owed to the poor membrane coverage allowing for a slight flux of lactate and O_2 into the enzyme layer despite an otherwise impermeable membrane. Openings in the membrane diminish its function as a diffusion barrier [65], resulting in an initially larger current flux and higher I_{init}. The membrane should additionally counteract efflux of enzymatically produced H_2O_2 and assists in enzyme immobilisation [28, 69]. Openings in the membrane more readily allow for leakage of both enzymes and H_2O_2 out to the bulk solution, reducing the I_{max}. Similarly, low enzyme loading or WE coverage upon casting would also result in a more rapid saturation of the enzyme layer and lower I_{max} values. The picture in Figure 4.5f clearly shows a partial deposition of enzyme and immobilisation matrix on the CE and in the WE/CE junction. Overall, the method of drop casting low solution volumes onto the small surface area of the WE proved challenging, resulting in inconsistency with respect to enzyme responsiveness and activity as well as the diffusion-limiting properties of the outer polymer membrane. The manual fabrication process facilitated irregularities with respect to loading amounts and WE coverage for individual sensors, irrespective of sensor batch.

Batch-to-batch variations could be owed to slight variations in curing conditions for the solution-cast polymers. Depending on the curing conditions such as humidity and ambient temperature, sensors produced in different batches could have different properties with respect to the structure and nature of the solution-cast polymers [67]. Drop-casting polymer membranes from solution generally yield a more unordered structure and organisation than commercially extruded membranes [67]. This applies both to the outer polymer membrane and to the chitosan-SWCNT immobilisation matrix. The difference in curing conditions between sensors could affect the enzyme immobilisation and the permeability of the outer diffusion membrane [65, 67], and thus contribute to low sensor repeatability.

Sensors with particularly low I_{max} values were presumably not limited by O_2 availability, but by properties of the enzyme or PB layer, with the exception of the complete impermeable cerium-membrane sensors. This can be seen by comparing the I_{max} of the enzyme-modified sensors in Table 4.2 and sensors tested in previous work (Tab. 2.2). One of the two PB|L^{Glu}|N sensor tested in this work reached an I_{max} of only $-0.155\,\mu A$, in stark contrast to the $-1.199\,\mu A$ signal obtained by the second PB|L^{Glu}|N sensor. Such low sensor responses were not observed for any PB|L|N sensors when examining the effect of Nafion membrane thickness on I_{max} and I_{init} in previous work, rendering it highly unlikely that the PB|L^{Glu}|N sensor was limited by low substrate availability at such low current values. Dismissing low substrate availability as a plausible cause, enzyme or PB layer saturation remains the most probable signal-limiting factor.

Low enzyme loading could be a result of poor WE coverage, as discussed above, but could also be due to an inhomogeneous distribution of LOx in the enzyme catalyst solution. As enzymes are proteins and prone to denaturation upon mechanical mixing, the catalyst solutions were never mixed or agitated before use. Possibly, some sensors received enzyme catalyst solution with a low presence of enzymes. Fur-

thermore, immobilisation is paramount for enzyme performance, and the immediate microenvironment can dramatically enhance or reduce enzyme activity [16, 19, 40]. The immobilisation matrix should also ensure that the enzymes were retained in close proximity to the WE. Considering the dependency of enzyme activity on the immobilisation medium [16, 19, 40], contaminations of the chitosan-SWCNT matrix upon casting or low immobilisation matrix loading amounts could have reduced enzymatic activity. Since several factors could contribute to a lowered enzyme activity, a variation in sensor saturation limits and thus reduced sensor repeatability would be expected.

The PB layer is expected to have had a low impact on sensor repeatability, despite variance in PB-film thickness between individual sensors. In the preliminary project work, it was found that the capacity of PB was not exceeded upon lactate titration testing, as seen from the S0 sensor in Figure 2.10. For the S0 sensor, having no membrane influencing H_2O_2 availability, maximum current signal was $-5.8\,\mu A$. The S0 sensor had exceedingly sufficient PB catalytic activity compared to the current signals generated in lactate titration measurements. Thus, variations in PB film thickness are not expected to have affected the overall sensor response. On the contrary, the method of PB electrodeposition could result in formation of thin PB films at the CE and/or RE of the sensor [34, 89]. The presence of PB increases the resistance against charge transfer in the counter and reference reactions, and could shift the operational potential of PB [89]. This would have a negative impact on the sensor response and possibly limit the maximum current signal. It could be assessed by optical inspection whether a thin layer of PB had formed on the CE or RE. PB has a bright blue colour and was readily visible on a Ag/AgCl electrode. Thus, sensors that were obviously discoloured after the PB deposition were disregarded. The post-treatment of PB|- was found to efficiently removed excess PB on the RE and CE from the deposition and diminish this effect. Consequently, the two remaining sensor layers are reckoned to be the largest sources of error regarding sensor repeatability.

Large variability in the response of PB|L|N** sensors could be owed to inhomogeneous dispersions of CeO_2 in the polymer membrane solutions. Embedding inorganic nanoparticles in a polymer matrix is challenging due to the strong preference of nanoparticles to form agglomerates [118]. Accordingly, it was difficult to obtain homogeneous dispersions with direct addition of CeO_2 to Nafion membrane solutions. Despite prolonged mechanical stirring, non-dispersed CeO_2 particles were readily observed in the solutions. Pearman et al. used a similar approach for preparing CeO_2-Nafion composite membranes, reporting on successful incorporation for 2 wt% CeO_2. However, mechanical mixing could be insufficient for achieving homogeneous dispersions for higher CeO_2 contents, such as the mixtures employed in this work. Weissbach et al. produced solution cast Nafion membranes with 10 wt% CeO_2 by direct addition followed by repeated cycles of mechanical stirring and sonication [74]. The sonication step was not adapted in this work, and could possibly have facilitated a more homogeneous dispersion of CeO_2 particles in the membrane solutions before casting. This could be investigated in future work. Overall, the method of solution casting CeO_2-membrane mixtures had low repeatability. The inhomogeneity of the dispersions resulted in uncertainty towards the actual weight percentage of CeO_2 in each of the solution-cast membranes.

5.1.4 Sensor Reproducibility

The reproducibility of the sensors upon lactate concentration fluctuations was not properly evaluated in the performed experiments. All sensors were chronoamperometrically tested 2-3 times, but the prolonged lag time between the repeated testing rounds allowed for the sensor layers to dry, which was not representative of continuous sweat measurements. The chronoamperometric data from all 2-3 testing rounds of all sensors are shown in Appendix B. Some sensors showed a good overlap for all 3 test rounds, as seen for the PB|L^{Glu}|N sensor in Figure B.13, indicating that properties both the PB, membrane and enzyme layers were retained between testing rounds. Contrastingly, Figure B.9 (PB|2L|N) shows a spread in current values associated with lactate concentrations of 1 mM, which complicates accurate lactate quantification.

Ideally, subsequent testing rounds should have been initiated immediately after one another, just renewing the test solution in between the measurements. The formation of cracks and occasionally delamination of the outer polymer membranes was readily observed after the first testing rounds, as seen in Figure 4.5. Membrane cracking was presumably owed to the hydration and dehydration process, as solution cast Nafion membranes are brittle and prone to crack formation [67]. As discussed above, openings in the membrane notably altered the sensor response by allowing for a larger influx of substrates [2, 65], but could also allow for efflux of enzymes and enzymatically produced H_2O_2 and thereby lowering the I_{max}. Consequently, the repeated testing format employed in the performed experiments was not representative of sensor reproducibility by definition, since the sensor architecture was not identical from one testing round to the next [2]. Moreover, the employed testing format was also not representative of single-use sweat sensors, as the sensors will be continuously wetted during practical sweat monitoring applications. In future work, the testing format should be adjusted to allow for a proper evaluation of sensor repeatability. To obtain a reliable signal for lactate quantification, it is paramount that the sensor generates reproducible responses when the lactate concentration is both decreased and increased under operational use [13].

For the step size, O_2 and Ar gas testing, the presented data include all 3 rounds of repeated testing. Despite the non-optimal testing format with respect to reproducibility, the results are still regarded as reliable. It was necessary to compare the sensor response at standard conditions in order to investigate the effect of adjusting the ambient conditions. To minimise the influence of varying sensor responses from one round to the next, two of the three testing rounds were performed under identical conditions in a sandwich format. For the step size testing, the +0.1 mM increment tests were performed first and last, with a standard testing round in between. Disregarding the differences in I_{max}, a similar behaviour was observed for both rounds of +0.1 mM testing with respect to current step sizes. Similarly, the O_2 testing was performed in between two rounds of standard conditions testing, thus discarding that the increase in I_{max} was purely a result of the change in sensor properties upon prior testing and repeated hydration and dehydration. To confirm the validity of the experimental findings, the step size and purging experiments could be repeated in future work without allowing for the sensor membranes to dry in between testing rounds.

5.2 Prussian Blue Stability

For optimal biosensor performance, the sensor response should not limited by the catalytic capacity of the PB layer towards H_2O_2 reduction. It was confirmed in previous work that the catalytic activity of PB towards H_2O_2 initially exceeded that of LOx towards lactate (Fig. 2.10). However, the explicit stability of PB activity over prolonged testing duration was not assessed. Electrocatalytic activity of PB is not only dependent on H_2O_2 availability, but also alkali ions for charge compensation upon reduction, evident from Equations (2.15) and (2.14) [34, 86]. It is known from literature that PB has good cycling stability in potassium-rich solutions [55, 86, 95, 119]. However, the concentration of potassium in sweat ranges only from 4-24 mM. The dominant alkali ion in sweat is sodium, which is present in concentrations between 10-100 mM [15]. Consequently, to employ PB for a reliable and stable sweat sensing signal, the activity and stability of PB must be sufficient in electrolytes where sodium is the dominating cationic specie. The PB activity retention must coincide with the length of a lactate threshold endurance training, preferably for more than 60 minutes. The following section is therefore concerned with understanding and evaluating the performance of PB under physiological conditions similar to a sweat environment to conclude whether PB is a suitable mediator for sweat lactate sensing purposes. Both alkali ion dependency and stability of PB will be discussed, and the effect of post-treatment procedures on the operational stability of PB will be evaluated.

5.2.1 Electrolyte Dependency

Sodium ions appeared to participate as charge compensators upon the reduction and oxidation of PB in PBS. The peak current position for cycling of PB|- sensors was contingent on the relative and absolute content of potassium and sodium ions in the electrolyte, as seen in Figure 4.6 and Table 4.5. Employing Equation 2.13, a shift in $E_{1/2}$ of -0.07 V is expected when the K^+ concentration is reduced from from 0.3 M (PPB) to 0.02 M (PBS). The experimentally observed $E_{1/2}$ shift was -0.14 V (Tab. 4.6), thus exceeding the theoretical prediction for potassium-mediated PB activity. The substantial shift in $E_{1/2}$ indicates that Na^+ participated in the reduction and oxidation of PB, resulting in a change in redox activity and/or electron transfer kinetics in the PB film [34, 85, 92]. The Na^+-dependent PB reduction and oxidation must consequently occur at lower potentials than the K^+-mediated process. An explanation behind the systematic reduction of $E_{1/2}$ in Na^+ electrolyte solutions has not yet been established in literature [85, 86, 92, 93].

EDS data obtained for a PBS-cycled PB|- sensor showed the presence of trace amounts of both sodium and potassium ions (Tab. 4.8), which could further strengthen the hypothesis in co-participation of both ions in the electrochemical activity of PB. However, EDS is not a considerably sensitive technique for detection of low elemental concentrations in a sample [120]. Consequently, no definite conclusion should be drawn on the basis of the EDS findings. The trace amounts of sodium detected with EDS could also be surface remnants from immersing the sensor in PBS during cycling, and not necessarily sodium incorporated within the PB structure.

The PB films appeared to be irreversibly damaged upon repeated cycling in PBS solution. Figure 4.7a) shows a gradual loss of electrochemical activity, which is in agreement with literature findings [86, 92, 121, 122]. The electrochemical activity of PB in potassium-rich solutions was not restored when the PBS-cycled PB|- sensor was subsequently cycled in a 0.1 M KCl/HCl solution (Fig. 4.8). Based on the voltammetric findings in this study, it cannot be evaluated whether PBS-cycling resulted in a decomposition or inactivation of PB. It could possibly have been evaluated by eye whether the film thickness was reduced before and after cycling in PBS, as the PB film has a strong blue colour. However, as the WE was black, the PB film was not visible by optical inspection. For future work, performing an identical test with platinum WEs could be relevant to enable a visual evaluation of whether PB films in sodium solutions are decomposed or if electroactivity is purely blocked upon cycling in PBS.

5.2.2 Optimising PB stability

Cycling stability of PB|- in PBS solution was significantly enhanced when introducing post-treatment procedures. Post-treated PB|- sensor displayed a smaller current decay over 30 cycles (Fig. 4.7b), especially at 0.0 V (Tab. 4.6), which is the potential employed for H_2O_2 reduction. Similar findings are also reported in literature, suggesting that ionic permeability is dependent on the PB deposition method and post-treatment procedures, which again dictates the structural disorder in the PB film [80, 85, 93]. Itaya et al. proposed that cycling of PB in 0.1 M KCl/HCl directly after deposition resulted in a structural change from the insoluble to the more stable soluble form of PB, thus improving cycling stability [80]. Another possibility is that cycling in KCl-rich solutions saturated the deeper layers of the PB film with potassium, resulting in improved retention and re-use of potassium ions upon oxidation and reduction, even in solutions with a low potassium content [85]. Overall, post-treatment of PB|- had a significantly positive effect on the stability of carbon-deposited PB films, and should thus be implemented as a part of the standard preparation procedure of PB films for sweat biosensing purposes.

Both cycling stability and durability of PB films were enhanced by applying a Nafion membrane, presumably owed to the ion-conductive and -retaining properties of the Nafion membrane [67, 94, 123]. For non-treated PB|- sensor, approximately all electrochemical activity was lost after 30 cycles (Fig. 4.7a). Contrastingly, both PB|N sensors were still electrochemically active after a total of 180 cycles, spread over 6 rounds of testing (Fig. 4.7). Similar findings were obtained by Garcia-Jareno et al. when cycling PB and PB-Nafion sensors in 1 M NaCl solutions (pH 3) [94]. The authors suggested that the Nafion membrane functioned as a sieve that stripped away the hydration shell around the sodium ions during transport across the membrane. Correspondingly, a review by Mauritz et al. similarly reports that sodium is in an intermediate hydration state when transported across the Nafion membrane [67]. Non-hydrated sodium ions are appropriately sized for transport through the PB lattice and can thus participate as charge compensators upon reduction and oxidation of PB [94]. The Nafion membrane could additionally facilitate retention of potassium ions already present within the PB film, preventing or slowing down the efflux to the bulk solution [94, 123]. Consequently, increased participation of both sodium and potassium ions as

charge compensators during reduction and oxidation of PB could explain the improved retention of electrochemical activity for PB|N sensors compared to PB|-.

The post-treated PB|N sensor showed relatively better retention of electrochemical activity around 0.0 V compared to the non-treated PB|N sensor upon repeated testing (Tab. 4.7). From Figure 4.9 it can be observed that both treated and non-treated PB|N had a similar decay in redox activity around 1.0 V, while post-treated PB|N had a lower relative reduction in current values at potentials around −0.05 V. The activity of PB around −0.05 V is presumed to be associated with sodium participation, as discussed above. Post-treatment of PB|N involved cycling in KCl/HCl solution, which does not explicitly clarify the observed retention in sodium affinity upon repeated testing. Rather opposite, cycling in KCl should be expected to improve potassium activity. A possible rationale is that KCl cycling resulted in a change from the insoluble to the soluble form of PB, which is more stable [86, 94]. The soluble PB form could be more suited for sodium transport, since the affinity of PB towards sodium is presumed to depend on the stochiometry, hydration state and crystallinity of the PB film [80, 85].

Overall, the combination of PB post-treatment and Nafion membrane application stabilised CV behaviour over both multiple cycles and repeated testing. Especially the activity around 0.0 V was retained by KCl cycling and Nafion membrane coating (Tab. 4.6), which is the relevant range of PB-mediated reduction of H_2O_2. Over 6 rounds of testing, the post-treated PB|N sensor was still electrochemically active at 0.0 V (Fig. 4.9b). The mechanism behind the observed improvement in stability and sodium activity by post-treatment of PB was not identified, but possibly resulted in a stochiometric change of insoluble PB to the soluble form [80], increased the presence of interstitial potassium within the PB lattice [85], or a combination of the two. The presence of a Nafion membrane presumably increased the amount of potassium retained in close proximity to the PB and increased sodium participation by partly dehydrating the ions upon transport across the membrane [94, 123]. The findings on the stability of post-treated PB|N in PBS do not undermine the suitability of PB as a catalyst for H_2O_2 reduction in sweat, which has an ionic composition of sodium and potassium similar to that of PBS. In total, the post-treated PB|N sensor was cycled for 96 minutes over 6 rounds of testing, which corresponds well with and even exceeds the duration of a lactate threshold endurance activity.

Chapter 6

Conclusion

The aim of this thesis was to identify the sensing range limitations of the biosensor formulation employed in previous work and adjust the formulation to overcome these constraints. The main objective was to extend the upper limit of the dynamic range to enable detection of physiologically relevant sweat lactate concentrations for wearable sweat lactate monitoring applications.

The experimental findings indicated that the maximum current signal of the biosensors used in previous work was ultimately limited by the availability of dissolved O_2 in the test solution. Increasing or depriving the testing solution of O_2 significantly affected the maximum current signal, whereas efforts to increase the activity of the enzyme layer had no positive effect. To overcome the influence of dissolved O_2 availability on the upper detection limit of the biosensors, properties of the outer polymer membrane were adjusted to reduce the current step sizes of the sensors. It was shown by reducing the bulk lactate concentration increment size that the sensors could generate at least 20 distinct current levels before signal saturation was reached, implying that the upper limit of the dynamic range could be increased if the diffusion of lactate across the outer polymer membrane was reduced.

Incorporation of cerium into the Nafion membrane by direct addition of cerium compound to the Nafion solution followed by immediate casting onto the sensors increased the upper lactate detection limit from 8 mM in previous work to 9 mM and 10 mM, employing $CeCl_3$ or CeO_2, respectively. The improvement was presumably owed to a cross-linking effect of cerium on the sulfonate groups of the membrane polymers, which reduced the lactate diffusion across the membrane. However, the significance of the findings is questionable due to the limited sample size and low sensor repeatability. Sensors made by direct addition of $CeCl_3$ could not be repeated because the $CeCl_3$-Nafion mixture had a low shelf life. For CeO_2-Nafion composite membranes, only one sensor displayed an improved dynamic and linear range, whereas all the attempts to repeat this sensor were unsuccessful. The low repeatability could be owed to the precipitation of cross-linked polymers from the mixture upon storage, an inhomogeneous dispersion of CeO_2 in the membrane polymer solutions, or the single improved sensor response could have been a statistical outlier. More tests should be performed to exclude all potential variables and evaluate whether CeO_2 and $CeCl_3$ had a significant effect on reducing the current step sizes of the sensors.

Other methods of cerium incorporation did not improve sensor performance compared to previous work. Immersing the sensors in aqueous $CeCl_3$ solutions for 24 hours had an adverse impact on the maximum current response. Storing the biosensor in an aqueous environment negatively affected the catalytic sensor layers, resulting in a decreased maximum current signal. Reducing the immersion time could possibly circumvent this problem, and should be examined in future work. The method of co-casting of $CeCl_3$ and membrane polymer solution in alternating layers was unsuccessful, as the $CeCl_3$ solvent evaporated too fast to allow for incorporation of Ce^{3+} into the polymer networks. The presence of solid $CeCl_3$ salts within the membrane both constituted a physical barrier towards lactate and O_2 diffusion and disrupted membrane integrity, facilitating membrane rupture. The co-casting method was thus not suited for cerium incorporation.

SBBP polymer membranes were tested as an alternative to Nafion, but none of the SBBP membrane sensors demonstrated reduced current step sizes or increased lactate detection ranges compared to previous work. However, considering the low sample size of only 4 sensors, the results could be biased by the low sensor repeatability. Moreover, solvent composition and wt% SBBP content appeared to influence the permeability of the solution-cast SBBP membranes, and thus optimising solvent and dissolved SBBP content could possibly enhance the sensor performance by improving membrane durability and by reducing the current step size. However, this is highly speculative and must be confirmed by further experimental testing.

The combination of post-treatment and Nafion membrane application should be sufficient for stabilising the PB film and ensuring sufficient delivery of ions for PB catalytic activity over the duration of an endurance training. Direct cycling of PB in 0.1 M KCl/HCl solution after preparation had a positive effect on the cycling stability of PB in PBS solution, and should be implemented in standard PB film preparation. Annealing was found useful to accelerate the drying of the PB film as an option for several days of desiccator storage. Applying a Nafion membrane further increased the cycling stability of PB, presumably due to retention of potassium ions and dehydration of sodium ions entering from the bulk solution.

Despite the lack of identifying an optimal method of loading cerium into the sensor membrane, testing results from direct mixing of cerium and Nafion solution demonstrated the prospect of cerium incorporation to increase the upper detection limit of the biosensors. Further research on cerium implementation approaches and identifying an optimal cerium loading could produce biosensors more suitable for quantification of physiologically relevant sweat lactate concentrations. The maximum dynamic range obtained in this work was 10 mM, which is about 10% of the required range for athlete sweat-sensing applications. Reducing the increment size of bulk lactate additions showed that at least 20 significant current steps were achievable, which would increase the dynamic range of the sensors up to 20 mM. Further efforts on tuning the permeability of lactate over the membrane could further increase the sensing range, but an excessive reduction in the step size will compromise sensor sensitivity. Consequently, it could ultimately be necessary to combine a reduced step size with sweat sample dilution or employ a lactate scavenger to enable practical applications of the sensor in a wearable sweat-sensing device.

Chapter 7

Future work

7.1 Cerium-Polymer Composite Membranes

As far as the author is concerned, the work in this thesis is the first to examine the effect of incorporating cerium in solution-cast membranes to improve the dynamic range of enzymatic biosensors. The objective was to investigate whether cerium-induced membrane cross-linking to reduce lactate permeability was feasible, which was performed by screening a wide range of implementation methods and loading contents. The improved performance of the PB|L|$N^{**}_{N/A\%}$ and PB|L|$N^{*1}{}_{3.1\%}$ sensors compared to previous work could serve as a proof of concept, while it should be kept in mind that the findings are based on a limited sensor sample size of only 3 sensors. If further investigations are done on the topic, emphasis should be on identifying how cerium incorporation method, loading content and type of cerium compound employed dictates membrane properties. An improved understanding of the cerium-Nafion or cerium-SBBP composite membranes can be obtained by studying the membranes as isolated systems, and could possibly accelerate the implementation of cerium-infused membranes in the biosensors. Investigating the entire biosensor system as a whole allows for more variables in each experiment due to the complex layer structure and accordingly low sensor repeatability. It is challenging to evaluate whether a low sensor response is owed to properties of the PB mediator, the enzyme immobilisation layer or the outer membrane. Isolated cerium-Nafion and cerium-SBBP permeability studies could be performed by layering solution-cast membranes directly onto the WE of the SPE sensors and investigating transport of species that can be directly oxidised or reduced at the WE surface, such as ascorbic or uric acid [22].

Direct mixing of $CeCl_3$ or CeO_2 into the membrane solutions generated the best sensor responses with respect to signal linearity and maximum detected lactate concentrations. However, practical issues complicated sensor reproducibility. For direct addition of $CeCl_3$ to a Nafion ionomer solution, precipitation of cross-linked Nafion could be observed (Appendix C Fig. C.1). Thus, it was not investigated whether increasing the $CeCl_3$ loading from 3.1 wt% resulted in a further reduction in I_{init}/I_{max} ratio, and only limited data on the effect of direct mixing of polymer solution and $CeCl_3$ were obtained. Further increasing the cerium loading content could be necessary to obtain a more pronounced reduction in lactate diffusion across the sensor

membrane. In the work of Tian, a Ce^{3+} loading of 4 wt% gave a noticeable reduction in SBBP-membrane conductivity, while 2 wt% had no influence [73]. Consequently, slightly increasing the Ce^{3+} loading content from the 3.1 wt% used in this work would be reasonable.

For CeO_2 implementation, reproducibility issues could have been related to the inhomogeneous dispersion of the CeO_2 in the membrane solutions and possibly precipitation issues, though a Nafion precipitate could not be directly observed. Storage stability of CeO_2-Nafion or CeO_2-SBBP mixtures should be investigated more closely to evaluate whether or not the dispersions are suitable for long-term storage. Possibly, a polymer-containing precipitate could be easier to observe if employing a more concentrated polymer solution containing only trace amounts of CeO_2. Moreover, inhomogeneity of the dispersions results in uncertainty towards the actual weight percentage of CeO_2 in each of the solution-cast membranes. Repeated cycles of mechanical mixing and sonication have been found to yield homogeneous dispersion of 10 wt% CeO_2 in Nafion solutions [74], and could be adapted to the preparation procedure. By homogenising the solutions, the content of CeO_2 loaded into the solution cast membranes will be approximately known, yielding more reproducible results.

If the impracticalities associated with the direct mixing of membrane solution and CeO_2 or $CeCl_3$ are not overcome, alternative methods of cerium ion implementation should be investigated more closely, including immersion of the sensors in aqueous $CeCl_3$. The method of $CeCl_3$(aq) immersion presented a viable approach where precipitation issues could be circumvented, but the immersion time employed in this work must be reduced to avoid adverse effects on the activity of the catalytic sensor layers. The time required for Ce^{3+}-proton exchange is not known, but a possible adjustment could be to let the sensors soak in a more concentrated $CeCl_3$ solution for a shorter period of time. Tian et al used a prolonged immersion time of 24 hours [73], which was the method adapted in this work. Contrastingly, Zaton et al. reported a complete uptake of Ce^{3+} in pre-cured Nafion membranes from a 0.04 mM immersion solution after only 90 minutes, obtaining a final doping concentration of approximately 0.9 wt% Ce^{3+} [75]. Identifying a suitable combination of [Ce^{3+}] and immersion time could be done in a larger scale screening assay, using various combinations of the two parameters.

7.2 SBBP Polymer Membranes

The SPPB presents an interesting alternative to employ in the lactate biosensors due to their improved durability compared to Nafion [71]. SBBP membranes were received as solid membranes and were dissolved in various solvent compositions and with different wt% pristine membrane content. Only three different combinations thereof were investigated, whereas a more optimal solvent and wt% membrane composition could exist. A limited amount of SBBP membrane sensors were presented in this work, with experimental data on 5 sensors lost due to issues experienced in 3 subsequent sensor batches, where all fabricated sensors were practically non-responsive for unknown reasons. Loading of Ce^{3+} into SPPB membrane was attempted with the co-casting method, which only resulted in solid $CeCl_3$ within the membrane layers and resulted in a highly permeable membrane (Appendix A Fig. A.1), similar to the

PB|L|N*[3] sensors. Consequently, there was a lack of experimental data on sensors with SBBP membranes in this work, both with and without incorporation of cerium. To properly evaluate the suitability of SBBP membranes, more sensors should be fabricated and tested, using various combinations of solvent and wt% dissolved SBBP. Furthermore, incorporation of Ce^{3+} into SBBP membranes has been investigated in literature, showing that the conductivity of the membrane was reduced with larger loading amounts of cerium [73]. SBBP membranes thus present a viable possibility of producing more durable membranes with a reduced lactate permeability and could possibly be employed to increase the dynamic range of the biosensors.

7.3 Sensor Response Limitations

The maximum catalytic capacity of the enzyme layer could be investigated more closely by performing more O_2 purging experiments. In this work, a maximum current signal of $-2.970\,\mu A$ was obtained with O_2 purging. However, as the signal did not exhibit a hyperbolic decrease in current signal, as would be expected from Michaelis-Menten kinetics [32], it was suggested that the capacity of the enzyme layer was not yet exceeded. The response could once again be limited by availability of O_2, as purging cannot infinitely increase the content of dissolved O_2 [124]. However, the sensor response indicated that the response was rather limited by a sudden drift in the sensor reference potential (Appendix B Fig. B.2). Thus, performing more O_2 purging experiments could provide useful data on the maximum catalytic capacity of the enzyme layer.

O_2 purging could additionally be employed to confirm that low sensor responses are owed to low catalytic activity of the PB or enzyme layer, and not by substrate availability. One of the two PB|L^{Glu}|N in Table 4.2 generated an I_{max} of only $-0.155\,\mu A$. Whether low substrate availability or enzyme activity was the signal limiting factor could have been confirmed by purging O_2 gas into the solution at signal saturation. If the PB|L^{Glu}|N sensor would still not respond to further lactate additions, the enzyme activity was the limiting factor. This was not performed in the current work due to the ordinary test station not being localised in close enough proximity to an O_2 supply and the inconvenience of the experimental set-up. However, it could be useful to perform a few experiments in further work on the topic to gain a better understanding of the mechanisms behind low sensor repeatability.

7.4 Wearable Sweat Lactate Biosensors

With a successful improvement of the dynamic range of the biosensor, the next step should be to test the sensor with a continuous flow of liquid over the electrode surface. Rather than employing a stepwise increment in lactate concentration, the lactate content should be continuously increased and decreased to evaluate the ability of the sensor for accurate lactate quantification when concentrations are fluctuating. This would be more similar to a wearable sweat-sensing environment, where lactate concentrations are continuously changing [21, 22, 104]. Such experiments could be performed

by employing a flow cell system, using a simple microfluidic design to ensure supply and discharge of solution over the electrodes.

Moreover, the response of the biosensors in a more complex test solution should be assessed to confirm the specificity of the biosensor towards lactate [13, 16, 21]. Sweat is abundant in biomarkers which could potentially interfere with the biosensor response [13, 15, 21, 91]. Employing an operating potention of 0.0 V reduces the number of potential interfering agents, but explicit sweat sensor testings should be performed to experimentally confirm sensor specificity [87].

Lastly, the biosensor should be integrated into a wearable device and tested on the skin during physical activity. The wearable would need to contain a microfluidic system for collection, delivery and discharge of sweat, suitable for low sample volumes [3, 13, 22, 104]. The sweat sampling and transport for real-time lactate monitoring still face challenges regarding irregular or low sweat generation, sample contamination by mixing with other skin components or with old sweat, air bubble entrapment and sweat evaporation, to mention a few [3, 104]. There will be a need for a careful and sophisticated designed microfluidic system to allow for accurate and real-time sweat monitoring of sweat lactate. Moreover, a wireless transmission device is necessary to read out the results in real-time [98, 104]. Testing the sensor under endurance activity could possibly induce noise in the measurements, which must also be considered when increasing the dynamic range of the sensor. The sensitivity of the sensor needs to be sufficient for on-body measurements during physical activity, and not only for a simple laboratory setup with minimal noise. Overall, there are still remaining components that must be constructed, tested and optimised in order to assemble a fully integrated wearable device for sweat lactate sport monitoring applications.

References

[1] Zimmer & Peacock. *Biosensors Metrics Glossary of Definitions.* https://www.zimmerpeacocktech.com/knowledge-base/faq/biosensors-glossary/ (Accessed: 21.06.23).

[2] D. R. Thevenot et al. 'Electrochemical Biosensors: Recommended Definitions and Classification'. In: *Pure and Applied Chemistry* 71.12 (1999), pp. 2333–2348. DOI: doi:10.1351/pac199971122333.

[3] J. Kim et al. 'Wearable biosensors for healthcare monitoring'. In: *Nature Biotechnology* 37.4 (2019). DOI: 10.1038/s41587-019-0045-y.

[4] M. U. Ahmed et al. 'Personalized diagnostics and biosensors: A review of the biology and technology needed for personalized medicine'. In: *Critical Reviews in Biotechnology* 34.2 (2014). DOI: 10.3109/07388551.2013.778228.

[5] Apple. *Apple Watch.* https://www.apple.com/no/watch/ (Accessed 24.04.23.)

[6] A. Sharma et al. 'Wearable Biosensors: An Alternative and Practical Approach in Healthcare and Disease Monitoring'. In: *Molecules* 26.3 (2021), p. 748. DOI: 10.3390/molecules26030748.

[7] A. J. Bandodkar, I. Jeerapan and J. Wang. 'Wearable Chemical Sensors: Present Challenges and Future Prospects'. In: *ACS Sensors* 1.5 (2016), pp. 464–482. DOI: 10.1021/acssensors.6b00250.

[8] S. Borgmann et al. 'Amperometric Biosensors'. In: *Advances in Electrochemical Science and Engineering*. John Wiley & Sons, Ltd, 2011. Chap. 1, pp. 1–83. DOI: https://doi.org/10.1002/9783527644117.ch1.

[9] P. Mehrotra. 'Biosensors and their applications – A review'. In: *Journal of Oral Biology and Craniofacial Research* 6.2 (2016), pp. 153–159. DOI: 10.1016/j.jobcr.2015.12.002.

[10] N. J. Ronkainen, H Brian Halsall and William R Heineman. 'Electrochemical biosensors'. In: *Chemical Society Reviews* 39.5 (2010), pp. 1747–1763. DOI: 10.1039/B714449K.

[11] Abbott. *Abbott Freestyle Libre.* https://www.freestyle.abbott/us-en/home.html (Accessed 24.04.23.)

[12] P. C. Pandey, G. Pandey and R. J. Narayan. 'Minimally Invasive Platforms in Biosensing'. In: *Frontiers in Bioengineering and Biotechnology* 8 (2020). DOI: 10.3389/fbioe.2020.00894.

[13] A. Martín et al. 'Epidermal Microfluidic Electrochemical Detection System: Enhanced Sweat Sampling and Metabolite Detection'. In: *ACS Sensors* 12.2 (2017), pp. 1869–1869. DOI: https://doi.org/10.1021/acssensors.7b00729.

[14] P. J. Derbyshire et al. 'Lactate in human sweat: a critical review of research to the present day'. In: *The Journal of Physiological Sciences* 62.6 (2012), pp. 429–440. DOI: 10.1007/s12576-012-0213-z.

[15] L.B. Baker. 'Physiology of sweat gland function: The roles of sweating and sweat composition in human health'. In: *Temperature* 6.3 (2019), pp. 211–259. DOI: 10.1080/23328940.2019.1632145.

[16] L. Rassaei et al. 'Lactate biosensors: current status and outlook'. In: *Analytical and Bioanalytical Chemistry* 406.1 (2014), pp. 123–137. DOI: 10.1007/s00216-013-7307-1.

[17] UC Davies Sports Medicine. *Lactate Profile*. https://www.health.ucdavis.edu/sports-medicine/resources/lactate (Accessed 24.04.23.)

[18] M. L. Goodwin et al. 'Blood lactate measurements and analysis during exercise: A guide for clinicians'. In: *Journal of Diabetes Science and Technology* 1.4 (2007). DOI: 10.1177/193229680700100414.

[19] K. Rathee et al. 'Biosensors based on electrochemical lactate detection: A comprehensive review'. In: *Biochemistry and Biophysics Reports* 5 (2016), pp. 35–54. DOI: 10.1016/J.BBREP.2015.11.010.

[20] V. Billat et al. 'Training effect on performance, substrate balance and blood lactate concentration at maximal lactate steady state in master endurance-runners'. In: *Pflugers Archiv European Journal of Physiology* 447.6 (2004). DOI: 10.1007/s00424-003-1215-8.

[21] W. Jia et al. 'Electrochemical tattoo biosensors for real-time noninvasive lactate monitoring in human perspiration'. In: *Analytical Chemistry* 85.14 (2013). DOI: 10.1021/ac401573r.

[22] I. Shitanda et al. 'Continuous sweat lactate monitoring system with integrated screen-printed MgO-templated carbon-lactate oxidase biosensor and microfluidic sweat collector'. In: *Electrochimica Acta* 368 (2021), p. 137620. DOI: 10.1016/J.ELECTACTA.2020.137620.

[23] Z. Sonner et al. 'The microfluidics of the eccrine sweat gland, including biomarker partitioning, transport, and biosensing implications'. In: *Biomicrofluidics* 9.3 (2015), p. 031301. DOI: 10.1063/1.4921039.

[24] J. M. Green et al. 'Sweat lactate response between males with high and low aerobic fitness'. In: *European Journal of Applied Physiology* 91.1 (2004), pp. 1–6. DOI: 10.1007/s00421-003-0968-2.

[25] E. V. Karpova et al. 'Relationship Between Sweat and Blood Lactate Levels During Exhaustive Physical Exercise'. In: *ChemElectroChem* 7.1 (2020), pp. 191–194. DOI: https://doi.org/10.1002/celc.201901703.

[26] Y. Seki et al. 'A novel device for detecting anaerobic threshold using sweat lactate during exercise'. In: *Scientific Reports* 11.1 (2021), p. 4929. DOI: 10.1038/s41598-021-84381-9.

[27] D. A. Sakharov et al. 'Relationship between Lactate Concentrations in Active Muscle Sweat and Whole Blood'. In: *Bulletin of Experimental Biology and Medicine* 150.1 (2010), pp. 83–85. DOI: 10.1007/s10517-010-1075-0.

[28] M. M. Pribil et al. 'Noninvasive Hypoxia Monitor Based on Gene-Free Engineering of Lactate Oxidase for Analysis of Undiluted Sweat'. In: *Analytical Chemistry* 86.11 (2014), pp. 5215–5219. DOI: 10.1021/ac501547u.

[29] M. Onor et al. 'Potentiometric sensor for non invasive lactate determination in human sweat'. In: *Analytica Chimica Acta* 989 (2017), pp. 80–87. DOI: 10.1016/j.aca.2017.07.050.

[30] K. Mitsubayashi et al. 'Analysis of metabolites in sweat as a measure of physical condition'. In: *Analytica Chimica Acta* 289.1 (1994), pp. 27–34. DOI: 10.1016/0003-2670(94)80004-9.

[31] C. A. Leinebø. 'Sensing Range Limitatios of Enzyme-Based Lactate Biosensor for Wearable Athletic Sweat Lactate Monitoring Applications'. Project report in TMT4510. Department of Materials Science Engineering, NTNU. Norwegian University of Science and Technology, 2022.

[32] J. Wang. *Analytical Electrochemistry*. 2rd ed. Hoboken, New Jersey: John Wiley & Sons, Inc., 2006.

[33] D. G. Rackus, M. H. Shamsi and A. R. Wheeler. 'Electrochemistry, biosensors and microfluidics: a convergence of fields'. In: *Chemical Society Reviews* 44.15 (2015), pp. 5320–5340. DOI: 10.1039/C4CS00369A.

[34] PalmSense. *Teacher's Guide to the PalmSens Educational Kit. A general introduction, information, and instructions for experiments*. January 2023. PalmSens BV, 2023.

[35] C.H. Hamann, A. Hamnett and W. Vielstich. *Electrochemistry*. 2nd ed. Wiley-VHC, 2007.

[36] M. Ciobanu et al. '1 - Fundamentals'. In: *Handbook of Electrochemistry*. Ed. by C. G. Zoski. Elsevier, 2007. Chap. 1, pp. 3–29. DOI: https://doi.org/10.1016/B978-044451958-0.50002-1.

[37] S. Petrovic. 'Basic Electrochemistry Concepts'. In: *Electrochemistry Crash Course for Engineers*. Cham: Springer International Publishing, 2021, pp. 3–10. DOI: 10.1007/978-3-030-61562-8{_}2.

[38] Bond A. M. Oldham K. B. Myland J. C. *Electrochemical Science and Technology: Fundamentals and Applications*. John Wiley & Sons, Ltd, 2012.

[39] N. Elgrishi et al. 'A Practical Beginner's Guide to Cyclic Voltammetry'. In: *Journal of Chemical Education* 95.2 (2018), pp. 197–206. DOI: 10.1021/acs.jchemed.7b00361.

[40] Brian R. Eggins. *Chemical Sensors and Biosensors*. Ed. by David J. Ando. 2002.

[41] *www.biorender.com*. 2023.

[42] A. A. Karyakin and E. E. Karyakina. 'Electroanalytical applications of Prussian Blue and its analogs'. In: *Izvestiya Akademii Nauk. Seriya Khimicheskaya* 50.10 (2001), pp. 1728–1734.

[43] A. A. Karyakin, E. E. Karyakina and L. Gorton. 'On the mechanism of H2O2 reduction at Prussian Blue modified electrodes'. In: *Electrochemistry Communications* 1.2 (1999), pp. 78–82. DOI: 10.1016/S1388-2481(99)00010-7.

[44] B. Alberts et al. *Molecular biology of the cell*. 5th ed. Garland Science, 2008.

[45] Y. C. Tsai, S. Y. Chen and H. W. Liaw. 'Immobilization of lactate dehydrogenase within multiwalled carbon nanotube-chitosan nanocomposite for application to lactate biosensors'. In: *Sensors and Actuators B: Chemical* 125.2 (2007), pp. 474–481. DOI: 10.1016/J.SNB.2007.02.052.

[46] T. D. Gibson. 'Biosensors: The Stability Problem'. In: *Analusis* 27.7 (1999), pp. 630–638.

[47] C. Mateo et al. 'Improvement of enzyme activity, stability and selectivity via immobilization techniques'. In: *Enzyme and Microbial Technology* 40.6 (2007), pp. 1451–1463. DOI: 10.1016/J.ENZMICTEC.2007.01.018.

[48] L. Cao. 'Introduction: Immobilized Enzymes: Past, Present and Prospects'. In: *Carrier-bound Immobilized Enzymes*. 2005, pp. 1–52. DOI: https://doi.org/10.1002/3527607668.ch1.

[49] Y. Haiquan et al. 'Molecular engineering of industrial enzymes: Recent advances and future prospects'. In: *Applied microbiology and biotechnology* 98 (2013). DOI: 10.1007/s00253-013-5370-3.

[50] W. Wang and J. G. Saven. 'Designing gene libraries from protein profiles for combinatorial protein experiments'. In: *Nucleic acids research* 30.21 (2002). DOI: https://doi.org/10.1093/nar/gnf119.

[51] V. Vagenende, M. G. S. Yap and B. L. Trout. 'Mechanisms of Protein Stabilization and Prevention of Protein Aggregation by Glycerol'. In: *Biochemistry* 48.46 (2009), pp. 11084–11096. DOI: 10.1021/bi900649t.

[52] I. Taurino et al. 'Comparative study of three lactate oxidases from Aerococcus viridans for biosensing applications'. In: *Electrochimica Acta* 93 (2013), pp. 72–79. DOI: 10.1016/J.ELECTACTA.2013.01.080.

[53] B. Lillis et al. 'Investigation into immobilisation of lactate oxidase to improve stability'. In: *Sensors and Actuators B: Chemical* 68.1-3 (2000), pp. 109–114. DOI: 10.1016/S0925-4005(00)00469-X.

[54] H. Cunha-Silva et al. 'Inhibited enzymatic reaction of crosslinked lactate oxidase through a pH-dependent mechanism'. In: *Colloids and Surfaces B: Biointerfaces* 184 (2019), p. 110490. DOI: 10.1016/j.colsurfb.2019.110490.

[55] F. Ricci and G. Palleschi. 'Sensor and biosensor preparation, optimisation and applications of Prussian Blue modified electrodes'. In: *Biosensors and Bioelectronics* 21.3 (2005), pp. 389–407. DOI: 10.1016/J.BIOS.2004.12.001.

[56] H. Minagawa et al. 'Development of long life lactate sensor using thermostable mutant lactate oxidase'. In: *Biosensors and Bioelectronics* 13.3-4 (1998), pp. 313–318. DOI: 10.1016/S0956-5663(97)00123-1.

[57] M. R.Romero et al. 'Amperometric Biosensor for Direct Blood Lactate Detection'. In: *Analytical Chemistry* 82.13 (2010), pp. 5568–5572. DOI: 10.1021/ac1004426.

[58] Sigma Aldrich. *Lactate Oxidase from Aerococcus viridans*. https://www.sigmaaldrich.com/NL/en/product/sigma/l9795 (Accessed: 21.06.23).

[59] J. Wang. 'Nanomaterial-based electrochemical biosensors'. In: *Analyst* 130.4 (2005), pp. 421–426. DOI: 10.1039/B414248A.

[60] J. Wang. 'Carbon-Nanotube Based Electrochemical Biosensors: A Review'. In: *Electroanalysis* 17.1 (2005), pp. 7–14. DOI: 10.1002/elan.200403113.

[61] J. Li et al. 'DNA biosensor based on chitosan film doped with carbon nanotubes'. In: *Analytical Biochemistry* 346.1 (2005), pp. 107–114. DOI: 10.1016/J.AB.2005.07.037.

[62] S. Bollo, N. F. Ferreyra and G. A. Rivas. 'Electrooxidation of DNA at Glassy Carbon Electrodes Modified with Multiwall Carbon Nanotubes Dispersed in Chitosan'. In: *Electroanalysis* 19.7-8 (2007), pp. 833–840. DOI: 10.1002/elan.200603782.

[63] J. Trzebinski et al. 'Hydrogel Membrane Improves Batch-to-Batch Reproducibility of an Enzymatic Glucose Biosensor'. In: *Electroanalysis* 23.12 (2011), pp. 2789–2795. DOI: https://doi.org/10.1002/elan.201100286.

[64] R. Garjonyte et al. 'Prussian Blue- and lactate oxidase-based amperometric biosensor for lactic acid'. In: *Sensors and Actuators B: Chemical* 79.1 (2001), pp. 33–38. DOI: 10.1016/S0925-4005(01)00845-0.

[65] M. G. Almeida, C. M. Silveira and José J.G. M. 'Biosensing nitrite using the system nitrite redutase/Nafion/methyl viologen—A voltammetric study'. In: *Biosensors and Bioelectronics* 22.11 (2007), pp. 2485–2492. DOI: 10.1016/J.BIOS.2006.09.027.

[66] J. J. Burmeister, M. Palmer and G. A. Gerhardt. 'l-lactate measures in brain tissue with ceramic-based multisite microelectrodes'. In: *Biosensors and Bioelectronics* 20.9 (2005), pp. 1772–1779. DOI: 10.1016/J.BIOS.2004.07.003.

[67] K. A. Mauritz and R. B. Moore. 'State of Understanding of Nafion'. In: *Chemical Reviews* 104.10 (2004), pp. 4535–4586. DOI: 10.1021/cr0207123.

[68] R. A. Rozendal, H. V. M. Hamelers and C. J. N. Buisman. 'Effects of Membrane Cation Transport on pH and Microbial Fuel Cell Performance'. In: *Environmental Science & Technology* 40.17 (2006), pp. 5206–5211. DOI: 10.1021/es060387r.

[69] G. Fortier, M. Vaillancourt and D. Bélanger. 'Evaluation of nafion as media for glucose oxidase immobilization for the development of an amperometric glucose biosensor'. In: *Electroanalysis* 4.3 (1992). DOI: 10.1002/elan.1140040304.

[70] W. D. Callister and D. G. Rethwisch. 'Characteristics, Applications, and Processing of Polymers'. In: *Materials Science and Engineering: An Introduction.* 10th. Wiley, 2018. Chap. 15, pp. 511–563.

[71] T. J. G. Skalski et al. 'Sulfophenylated Terphenylene Copolymer Membranes and Ionomers'. In: *ChemSusChem* 11.23 (2018), pp. 4033–4043. DOI: https://doi.org/10.1002/cssc.201801965.

[72] T. H. Yu et al. 'Mechanism for Degradation of Nafion in PEM Fuel Cells from Quantum Mechanics Calculations'. In: *Journal of the American Chemical Society* 133.49 (2011), pp. 19857–19863. DOI: 10.1021/ja2074642.

[73] L. Tian. 'Stabilizing proton exchange membranes using Cerium(III) ions'. Master's Thesis. Simon Fraser University, 2021.

[74] T. Weissbach, T. J. Peckham and S. Holdcroft. 'CeO2, ZrO2 and YSZ as mitigating additives against degradation of proton exchange membranes by free radicals'. In: *Journal of Membrane Science* 498 (2016), pp. 94–104. DOI: 10.1016/J.MEMSCI.2015.10.004.

[75] M. Zatoń et al. 'Migration of Ce and Mn Ions in PEMFC and Its Impact on PFSA Membrane Degradation'. In: *Journal of The Electrochemical Society* 165.6 (2018), F3281–F3289. DOI: 10.1149/2.0311806jes.

[76] Q. Zhao, P. Majsztrik and J. Benziger. 'Diffusion and Interfacial Transport of Water in Nafion'. In: *The Journal of Physical Chemistry B* 115.12 (2011), pp. 2717–2727. DOI: 10.1021/jp1112125.

[77] F. D. Coms, H. Liu and J. E. Owejan. 'Mitigation of Perfluorosulfonic Acid Membrane Chemical Degradation Using Cerium and Manganese Ions'. In: *ECS Transactions* 16.2 (2008), pp. 1735–1747. DOI: 10.1149/1.2982015.

[78] B. P. Pearman et al. 'The degradation mitigation effect of cerium oxide in polymer electrolyte membranes in extended fuel cell durability tests'. In: *Journal of Power Sources* 225 (2013), pp. 75–83. DOI: 10.1016/j.jpowsour.2012.10.015.

[79] Z. Wang et al. 'Synthesis of Nafion/CeO2 hybrid for chemically durable proton exchange membrane of fuel cell'. In: *Journal of Membrane Science* 421-422 (2012), pp. 201–210. DOI: 10.1016/j.memsci.2012.07.014.

[80] K. Itaya, I. Uchida and V. D. Neff. 'Electrochemistry of polynuclear transition metal cyanides: Prussian blue and its analogues'. In: *Accounts of Chemical Research* 19.6 (1986), pp. 162–168. DOI: 10.1021/ar00126a001.

[81] A. A. Karyakin. 'Prussian blue and its analogues: Electrochemistry and analytical applications'. In: *Electroanalysis* 13.10 (2001), pp. 813–819. DOI: 10.1002/1521-4109(200106)13:10<813::AID-ELAN813>3.0.CO;2-Z.

[82] J. F. Keggin and F. D. Miles. 'Structures and formulæ of the prussian blues and related compounds [4]'. In: *Nature* 137.3466 (1936). DOI: 10.1038/137577a0.

[83] F. Tian and N. Dale. 'Hexacyanoferrates as Mediators for Microelectrode Biosensors'. In: *Microelectrode Biosensors*. Ed. by S. Marinesco and N. Dale. Humana Press, 2013, pp. 69–93. DOI: 10.1007/978-1-62703-370-1{_}4.

[84] V. D. Ivanov. 'Four decades of electrochemical investigation of Prussian blue'. In: *Ionics* 26.2 (2020). DOI: 10.1007/s11581-019-03292-y.

[85] C. A. Lundgren and R. W. Murray. 'Observations on the composition of Prussian blue films and their electrochemistry'. In: *Inorganic Chemistry* 27.5 (2002), pp. 933–939. DOI: 10.1021/ic00278a036.

[86] K. Itaya, T. Ataka and S. Toshima. 'Spectroelectrochemistry and electrochemical preparation method of Prussian blue modified electrodes'. In: *Journal of the American Chemical Society* 104.18 (1982), pp. 4767–4772. DOI: 10.1021/ja00382a006.

[87] A. A. Karyakin, E. E. Karyakina and L. Gorton. 'Prussian-Blue-based amperometric biosensors in flow-injection analysis'. In: *Talanta* 43.9 (1996), pp. 1597–1606. DOI: 10.1016/0039-9140(96)01909-1.

[88] K. Itaya, H. Akahoshi and S. Toshima. 'Electrochemistry of Prussian Blue Modified Electrodes: An Electrochemical Preparation Method'. In: *Journal of The Electrochemical Society* 129.7 (1982). DOI: 10.1149/1.2124191.

[89] F. Ricci et al. 'Prussian Blue based screen printed biosensors with improved characteristics of long-term lifetime and pH stability'. In: *Biosensors and Bioelectronics* 18.2-3 (2003), pp. 165–174. DOI: 10.1016/S0956-5663(02)00169-0.

[90] A. A. Karyakin and E. E. Karyakina. 'Prussian Blue-based 'artificial peroxidase' as a transducer for hydrogen peroxide detection. Application to biosensors'. In: *Sensors and Actuators B: Chemical* 57.1-3 (1999), pp. 268–273. DOI: 10.1016/S0925-4005(99)00154-9.

[91] I. L. De Mattos et al. 'Sensor for hydrogen peroxide based on Prussian Blue modified electrode: Improvement of the operational stability'. In: *Analytical Sciences* 16.8 (2000). DOI: 10.2116/analsci.16.795.

[92] S. Saeed et al. 'Understanding electrochemical cation insertion into prussian blue from electrode deformation and mass changes'. In: *Chemical Communications* 57.55 (2021). DOI: 10.1039/d1cc01681d.

[93] A. L. Crumbliss, P. S. Lugg and N. Morosoff. 'Alkali metal cation effects in a Prussian blue surface modified electrode'. In: *Inorganic Chemistry* 23.26 (1984), pp. 4701–4708. DOI: 10.1021/ic00194a057.

[94] J. J. García-Jareño et al. 'Study of Prussian Blue (PB) films by ac-electrogravimetry: influence of PB morphology on ions movement'. In: *Electrochimica Acta* 45.22-23 (2000), pp. 3765–3776. DOI: 10.1016/S0013-4686(00)00470-9.

[95] B. J. Feldman and O. R. Melroy. 'Ion flux during electrochemical charging of Prussian Blue films'. In: *Journal of Electroanalytical Chemistry and Interfacial Electrochemistry* 234.1-2 (1987), pp. 213–227. DOI: 10.1016/0022-0728(87)80173-0.

[96] K. C. Lin, S. Muthukumar and S. Prasad. 'Flex-GO (Flexible graphene oxide) sensor for electrochemical monitoring lactate in low-volume passive perspired human sweat'. In: *Talanta* 214 (2020), p. 120810. DOI: 10.1016/j.talanta.2020.120810.

[97] X. Xuan et al. 'Lactate Biosensing for Reliable On-Body Sweat Analysis'. In: *ACS Sensors* 6.7 (2021), pp. 2763–2771. DOI: 10.1021/acssensors.1c01009.

[98] W. Gao et al. 'Fully integrated wearable sensor arrays for multiplexed in situ perspiration analysis'. In: *Nature* 529.7587 (2016), pp. 509–514. DOI: 10.1038/nature16521.

[99] M. Cuartero, M. Parrilla and G. Crespo. 'Wearable Potentiometric Sensors for Medical Applications'. In: *Sensors* 19.2 (2019), p. 363. DOI: 10.3390/s19020363.

[100] C. J. Harvey, R. F. LeBouf and A. B. Stefaniak. 'Formulation and stability of a novel artificial human sweat under conditions of storage and use'. In: *Toxicology in Vitro* 24.6 (2010), pp. 1790–1796. DOI: 10.1016/J.TIV.2010.06.016.

[101] I. Alvear-Ordenes et al. 'Sweat Lactate, Ammonia, and Urea in Rugby Players'. In: *International Journal of Sports Medicine* 26.8 (2005), pp. 632–637. DOI: 10.1055/s-2004-830380.

[102] J. M. Green et al. 'Effects of High and Low Blood Lactate Concentrations on Sweat Lactate Response'. In: *International Journal of Sports Medicine* 21.8 (2000), pp. 556–560. DOI: 10.1055/s-2000-8483.

[103] M. J. Patterson, S. D. R. Galloway and M. A. Nimmo. 'Variations in Regional Sweat Composition in Normal Human Males'. In: *Experimental Physiology* 85.6 (2000), pp. 869–875. DOI: https://doi.org/10.1111/j.1469-445X.2000.02058.x.

[104] I. Shitanda et al. 'Air-Bubble-Insensitive Microfluidic Lactate Biosensor for Continuous Monitoring of Lactate in Sweat'. In: *ACS Sensors* (2023). DOI: 10.1021/acssensors.3c00490.

[105] E. V. Karpova and A. A. Karyakin. 'Noninvasive monitoring of diabetes and hypoxia by wearable flow-through biosensors'. In: *Current Opinion in Electrochemistry* 23 (2020), pp. 16–20. DOI: 10.1016/J.COELEC.2020.02.018.

[106] S. Biagi et al. 'Simultaneous determination of lactate and pyruvate in human sweat using reversed-phase high-performance liquid chromatography: a noninvasive approach'. In: *Biomedical Chromatography* 26.11 (2012), pp. 1408–1415. DOI: 10.1002/bmc.2713.

[107] S. Søpstad et al. 'Long-term stability of screen-printed pseudo-reference electrodes for electrochemical biosensors'. In: *Electrochimica Acta* 287 (2018), pp. 29–36. DOI: 10.1016/j.electacta.2018.08.045.

[108] Y. Wu et al. 'Water transport through hydrocarbon-based proton exchange membranes'. In: *Journal of Membrane Science* 610 (2020), p. 118276. DOI: 10.1016/j.memsci.2020.118276.

[109] J. Peron et al. 'Properties of Nafion® NR-211 membranes for PEMFCs'. In: *Journal of Membrane Science* 356.1-2 (2010), pp. 44–51. DOI: 10.1016/J.MEMSCI.2010.03.025.

[110] K. A. Striebel, G. G. Scherer and O. Haas. 'Effect of curing-humidity on recast-nation films'. In: *Journal of Electroanalytical Chemistry and Interfacial Electrochemistry* 304.1-2 (1991), pp. 289–296. DOI: 10.1016/0022-0728(91)85512-N.

[111] S. Vengatesan et al. 'Effects of curing condition of solution cast Nafion® membranes on PEMFC performance'. In: *Korean Journal of Chemical Engineering* 26.3 (2009), pp. 679–684. DOI: 10.1007/s11814-009-0113-y.

[112] X. Gao et al. 'Impact of the Composition of Alcohol/Water Dispersion on the Proton Transport and Morphology of Cast Perfluorinated Sulfonic Acid Ionomer Thin Films'. In: *ACS Omega* 6.22 (2021), pp. 14130–14137. DOI: 10.1021/acsomega.1c00607.

[113] P. Trogadas, J. Parrondo and V. Ramani. 'Degradation Mitigation in Polymer Electrolyte Membranes Using Cerium Oxide as a Regenerative Free-Radical Scavenger'. In: *Electrochemical and Solid-State Letters* 11.7 (2008), B113. DOI: 10.1149/1.2916443.

[114] V. D. Thuc, V. D. Cong Tinh and D. Kim. 'Simultaneous improvement of proton conductivity and chemical stability of Nafion membranes via embedment of surface-modified ceria nanoparticles in membrane surface'. In: *Journal of Membrane Science* 642 (2022), p. 119990. DOI: 10.1016/j.memsci.2021.119990.

[115] R. F. Silva, M. De Francesco and A. Pozio. 'Solution-cast Nafion® ionomer membranes: preparation and characterization'. In: *Electrochimica Acta* 49.19 (2004), pp. 3211–3219. DOI: 10.1016/J.ELECTACTA.2004.02.035.

[116] Sigma Aldrich. *Cerium(III) chloride heptahydrate.* https://www.sigmaaldrich.com/NO/en/product/aldrich/228931 (Accessed: 21.06.23).

[117] T. Agarwal et al. 'Mitigating cerium migration for perfluorosulfonic acid membranes using organic ligands'. In: *Journal of Power Sources* 554 (2023), p. 232320. DOI: 10.1016/j.jpowsour.2022.232320.

[118] H. Zou, S. Wu and J. Shen. 'Polymer/Silica Nanocomposites: Preparation, Characterization, Properties, and Applications'. In: *Chemical Reviews* 108.9 (2008), pp. 3893–3957. DOI: 10.1021/cr068035q.

[119] R. J. Mortimer and D. R. Rosseinsky. 'Electrochemical polychromicity in iron hexacyanoferrate films, and a new film form of ferric ferricyanide'. In: *Journal of Electroanalytical Chemistry* 151.1-2 (1983). DOI: 10.1016/S0022-0728(83)80429-X.

[120] S. Nasrazadani and S. Hassani. 'Modern analytical techniques in failure analysis of aerospace, chemical, and oil and gas industries'. In: *Handbook of Materials Failure Analysis with Case Studies from the Oil and Gas Industry*. Elsevier, 2016, pp. 39–54. DOI: 10.1016/B978-0-08-100117-2.00010-8.

[121] R. Vittal et al. 'CTAB-Promoted Prussian Blue-Modified Electrode and Its Cation Transport Characteristics for K+, Na+, Li+, and NH4+ Ions'. In: *The Journal of Physical Chemistry B* 112.4 (2008), pp. 1149–1156. DOI: 10.1021/jp074994s.

[122] J. Q. Ang et al. 'Ion-selective detection of non-intercalating Na+ using competitive inhibition of K+ intercalation in Prussian blue nanotubes sensor'. In: *Electrochimica Acta* 55.27 (2010), pp. 7903–7908. DOI: 10.1016/J.ELECTACTA.2010.04.025.

[123] H. L. Yeager and A. Steck. 'Cation and Water Diffusion in Nafion Ion Exchange Membranes: Influence of Polymer Structure'. In: *Journal of The Electrochemical Society* 128.9 (1981), pp. 1880–1884. DOI: 10.1149/1.2127757.

[124] W. Xing et al. 'Oxygen Solubility, Diffusion Coefficient, and Solution Viscosity'. In: *Rotating Electrode Methods and Oxygen Reduction Electrocatalysts*. Elsevier, 2014, pp. 1–31. DOI: 10.1016/B978-0-444-63278-4.00001-X.

Appendix A

Extended Results Cerium-Incorporated Membrane Sensors

Chronoamperometric data from the first testing round of all 19 sensors where cerium was incorporated in the sensor membrane. The following sensors are presented in addition to what was included in the Results section: PB|L|N*$^3_{50.0\%}$, PB|L|N*$^3_{9.3\%}$, PB|L|N*$^3_{4.6\%}$, PB|L|S*$^3_{9.3\%}$ and 2 PB|L|N**$_{24.3\%}$. Figure A.1 present testing results from PB|L|N* and PB|L|S* sensors and Figure A.2 from PB|L|N** sensors. Table A.1 summarises the I_{max}/I$_{init}$ ratio and c_{max} for all tested sensors, sorted by decreasing c_{max}.

It can be observed from Figure A.1 that I_{max} was strictly increasing with a decrease in Ce^{3+} membrane content, with the exception of the PB|L|N*$^3_{50\%}$ sensor. The slightly higher responsiveness of one of the PB|L|N*$^3_{60.7\%}$ sensors was presumably owed to a non-sufficient membrane coverage of the WE. It is evident from the photo in Figure 4.5a that there was an opening in the membrane at the right edge of the WE, which would allow for a slight flux of lactate and O2 into the enzyme layer despite an otherwise impermeable membrane. When reducing the molarity of the cast $CeCl_3$(aq) solution, the density of the solid $CeCl_3$ layer is expected to have decreased, thus increasing membrane permeability and explaining the observed trend.

Only one PB|L|S* sensor was tested, made with the co-casting method. It was evaluated that this method was not suitable for cerium incorporation into the sensor membranes, and thus the performance of cerium-SPPB membranes was not investigated in this work. The PB|L|S*$_{9.3\%}$ sensor behaved similar to the PB|L|N* sensors, with a high I_{init}/I_{max} ratio.

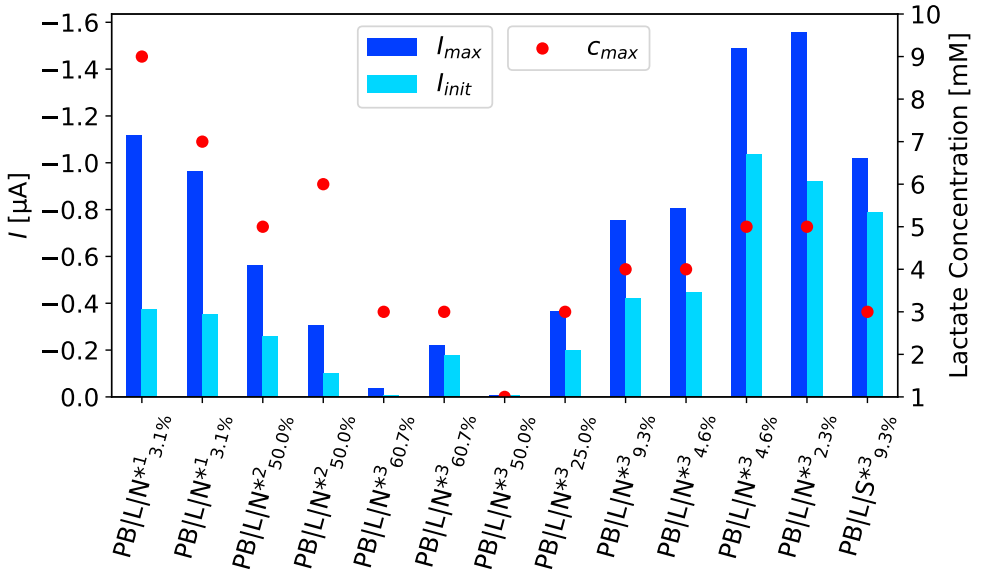

Figure A.1. Responses of all PB|L|N* and PB|L|S* sensors to increasing lactate concentrations, displaying the current signal at the first (I_{init}) and last (I_{max}) lactate increment (left axis). The c_{max} markers denote the maximum detected lactate concentration (right axis). The x-axis specifies the sensor formulation, with cerium loading method (1,2,3) and content (%). * = Ce^{3+}.

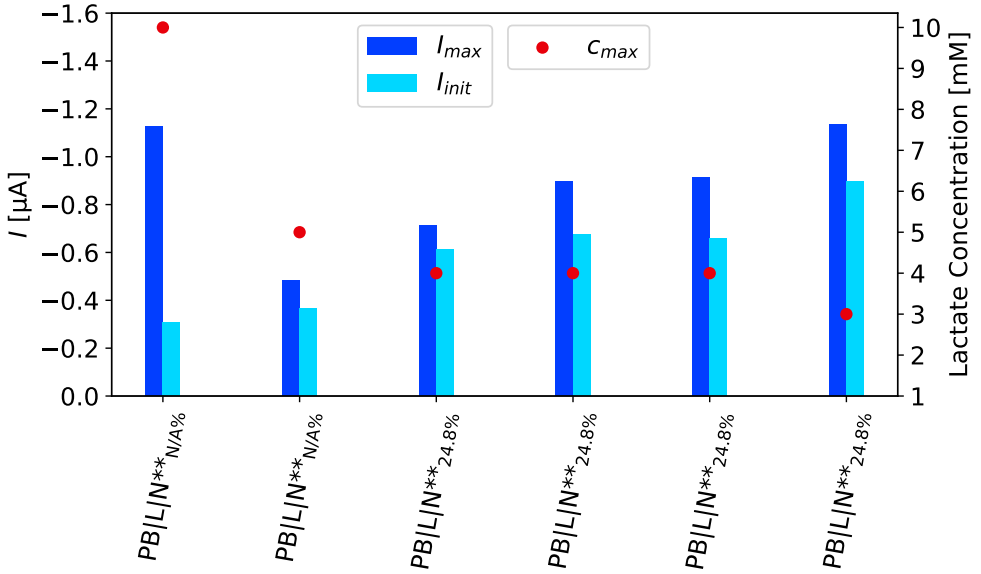

Figure A.2. Responses of all PB|L|N** sensors to increasing lactate concentrations, displaying the current signal at the first (I_{init}) and last (I_{max}) lactate increment (left axis). The c_{max} markers denote the maximum detected lactate concentration (right axis). The x-axis specifies the sensor formulation, with cerium loading content (%). ** = CeO_2.

Table A.1. Ratio between initial current step (I_{init}) and maximum current signal (I_{max}) and maximum detected lactate concentration (c_{max}) for sensors with cerium-modified membranes. The sensor formulation is specified, with cerium loading method (1,2,3) and content (%). * = Ce^{3+} and ** = CeO_2

Sensor Formulation	$\boldsymbol{I_{init}/I_{max}}$	$\boldsymbol{c_{max}}$
PB|L|N**$_{N/A\%}$	0.270	10
PB|L|N**$_{N/A\%}$	0.742	5
PB|L|N*1$_{3.1\%}$	0.336	9
PB|L|N*1$_{3.1\%}$	0.365	7
PB|L|N*2$_{50\%}$	0.347	6
PB|L|N*2$_{50\%}$	0.329	5
PB|L|N*3$_{4.6\%}$	0.551	5
PB|L|N*3$_{4.6\%}$	0.696	4
PB|L|N*3$_{2.3\%}$	0.591	5
PB|L|N*3$_{9.3\%}$	0.557	4
PB|L|N**$_{24.8\%}$	0.720	4
PB|L|N**$_{24.8\%}$	0.752	4
PB|L|N**$_{24.8\%}$	0.856	4
PB|L|N**$_{24.8\%}$	0.789	3
PB|L|N*3$_{60.7\%}$	0.191	3
PB|L|N*3$_{60.7\%}$	0.811	3
PB|L|N*3$_{25\%}$	0.548	3
PB|L|S*3$_{9.3\%}$	0.773	3
PB|L|N*3$_{50\%}$	1.000	1

Appendix B

Chronoamperometry Raw Data

All presented lactate sensors were chronoamperometrically tested in PBS for 2 or 3 rounds, with approximately 1 hour between each subsequent testing round. The raw testing data for all testing rounds are presented below. The figure captions specify the sensor formulation and testing conditions if relevant.

B.1 Lactate Increment Size

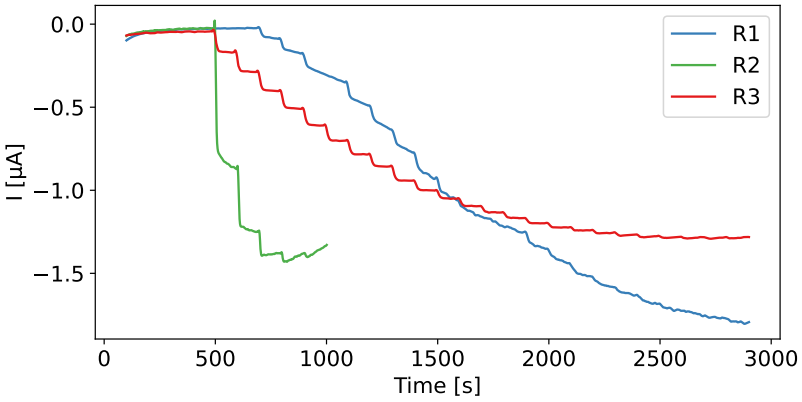

Figure B.1. 3 rounds of chronoamperometry measurements of PB|L|N sensor with 2 rounds of +0.1 mM and 1 round of +1 mM. Applied voltage was 0.0 V vs. Ag/AgCl.

B.2 Dissolved Oxygen Availability

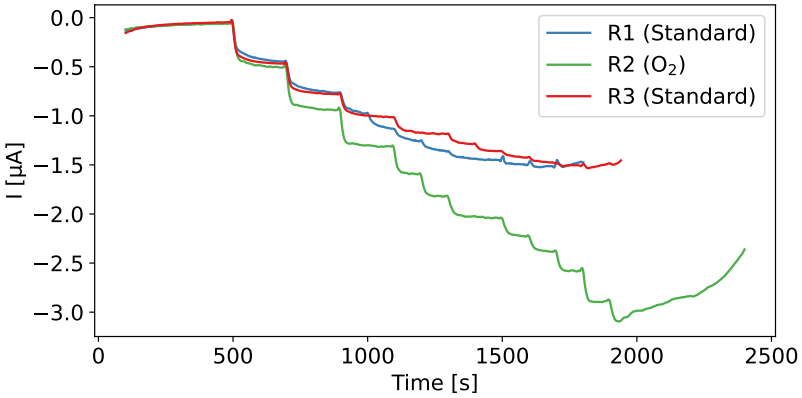

Figure B.2. 3 rounds of chronoamperometry measurements of PB|L|N sensor with O_2 gas purging into the solution. Applied voltage was 0.0 V vs. Ag/AgCl.

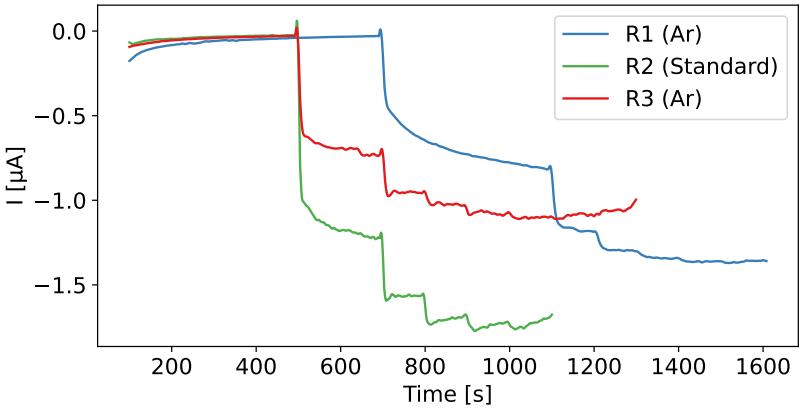

Figure B.3. 3 rounds of chronoamperometry measurements of PB|L|N sensor with Ar gas purging into the solution. Applied voltage was 0.0 V vs. Ag/AgCl.

B.3 Adjusting Enzyme Activity

Testing at 37°C

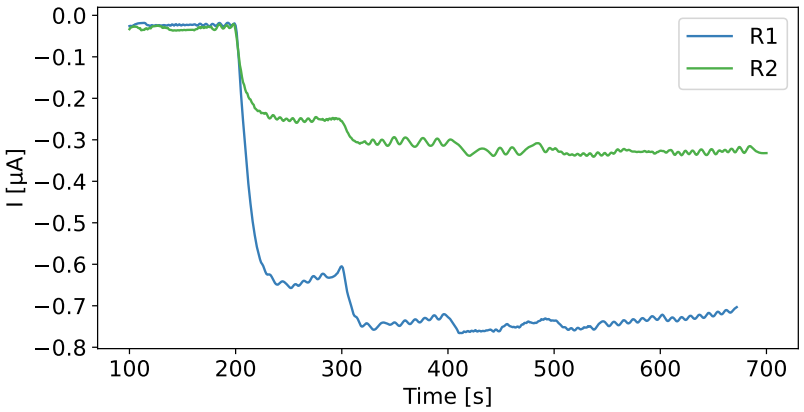

Figure B.4. 2 rounds of chronoamperometry measurements of a PB|L|N sensor at 37°C. Applied voltage was 0.0 V vs. Ag/AgCl.

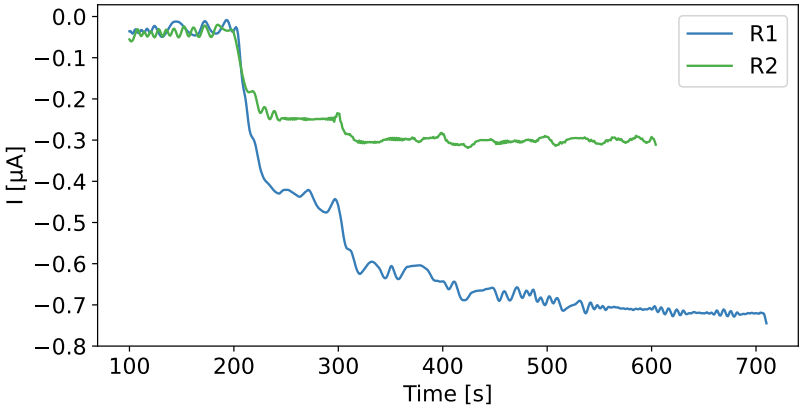

Figure B.5. 2 rounds of chronoamperometry measurements of a PB|L|N sensor at 37°C. Applied voltage was 0.0 V vs. Ag/AgCl.

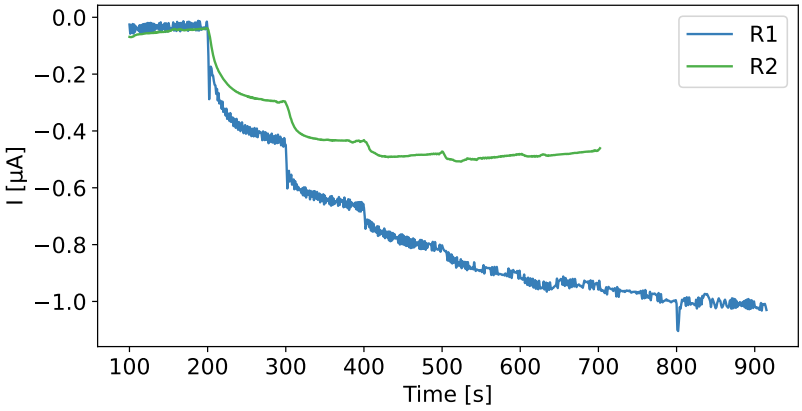

Figure B.6. 2 rounds of chronoamperometry measurements of a PB|L|N sensor at 37°C. Applied voltage was 0.0 V vs. Ag/AgCl.

Testing with 0.75 μL Loading

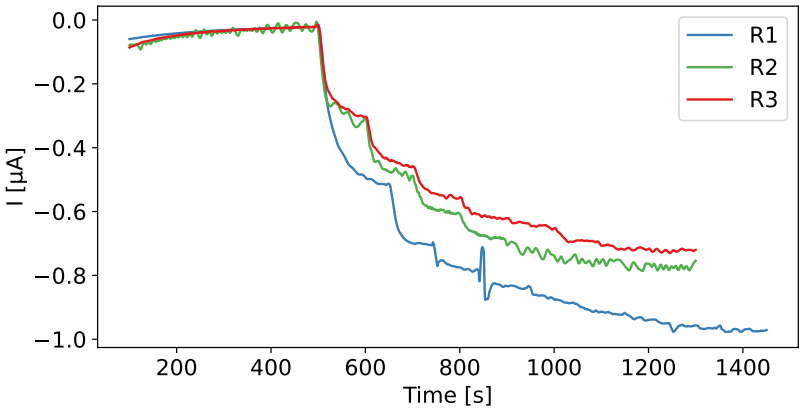

Figure B.7. 3 rounds of chronoamperometry measurements of a PB|1.5L|N. Applied voltage was 0.0 V vs. Ag/AgCl.

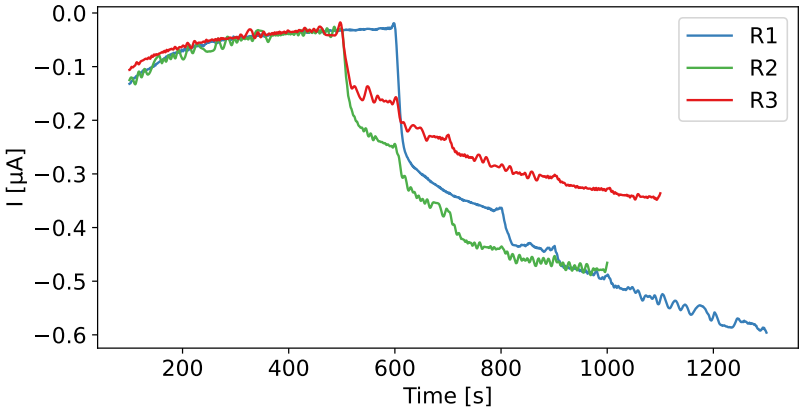

Figure B.8. 3 rounds of chronoamperometry measurements of a PB|1.5L|N. Applied voltage was 0.0 V vs. Ag/AgCl.

Testing with 1 μL Loading

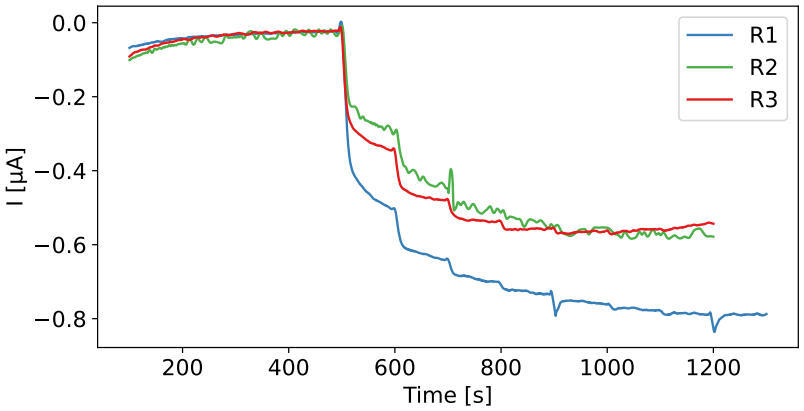

Figure B.9. 3 rounds of chronoamperometry measurements of a PB|2L|N. Applied voltage was 0.0 V vs. Ag/AgCl.

Testing with Glycerol Additive

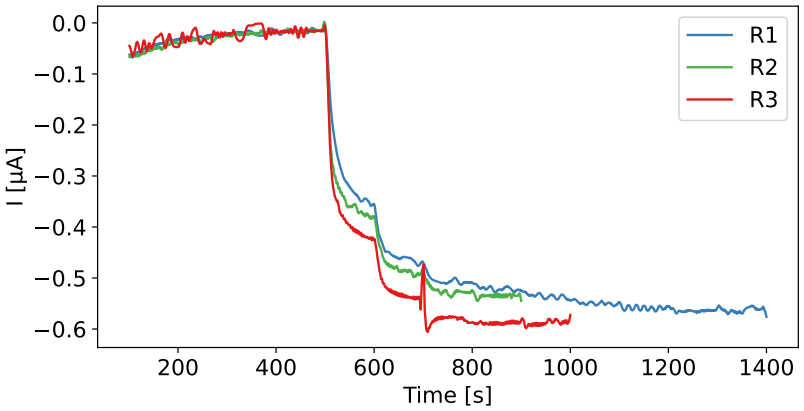

Figure B.10. 3 rounds of chronoamperometry measurements of a PB|L^{Gly}|N. Applied voltage was 0.0 V vs. Ag/AgCl.

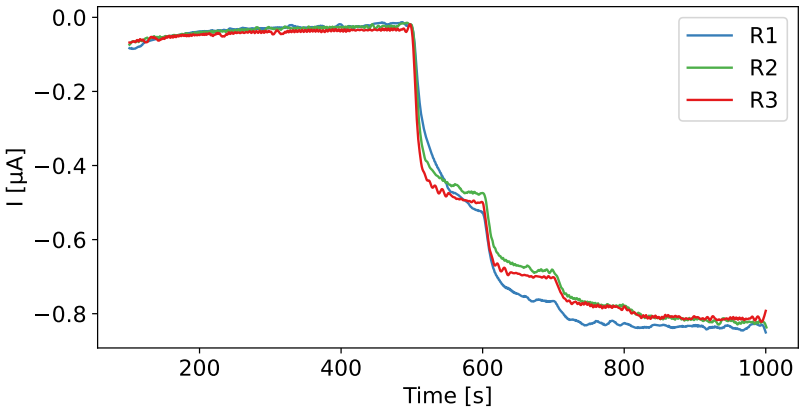

Figure B.11. 3 rounds of chronoamperometry measurements of a PB|L^{Gly}|N. Applied voltage was 0.0 V vs. Ag/AgCl.

Testing with Glucose Additive

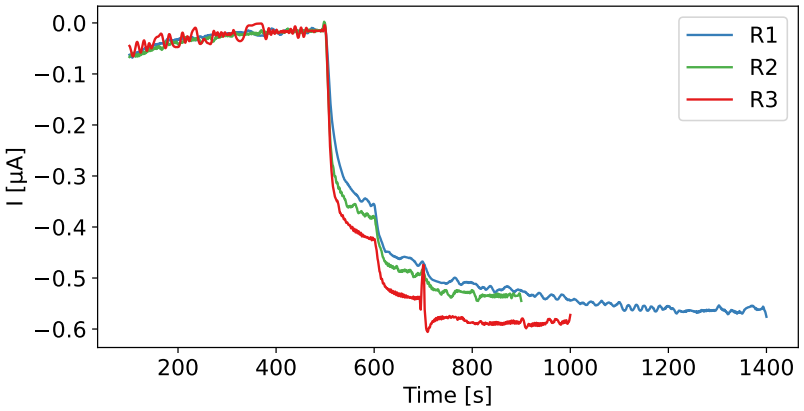

Figure B.12. 3 rounds of chronoamperometry measurements of a PB|L^{Glu}|N. Applied voltage was 0.0 V vs. Ag/AgCl.

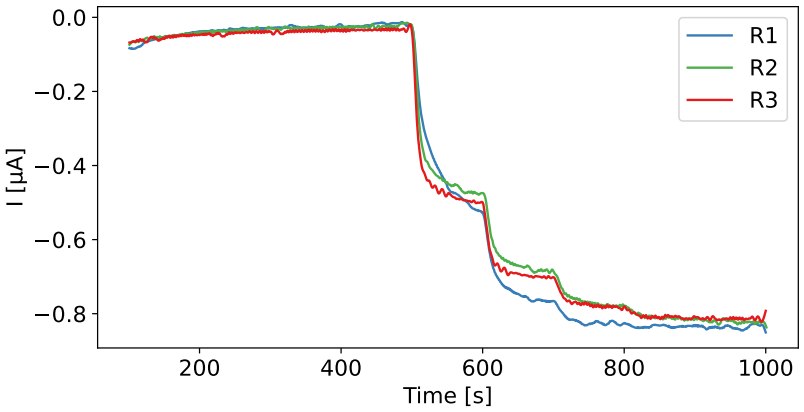

Figure B.13. 3 rounds of chronoamperometry measurements of a PB|L^{Glu}|N. Applied voltage was 0.0 V vs. Ag/AgCl.

B.4 Adjusting Membrane Permeability

SPPB Membranes

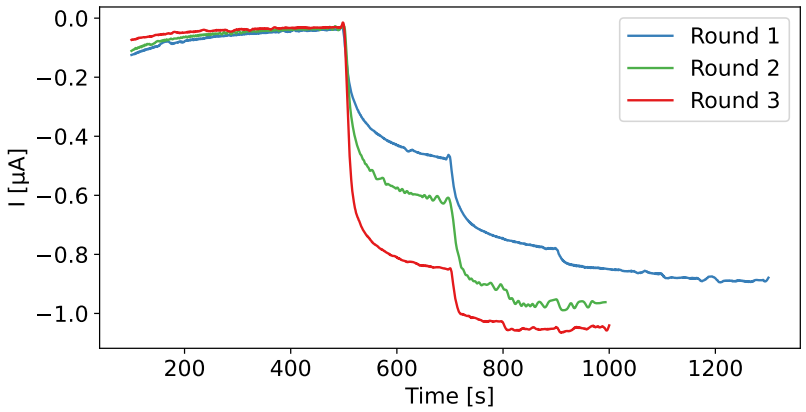

Figure B.14. 3 rounds of chronoamperometry measurements of a PB|L|S (7.5 wt% SPPB in ethanol). Applied voltage was 0.0 V vs. Ag/AgCl.

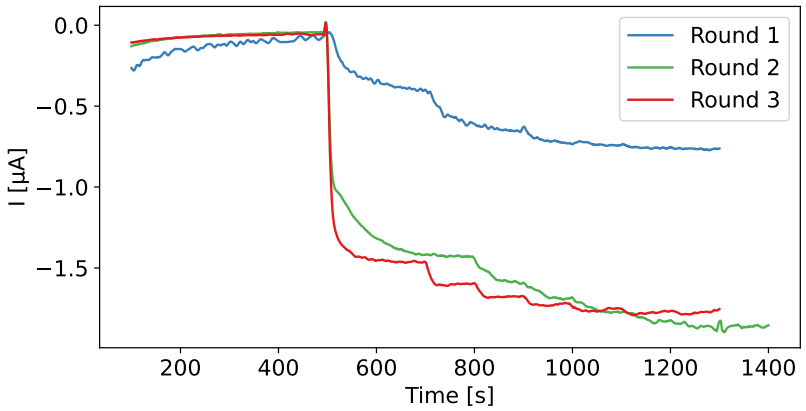

Figure B.15. 3 rounds of chronoamperometry measurements of a PB|L|S (7.5 wt% SPPB in ethanol). Applied voltage was 0.0 V vs. Ag/AgCl.

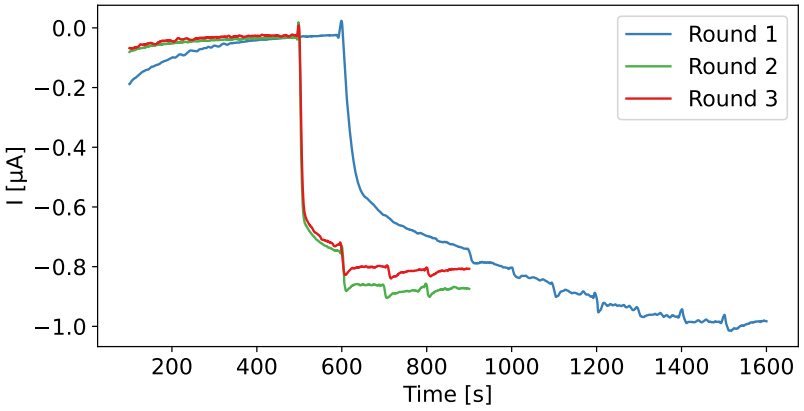

Figure B.16. 3 rounds of chronoamperometry measurements of a PB|L|S (2.5 wt% SPPB in ethanol). Applied voltage was 0.0 V vs. Ag/AgCl.

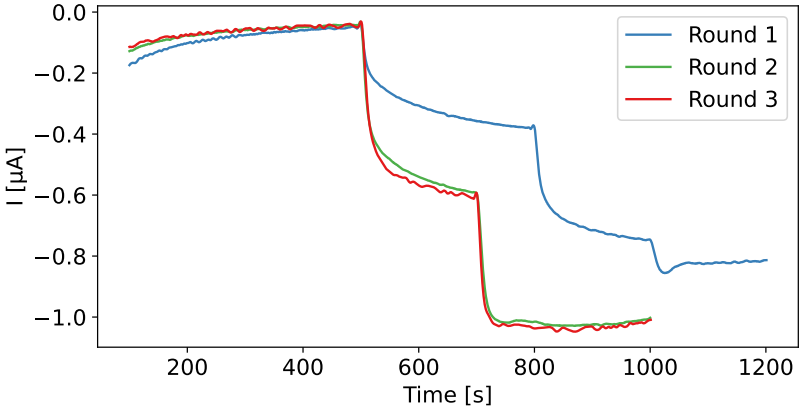

Figure B.17. 3 rounds of chronoamperometry measurements of a PB|L|S (2.5 wt% SPPB in ethanol and water). Applied voltage was 0.0 V vs. Ag/AgCl.

Cerium-Incorporated Membranes

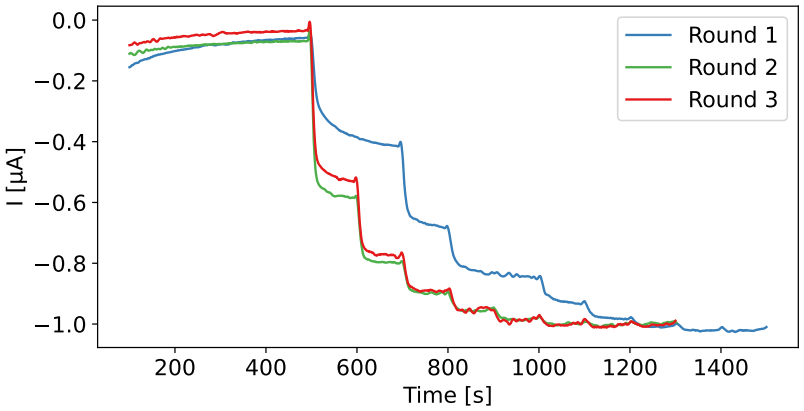

Figure B.18. 3 rounds of chronoamperometry measurements of a PB|L|N*1$_{3.1\%}$. Applied voltage was 0.0 V vs. Ag/AgCl.

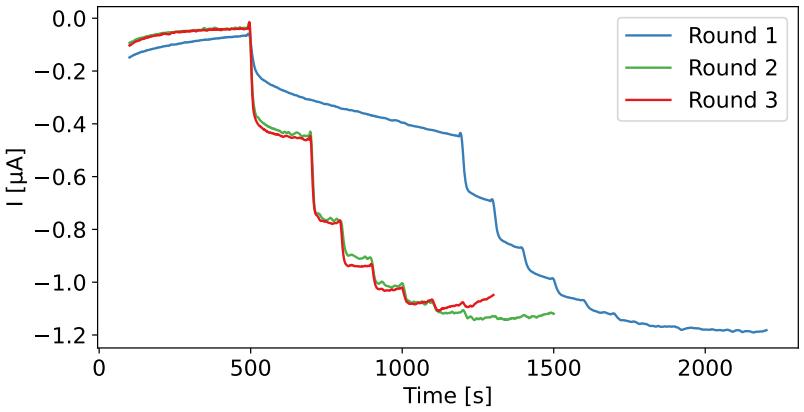

Figure B.19. 3 rounds of chronoamperometry measurements of a PB|L|N*1$_{3.1\%}$. Applied voltage was 0.0 V vs. Ag/AgCl.

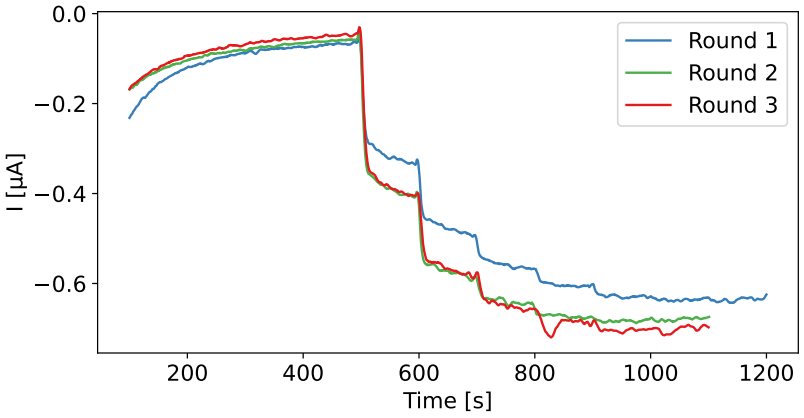

Figure B.20. 3 rounds of chronoamperometry measurements of a PB|L|N*$^{2}_{50\%}$. Applied voltage was 0.0 V vs. Ag/AgCl.

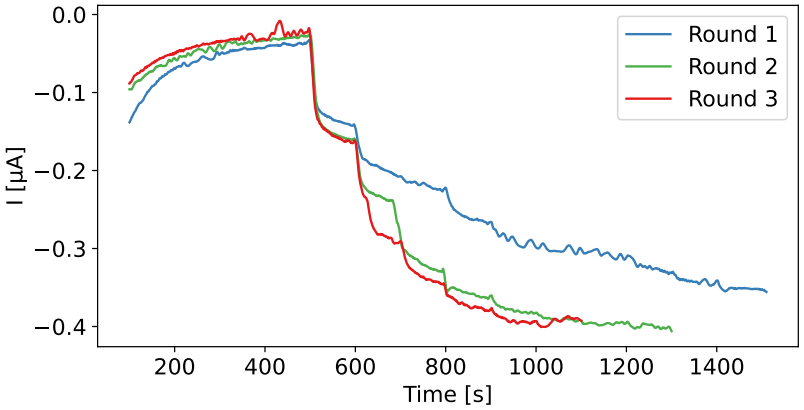

Figure B.21. 3 rounds of chronoamperometry measurements of a PB|L|N*$^{2}_{50\%}$. Applied voltage was 0.0 V vs. Ag/AgCl.

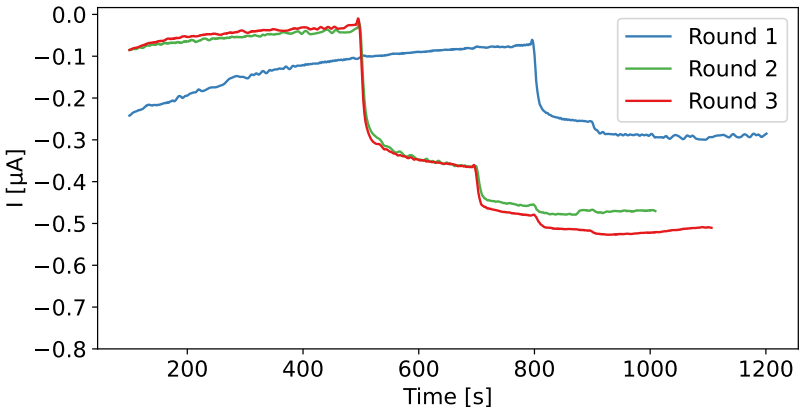

Figure B.22. 3 rounds of chronoamperometry measurements of a PB|L|N*$^{3}_{60.7\%}$. Applied voltage was 0.0 V vs. Ag/AgCl.

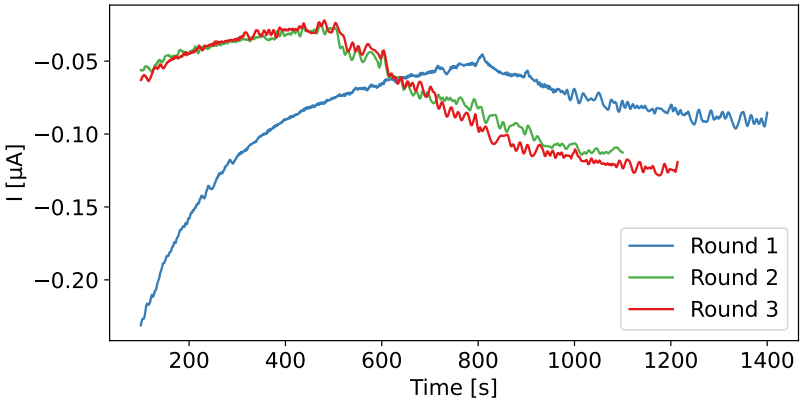

Figure B.23. 3 rounds of chronoamperometry measurements of a PB|L|$N^{*3}_{60.7\%}$. Applied voltage was 0.0 V vs. Ag/AgCl.

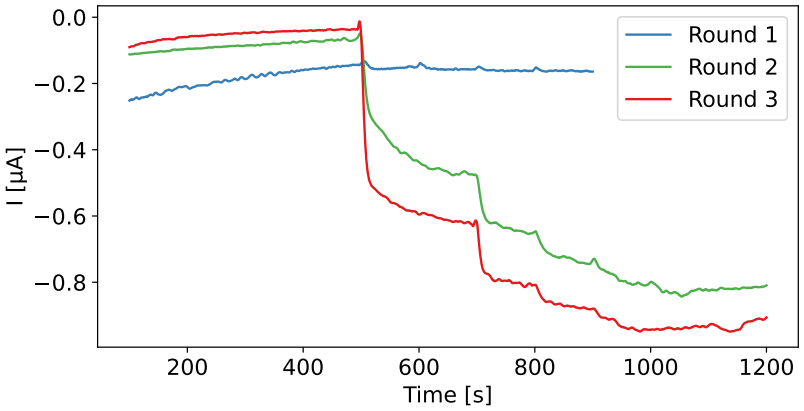

Figure B.24. 3 rounds of chronoamperometry measurements of a PB|L|$N^{*3}_{50\%}$. Applied voltage was 0.0 V vs. Ag/AgCl.

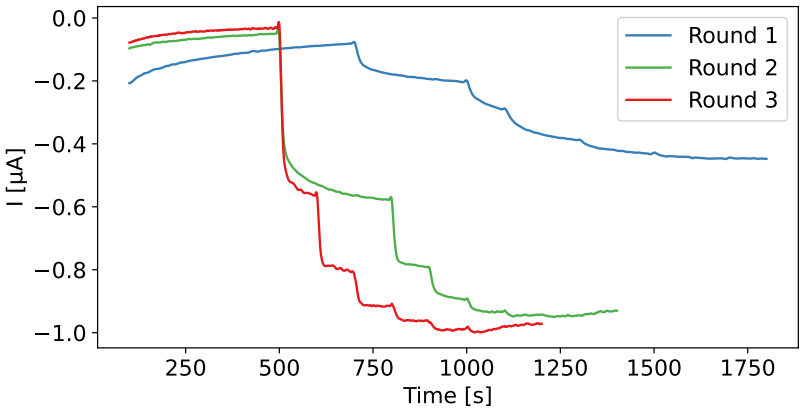

Figure B.25. 3 rounds of chronoamperometry measurements of a PB|L|$N^{*3}_{25\%}$. Applied voltage was 0.0 V vs. Ag/AgCl.

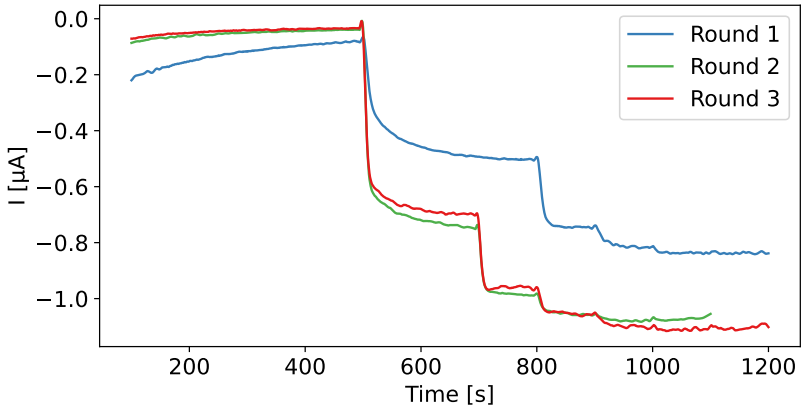

Figure B.26. 3 rounds of chronoamperometry measurements of a PB|L|N*$^{3}_{9.3\%}$. Applied voltage was 0.0 V vs. Ag/AgCl.

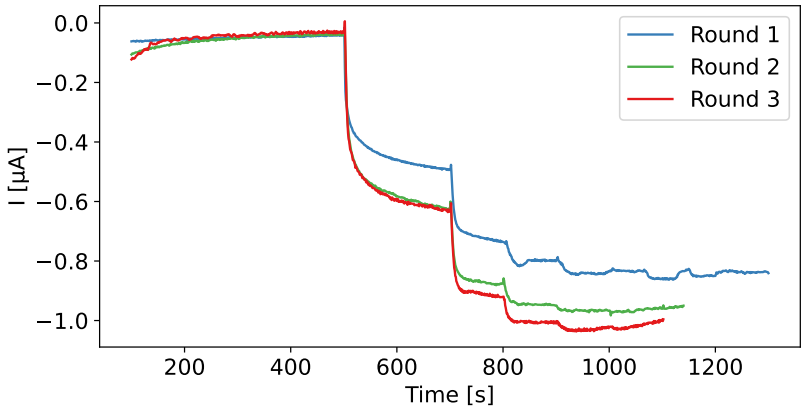

Figure B.27. 3 rounds of chronoamperometry measurements of a PB|L|N*$^{3}_{4.6\%}$. Applied voltage was 0.0 V vs. Ag/AgCl.

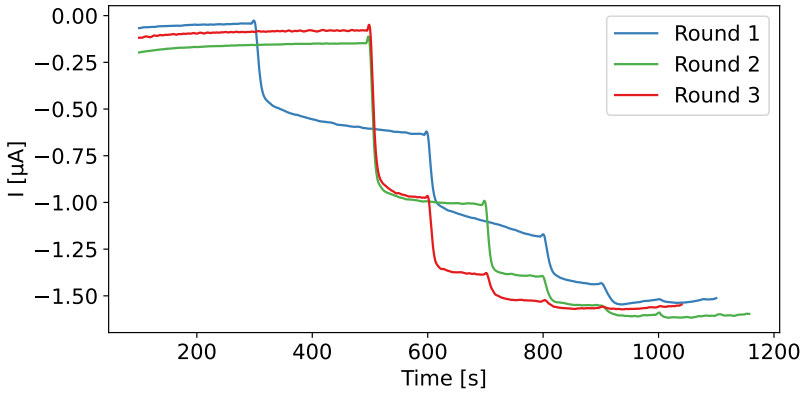

Figure B.28. 3 rounds of chronoamperometry measurements of a PB|L|N*$^{3}_{4.6\%}$. Applied voltage was 0.0 V vs. Ag/AgCl.

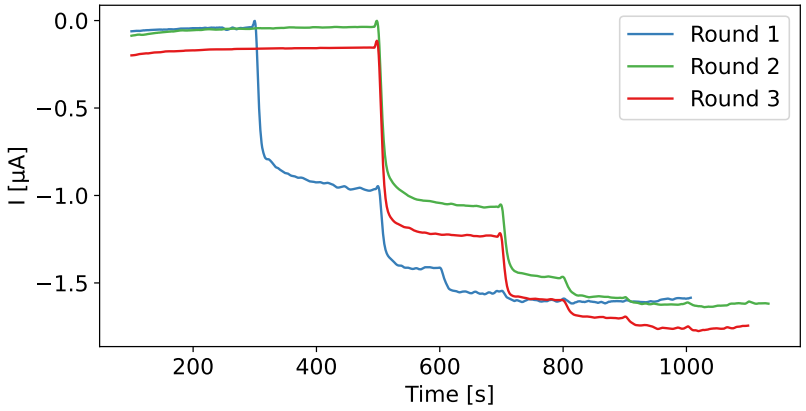

Figure B.29. 3 rounds of chronoamperometry measurements of a PB|L|N*$^{3}_{3.2\%}$. Applied voltage was 0.0 V vs. Ag/AgCl.

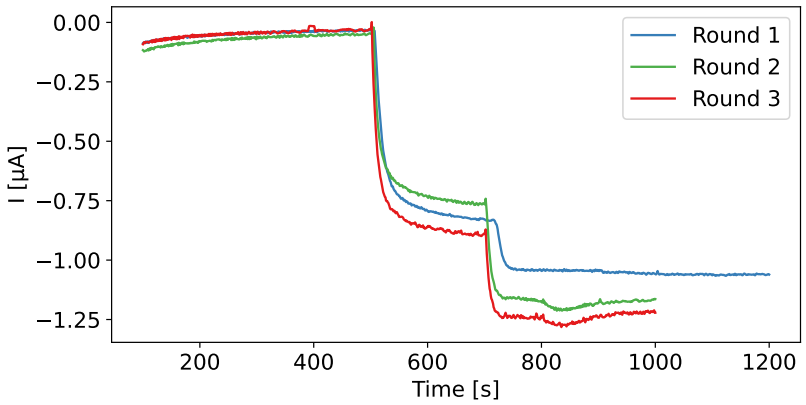

Figure B.30. 3 rounds of chronoamperometry measurements of a PB|L|S*$^{3}_{9.3\%}$. Applied voltage was 0.0 V vs. Ag/AgCl.

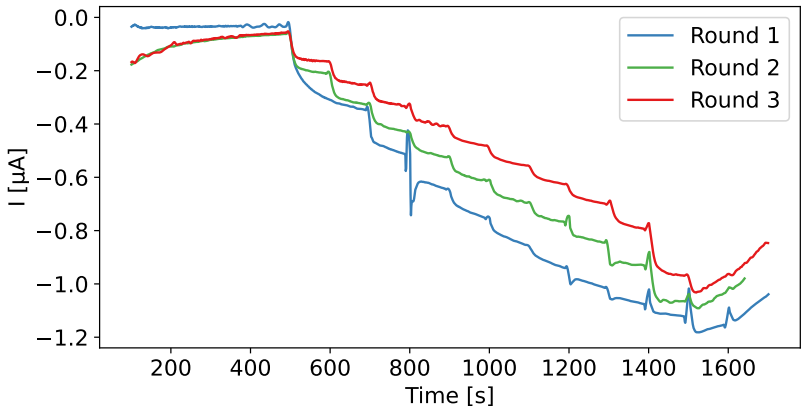

Figure B.31. 3 rounds of chronoamperometry measurements of a PB|L|N**$_{N/A\%}$. Applied voltage was 0.0 V vs. Ag/AgCl.

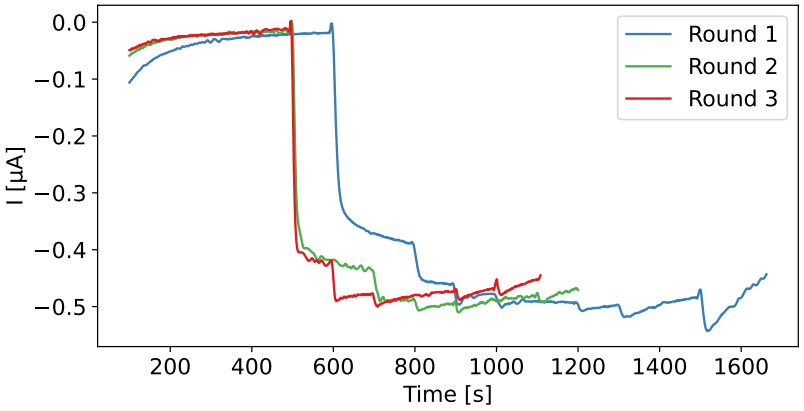

Figure B.32. 3 rounds of chronoamperometry measurements of a PB|L|N**$_{N/A\%}$. Applied voltage was 0.0 V vs. Ag/AgCl.

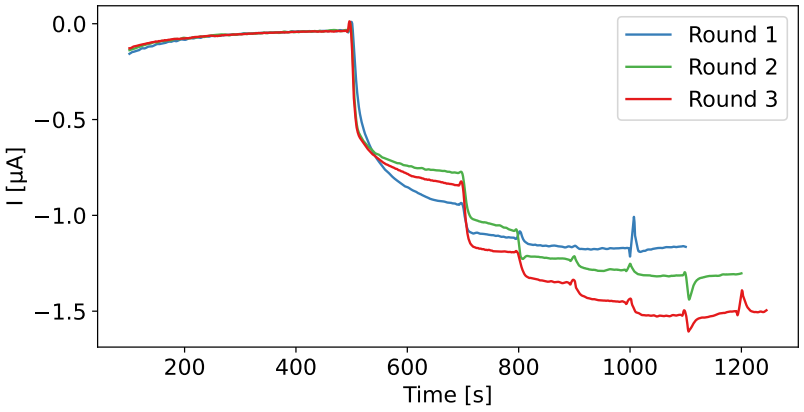

Figure B.33. 3 rounds of chronoamperometry measurements of a PB|L|N**$_{24.1\%}$. Applied voltage was 0.0 V vs. Ag/AgCl.

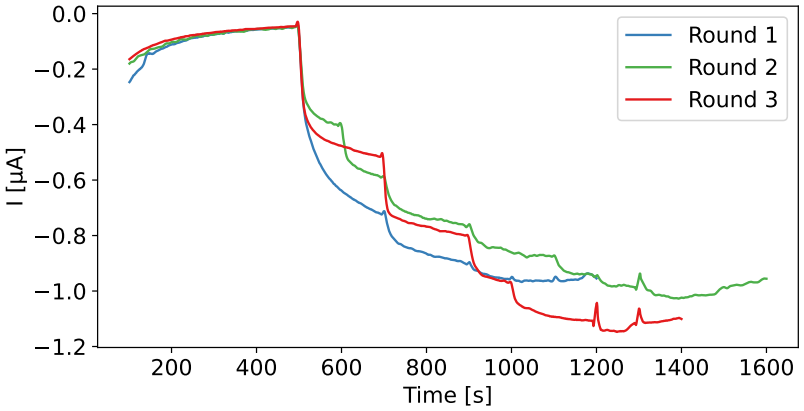

Figure B.34. 3 rounds of chronoamperometry measurements of a PB|L|N**$_{24.1\%}$. Applied voltage was 0.0 V vs. Ag/AgCl.

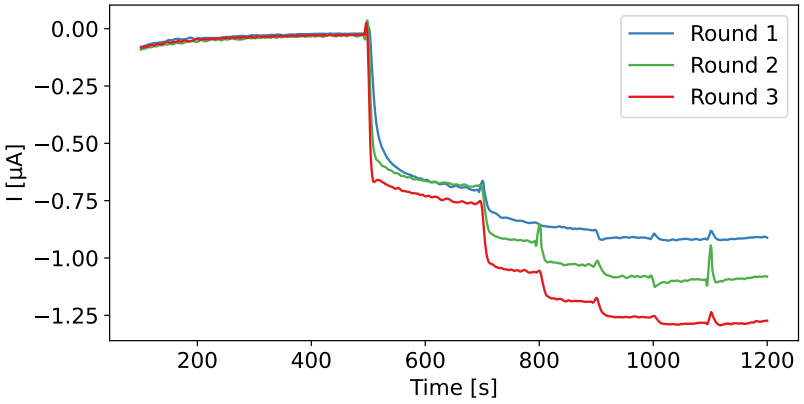

Figure B.35. 3 rounds of chronoamperometry measurements of a PB|L|N**$_{24.1\%}$. Applied voltage was 0.0 V vs. Ag/AgCl.

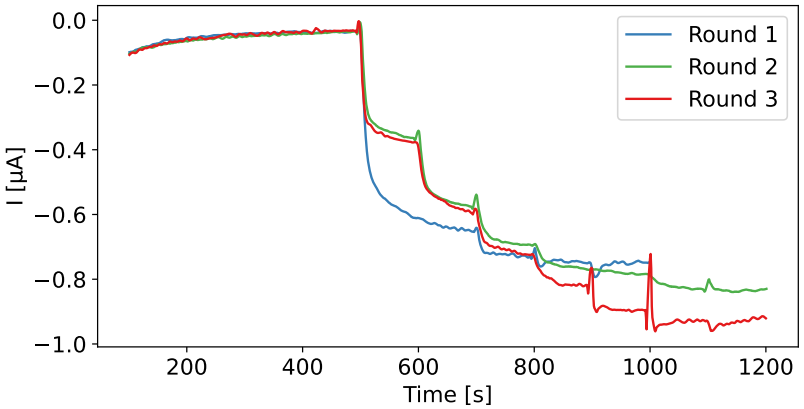

Figure B.36. 3 rounds of chronoamperometry measurements of a PB|L|N**$_{24.1\%}$. Applied voltage was 0.0 V vs. Ag/AgCl.

Appendix C

Cerium-Nafion Solution Precipitation

Pictures were captured of the CeCl-Nafion and CeO_2-Nafion membrane solutions made from direct mixing of cerium salt and Nafion. Figure C.1 shows the CeCl-Nafion, with the red arrow indicating a cross-linked Nafion precipitation. Figure C.2 shows the CeO_2-Nafion solution, where non-dispersed and agglomerated CeO_2 is readily visible, as indicated by the red arrow.

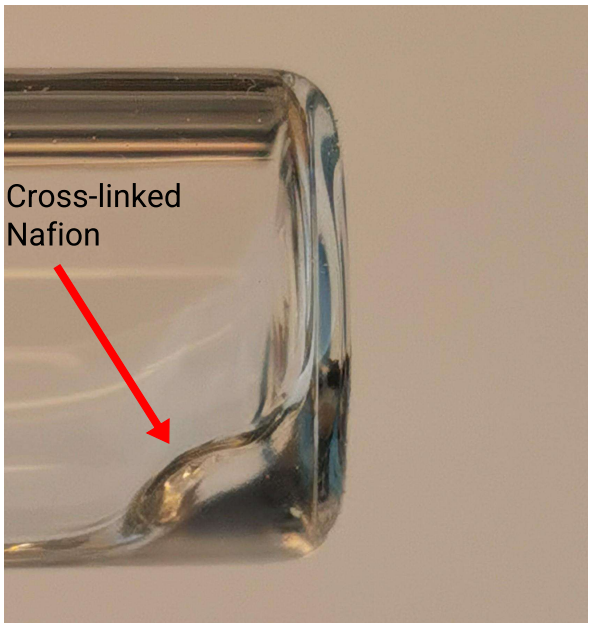

Figure C.1. Picture showing precipitation of cross-linked Nafion after the direct addition of $CeCl_3$(s) to the Nafion ionomer solution.

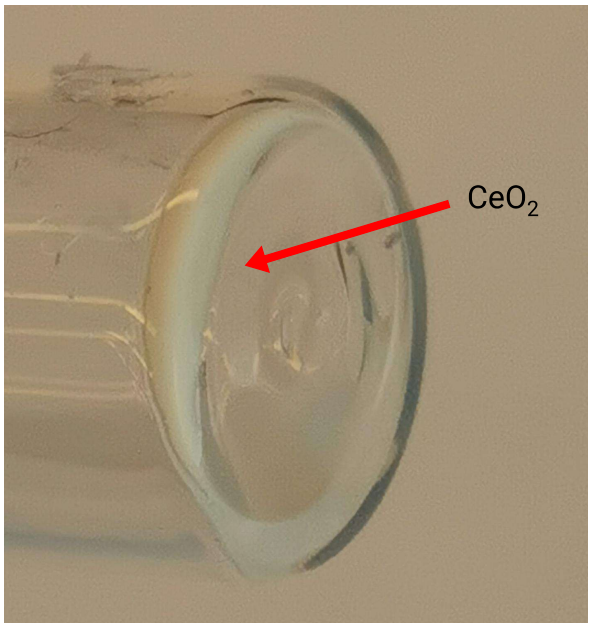

Figure C.2. Picture showing the presence of non-dispersed and agglomerated CeO_2 in the Nafion-CeO_2 mixture. Precipitation of Nafion polymers could not be directly observed or concluded with.

Appendix D

Prussian Blue CV

D.1 PB|- Cycling in Buffer Solutions

CVs obtained from cycling of PB|- in PPB and PPB+NaCl solutions, including both the second and the last (30th) cycle. The CVs were relatively stable over 30 cycles.

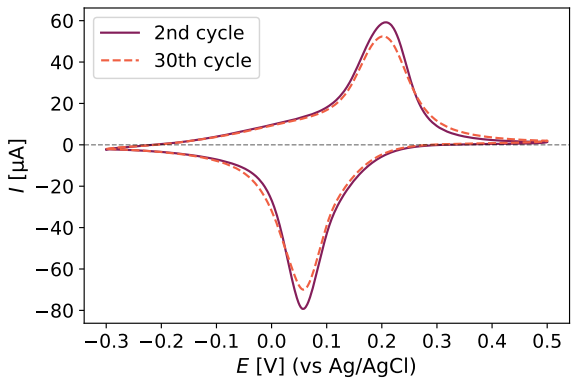

(a) CV of PB in PPB

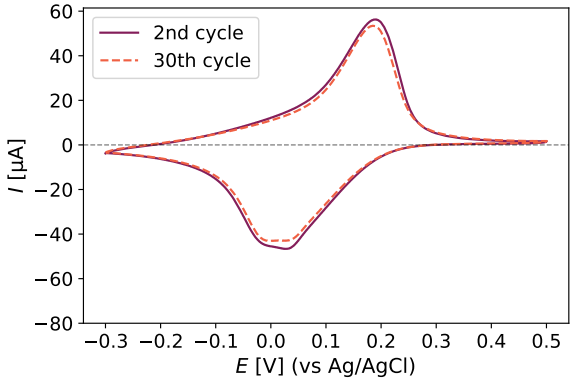

(b) CV of PB in PPB + NaCl

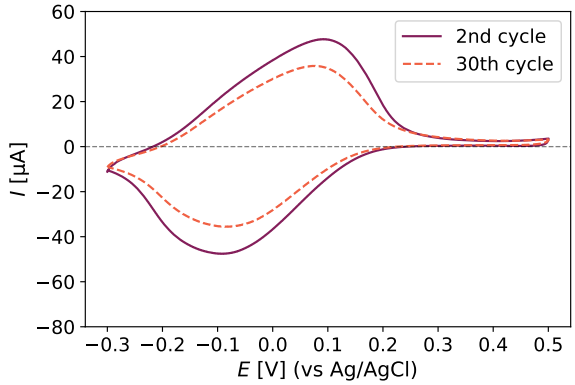

(c) CV of PB in PBS

Figure D.1. The second and last (30th) cycle for CVs of PB|- sensors in (a) PPB (pH 6.83), (b) PPB+NaCl (pH 6.78) and (c) PBS (pH 7.48) at $50\,\mathrm{mV\,s^{-1}}$ showing both the second and the last (30th) cycle.

D.2 Repeated PB|N Cycling in PBS

CVs obtained from cycling of non-treated and post-treated PB|- and PB|N sensors in PBS solution for a total of 5 rounds, showing the 2nd and 30th cycles from all 5 testing rounds.

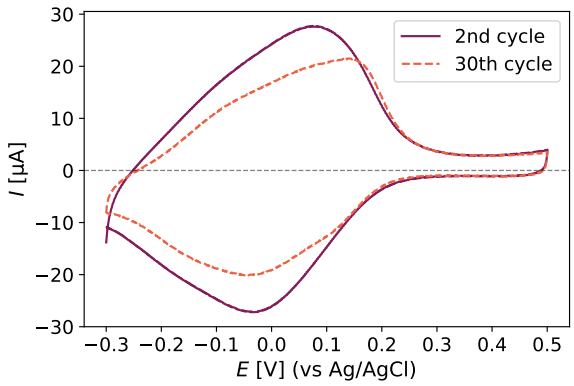

(a) PB|-

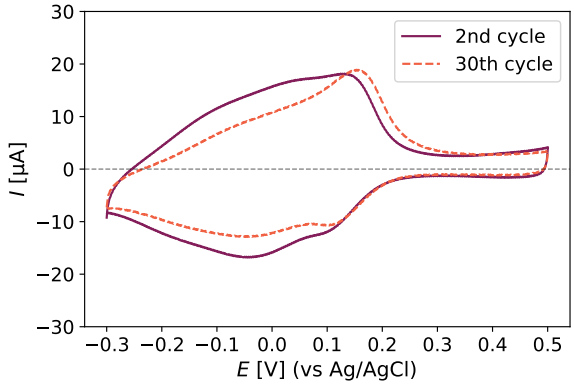

(b) Post-treated PB|-

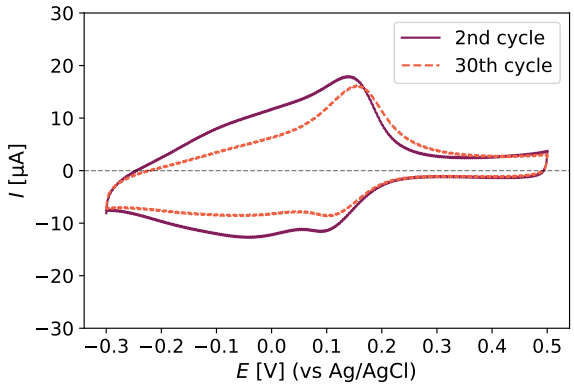

(c) PB|N

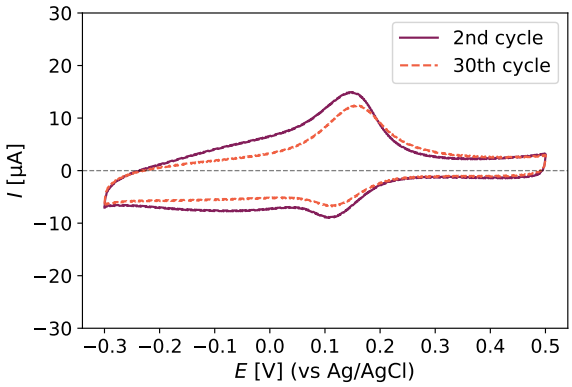

(d) Post-treated PB|N

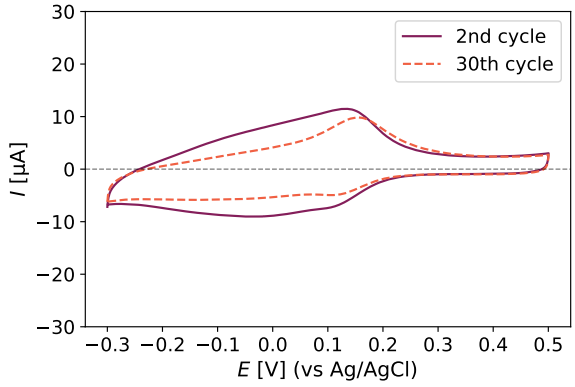

(e) PB|N

Figure D.2. The second and last (30th) cycle for repeated CV of a PB|N sensor in PBS. There were at least 5 days between each round of CV. The first round is shown in (a) and the last in (e). Scan rate was $50\,\mathrm{mV\,s^{-1}}$

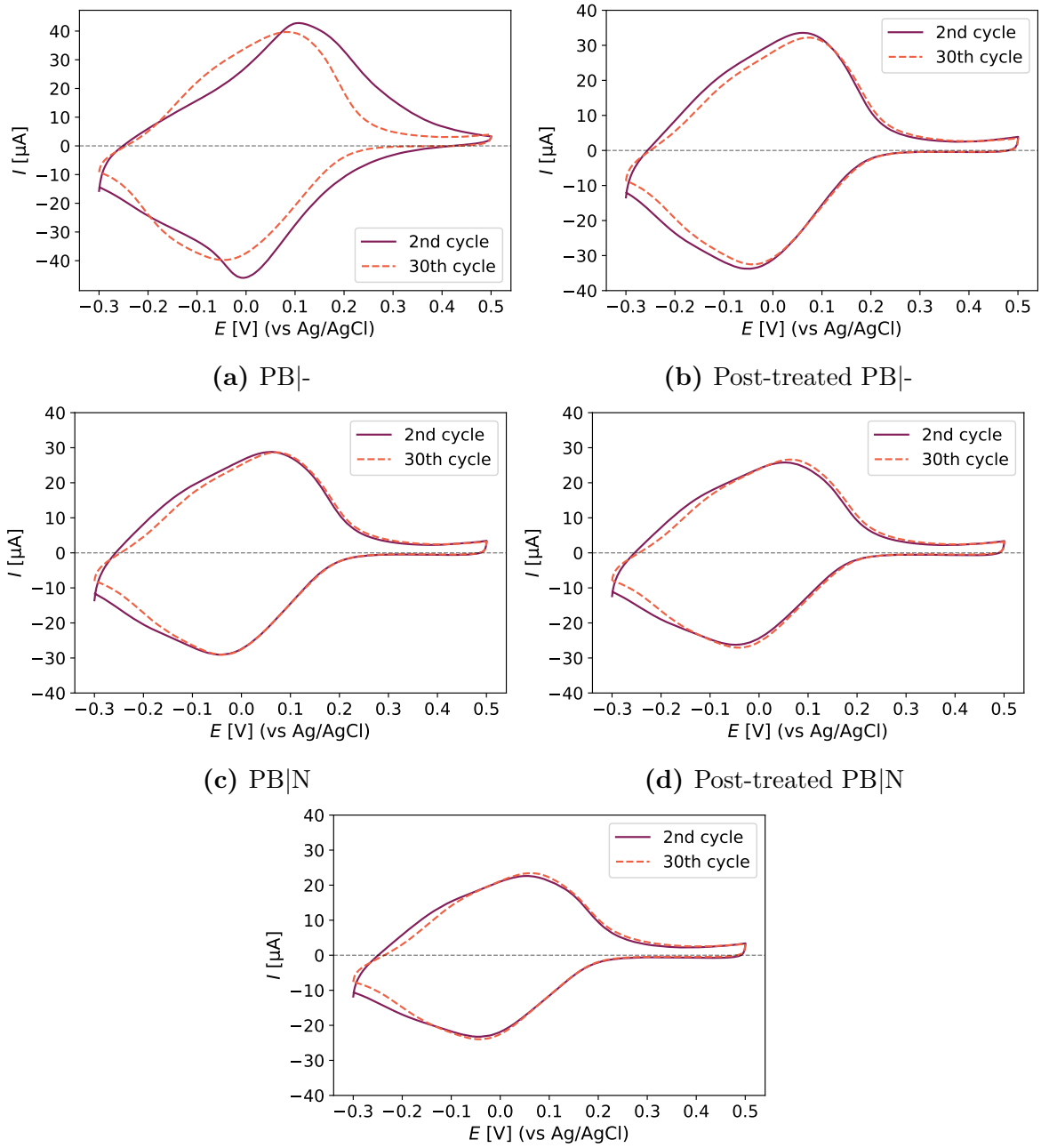

(a) PB|-

(b) Post-treated PB|-

(c) PB|N

(d) Post-treated PB|N

(e) PB|N

Figure D.3. The second and last (30th) cycle for repeated CV of a post-treated PB|N sensor in PBS. There were at least 5 days between each round of CV. The first round is shown in (a) and the last in (e). Scan rate was $50\,\mathrm{mV\,s^{-1}}$

D.3 PB Deposition Data

PB deposition data for the non-treated and post-treated PB|- and PB|N sensors presented in Figures 4.7 and 4.9. Only the last (10th) cycle from the deposition is shown. It is expected that thicker PB films were formed from sensors with larger deposition peak currents.

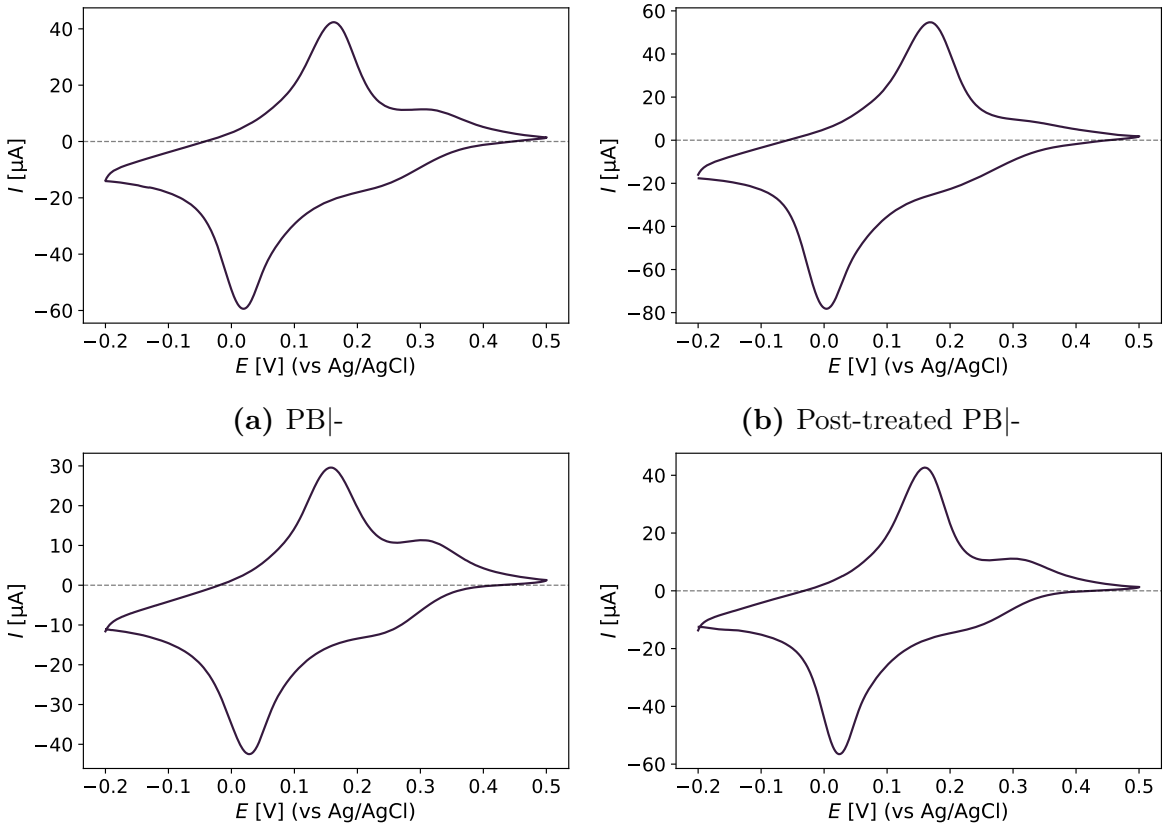

(a) PB|-

(b) Post-treated PB|-

(c) PB|N

(d) Post-treated PB|N

Figure D.4. The last (10th) cycle in the electrodeposition of PB for non-treated and post-treated PB|- and PB|N sensors. Scan rate was $50\,\mathrm{mV\,s^{-1}}$.

Appendix E

Prussian Blue EDS Spectra

Raw EDS spectra obtained for a post-treated PB|- sensor and a non-treated PB|- sensor previously cycled in PBS.

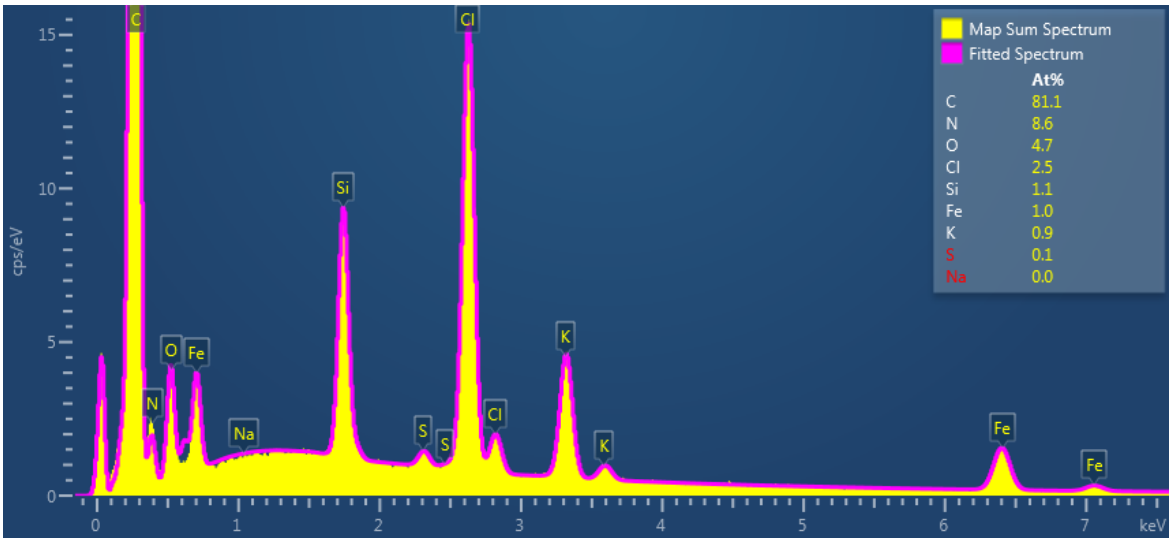

Figure E.1. EDS spectra for post-treated PB|- sensor.

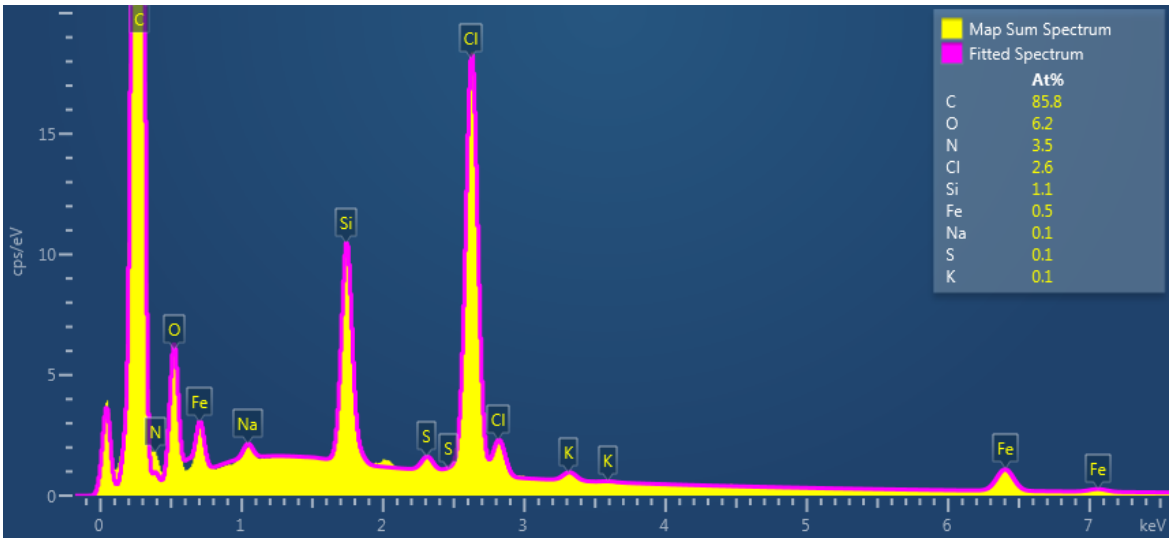

Figure E.2. EDS spectra for a post-treated PB|- previously cycled in PBS.

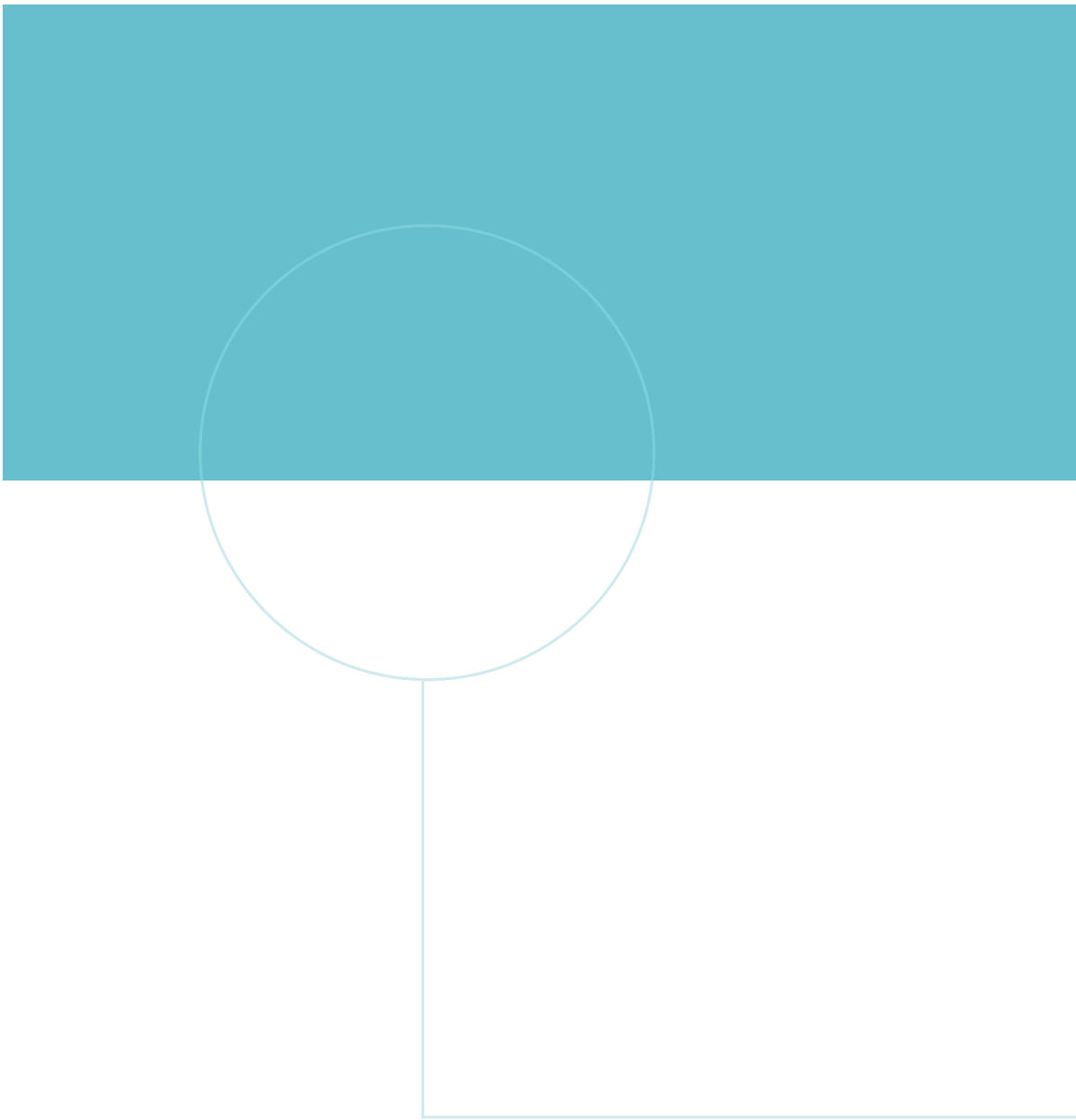

NTNU

Norwegian University of
Science and Technology